Studying Ventral Enclosure during *C. elegans*

Epidermal Morphogenesis

Denise Wernike

A

Thesis

in the Department

of

Biology

Presented in Partial Fulfillment of the Requirements

For the Degree of

Doctor of Philosophy (Biology) at

Concordia University

Montréal, Quebec, Canada

September 2015

CONCORDIA UNIVERSITY

School of Graduate Studies

This is to certify that the thesis prepared

By: Denise Wernike

Entitled: Studying Ventral Enclosure during *C. elegans* Epidermal Morphogenesis

and submitted in partial fulfillment of the requirements for the degree of

Doctor of Philosophy (Biology)

complies with the regulations of the University and meets the accepted standards with respect to originality and quality.

Signed by the final Examining Committee:

_____Chair

Dr. Xavier Ottenwaelder

_____External Examiner

Dr. Sarah Jenna

_____External Examiner

Dr. Andreas Bergdahl

_____Examiner

Dr. Catherine Bachewich

_____Examiner

Dr. Christopher Brett

_____Supervisor

Dr. Alisa Piekny

Approved by

_____

Dr. Selvadurai Dayanandan, Graduate Program Director

_____2015   _____

                                                  Dean of Faculty

ABSTRACT

Studying Ventral Enclosure during *C. elegans* Epidermal Morphogenesis

Denise Wernike, Ph.D.

Concordia University, 2015

Tissue morphogenesis is essential for metazoan development, yet is poorly understood as it requires the coordination of multiple cellular events such as migration, adhesion and shape changes. Furthermore, cells from neighboring tissues also must be coordinated during development, but few studies have addressed this. *Caenorhabditis elegans* is an ideal model to study tissue morphogenesis, since tissues are formed in a highly reproducible manner from a relatively small number of cells of known origin.

I study *C. elegans* ventral enclosure, when epidermal cells migrate over the ventral side of the embryo using cues from the underlying neurons. F-actin accumulates into a supracellular ring along the margins of the ventral epidermal cells, which was predicted to close by non-muscle myosin contractility. We found that anillin (*ani-1*), an actomyosin binding protein, and RhoA (*rho-1*), an upstream regulator of myosin contractility, are required for ventral enclosure. Interestingly, we found that anillin is required for neuroblast cytokinesis, and non-autonomously facilitates ventral epidermal cell migration. We also found that ventral enclosure phenotypes caused by *ani-1* depletion were alleviated or strengthened by mutants that altered actomyosin contractility. Based on these data, we hypothesized that myosin contractility regulates ventral enclosure, and that tissue-tissue interactions are crucial for this process.

Further studies revealed that myosin is indeed required for ventral enclosure. In ventral epidermal cells, myosin localizes as foci in a pattern reminiscent of F-actin. However, myosin also localizes as dynamic foci that form intercellular networks in the neuroblasts, and we found that myosin is required in the neuroblasts for ventral enclosure. In the area underlying the ventral epidermal pocket cells, neuroblasts organize into a rosette-like pattern, and their exposed surface area decreases as the epidermal cells are drawn together. Interestingly, myosin distribution is altered in epidermal cells when neuroblast shape is altered, suggesting that they sense changes in neuroblast tension.

We propose that mechanical forces in the neuroblasts may influence actomyosin in the epidermal cells to facilitate ventral enclosure. This work emphasizes the importance of the interplay between different cell types during tissue morphogenesis, where contractility could be uniquely organized in non-epidermal tissues.

Acknowledgements

First of all, and most importantly, I would like to thank my supervisor Dr. Alisa Piekny. Alisa, I am grateful for the opportunity to perform my PhD studies under your supervision and for being blessed with such an interesting research topic. You have always been a great mentor giving me guidance when needed, but also allowing me to develop my own ideas and approaches to improve this research project.

In addition, I would like to thank my committee members Dr. Sarah Jenna, Dr. Catherine Bachewich and Dr. Christopher Brett for their support and valuable input.

I would also like to give a special thanks to *The Centre for Microscopy and Cellular Imaging* (CMCI) at Concordia University and the constant help provided by the centre's operations manager Dr. Chloë van Oostende. Chloë, thank you for your patience and the countless hours of troubleshooting.

Also, I would like to thank my lab members Karina, Danny, Alexa, Yun, Melina, Madhav, and Tara for their scientific feedback and the little in-between pep talks.

Finally, I appreciated working with Nellie Fotopoulos, who laid the foundation for this project, for which I will be forever thankful.

Dedications

I decided to dedicate this thesis to my parents, Iris and Frank, and my boyfriend Julien, who supported me on every single step of the way. Even though university taught me a lot, you taught me the most important lesson in life, which is that – no matter where you come from or who you are – you can achieve anything in life if you demonstrate wits, will and endurance. So, thank you for this precious lecture, your love and for believing in me.

Contribution of Authors

Figure 11: Nellie Fotopoulos and I both contributed to the time-lapse images.

Figure 12: Nellie Fotopoulos contributed the AJM-1:GFP/ANI-1 immunostaining images.

Figure 15: Nellie Fotopoulos and I both contributed to the time-lapse images.

Figure 16: Alvaro Marte contributed data to the velocity of epidermal cell migration (part A).

Figure 17: Yun Chen and I both contributed to the time-lapse images (part A). Yun Chen contributed the immunostaining images (part B).

Figure 18: Yun Chen contributed the immunostaining images (part B).

Figure 19: Yun Chen and I both contributed to the time-lapse images and analysis of phenotypic ratios (part A and B).

Figure 20: Yun Chen and I both contributed to the immunostaining images (part A and C).

Figure 21: Yun Chen contributed the immunostaining images (part A).

Figure 23: Yun Chen and I both contributed to the time-lapse images (A).

Figure 25: Yun Chen and I both contributed data for measurements (part A and B).

Figure 26: Yun Chen contributed the *ect-2 (ax751)* time-lapse images (part A).

Table 1: Yun Chen, Karina Mastronardi and I contributed data for genetic analysis.

Table 2: Yun Chen, Karina Mastronardi and I contributed data for genetic analysis.

Table of Contents

List of Figures

List of Tables

List of Abbreviations

ABD – actin binding domain

AJM-1 – adherens junction marker 1

ani-1/2/3 – anillin 1/2/3 (*Drosophila* Scraps/Scr)

Arp2/3 – actin-related protein-2/3 (*C. elegans* ARX-2/3)

ATP – adenosine triphosphate

bp – base pairs

*Ce*AJ – *C. elegans* adherens junction

CCC – catenin-cadherin complex

CDC42 – cell division control protein 42 (*C. elegans* CDC-42)

CGC – *Caenorhabditis* Genetics Center

Cyk4 – cytokinesis defect 4 (*C. elegans* CYK-4; human MgcRacGAP; *Drosophila* RacGAP50C)

CRISPR/Cas9 – clustered regularly interspaced short palindromic repeats/CRISPR associated

protein 9

DAC – DLG-1/AJM-1 complex

DIC – differential interference contrast (microscopy)

DLG-1 – *Drosophila* discs large homologue 1

dpy – dumpy

E-cadherin – epidermal cadherin

Ect2 – epithelial cell transformer sequence 2 (*C. elegans* ECT-2; *Drosophila* Pebble/Pbl)

ELC – (myosin) essential light chain

F2/3 – filial generation 2/3

F-actin – filamentous actin

FH1/2 – formin homology (domain) 1/2

GAP – guanine nucleotide activating protein

GEF – guanine nucleotide exchange factor

Gex – gut on the exterior

GFP – green fluorescent protein

GDP – guanosine diphosphate

gof – gain-of-function

GTP – guanosine triphosphate

GTPase – guanosine triphosphatase

HAM-1 – HSN abnormal migration

HMP-1/2 – humpback dorsal lumps 1/2

HMR-1 – hammerhead embryonic lethal 1

KAL-1 – Kallmann syndrome 1

L1/2/3/4 – *C. elegans* larval stage (1-4)

L4440 – ligation number 4440/feeding vector

ROCK – Rho kinase (*C. elegans* LET-502)

LIMK – Lim kinase

LIN-15B – abnormal cell lineage 15B

lof – loss-of-function

lpy – lumpy

MAB-20 – male abnormal (human semaphorin-2A)

mCherry – monomeric cherry fluorescent protein

mDia1/2 – mammalian diaphanous 1/2

MEL-11 – myosin phosphatase

MHC – myosin heavy chain (*C. elegans* nmy-1/2; *Drosophila* Zipper/zip)

MIG-2 – mitogen inducible gene 2

MLC – myosin light chain

MLCK – myosin light chain kinase

MLCP – myosin light chain phosphatase

N2 – *C. elegans* wild-type (Bristol)

N-cadherin – neuronal cadherin

NDS – normal donkey serum

NGM – nematode growth media

NPF – nucleation-promoting factors

OP-50 – *Escherichia coli* strain OP50/*C. elegans* feeding bacteria

PAK-1 – p21-activated kinase

PAR-3/6 – abnormal embryonic partitioning of cytoplasm 3/6

Pat – paralyzed arrest at twofold

PH – pleckstrin homology PLCdelta1

PIE-1 – pharynx and intestine in excess 1

PIX-1 – PAK interacting exchange factor homolog 1

PLX-2 – plexin 2

Rac1 – receptor-adenylate cyclase protein (*C. elegans* CED-10)

RDE-1 – RNAi defective 1

RGA-2 – Rho GTPase activating protein 2

RHGF-2 – Rho guanine nucleotide exchange factor 2

RhoA – Ras homolog family, member A (*C. elegans* RHO-1)

RLC – (myosin) regulatory light chain

RNAi – RNA interference

ROI – region of interest

S2 (cells) – Schneider 2 (*Drosophila* embryonic cells)

SAX-3 – sensory axon guidance 3

SMA-1 – small 1

TBST – Tris buffer saline (Triton X)

TIRF – total internal reflection fluorescence (microscope)

ts – temperature sensitive

UNC-4/40/119 – uncoordinated 4/40/119

VAB-1/2/10 – variable abnormal morphology 1/2/10

VE – ventral enclosure

WASp – Wiskott-Aldrich syndrome protein (*C. elegans* WSP-1)

WAVE/SCAR – WASp-family verprolin homology protein/suppressor of cAMP receptor (*C. elegans* WVE-1, GEX-2/3)

Wnt – *Drosophila* wingless

Chapter 1. Introduction

The formation of tissues, also known as morphogenesis, is crucial for the development of all metazoans. Morphogenesis relies on a series of concerted cellular events such as cell shape changes, migration and adhesion. All of these events are tightly regulated in response to cues, which can be mechanical or chemical, and can come from neighboring tissues. Although not well understood, these cues can promote the activation of intracellular signaling pathways that cause changes in the actomyosin cytoskeleton in distinct areas of the cortex to create symmetry breaks (polarity) that mediate cell shape changes and migration. However, how these events are coordinated for tissue morphogenesis is poorly understood, since few studies have explored this on both the intra and intercellular levels.

Caenorhabditis elegans is an excellent model organism to study tissue morphogenesis. *C. elegans* is amenable to microscopy due to its transparency and simple tissue organization. In addition, the wild-type strain undergoes the various stages of embryogenesis with high reproducibility making it easy to identify phenotypes that deviate from wild-type. *C. elegans* is also amenable to genetics due to the high number of mutant strains that have been generated, their short generation cycle of ~2-3 days (**Figure 1**), and high number of progeny produced by hermaphrodites (Brenner, 1974). Furthermore, many of the *C. elegans* genes have human homologues making them ideal for studying conserved pathways (Sulston et al., 1983; Fire et al., 1998; Tabara et al., 1999).
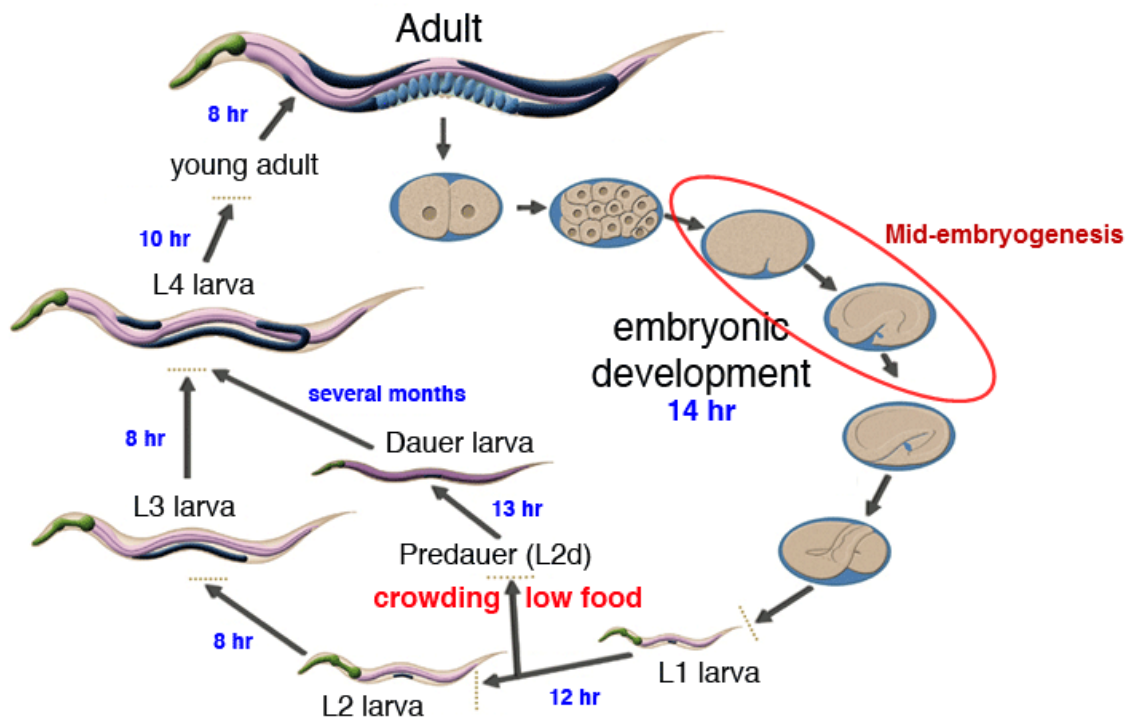
Figure 1. Life cycle of *Caenorhabditis elegans*. The zygote's first cell division occurs in utero. Subsequent developmental stages (gastrulation, mid-embryogenesis (red circle) and late embryogenesis) typically occur ex utero, depending on the availability of food. The embryo then hatches into the L1 larva, which subsequently develops into L2, L3 and L4 stages and finally an adult hermaphrodite. If sources of food are low and/or population density is high, the L1 larva enters a dauer stage. The times shown are for development at room temperature. The times are longer at lower temperatures, and faster at higher temperatures. Figure adapted from Hall and Altun, 2008.

1.1 *C. elegans* epidermal morphogenesis

All metazoans are covered in skin and, apart from providing an outer protective layer that acts as a permeability and structural barrier, the skin functions to provide mechanosensation and homeostasis (e.g. wound healing; Grose and Martin, 1999). Using *C. elegans* as a model to study the mechanisms of tissue morphogenesis can shed light on key aspects of epidermal development that are conserved amongst metazoans (Schmidt-Rhaesa, 2007).

Development of the *C. elegans* epidermis (formerly termed hypodermis) occurs during mid to late-embryogenesis and spans over ~4 hours (**Figure 2**). In addition to enclosing the embryo in a layer of skin, epidermal morphogenesis helps transform the embryo from an ovoid ball of cells into the typical elongated shape of a worm. Epidermal morphogenesis is characterized by three major events: dorsal intercalation, ventral enclosure and elongation (Chisholm and Hardin, 2005).

1.1.1 Ventral enclosure

Ventral enclosure is part of *C. elegans* epidermal morphogenesis where ten pairs of ventral epidermal cells change shape, migrate and adhere with one another to encase the embryo in a single layer of epithelium (Williams-Masson et al., 1997; Chisholm and Hardin, 2005; Zhang et al., 2010). Ventral enclosure is an example of epiboly, which describes the spreading of cells over a substrate to form an epithelium. Studies on epiboly such as in *C. elegans*, zebrafish or *Drosophila* embryos are of broad interest since they may relate to analogous mechanisms involved in wound healing and cancer (Martin and Parkhust, 2004; Jacinto et al., 2002A; Lepage and Bruce, 2010; Wong and Schwarzbauer, 2012).

Ventral enclosure is a two-step process, which involves two functionally distinct subsets
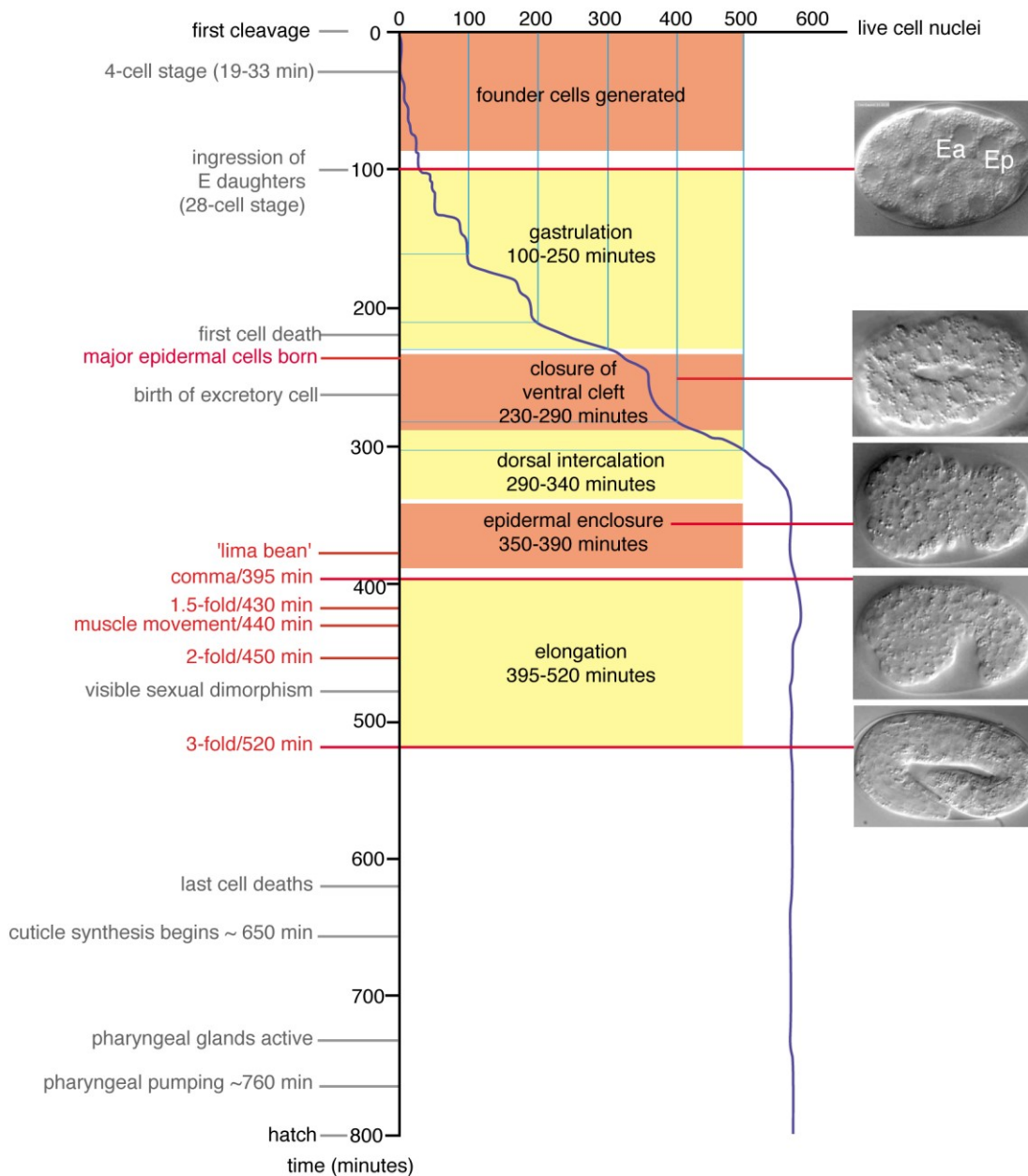
Figure 2. Schematic overview of developmental timing of morphogenetic events during *C. elegans* embryogenesis. Developmental landmarks are shown with representative Differential Interference Contrast (DIC) microscopy images of embryos at corresponding stages. Epidermal morphogenesis occurs between ~290-520 minutes after the first cleavage and includes dorsal intercalation, epidermal (ventral) enclosure and elongation. Figure adapted from Chisholm and Hardin, 2005.

4

of ventral epidermal cells. It is initiated by the migration of two pairs of anterior cells (leading cells) that form actin-rich protrusions (lamellipodia and filopodia) at their leading tips as they migrate towards the ventral midline (**Figure 3**; Chisholm and Hardin, 2005). Inactivation of the leading cells via laser ablation blocks ventral enclosure, indicating that these cells are required for the collective migration of all of the ventral epidermal cells (Williams-Masson et al., 1997). The migration of these cells is actin-dependent, because treatment with cytochalasin D, an inhibitor of actin polymerization, blocks their migration (Williams-Masson et al., 1997). Further studies showed that the WAVE/SCAR complex (GEX-2/3 in *C. elegans*) promotes the formation of short, branched F-actin required for lamellipodia or filopodia through the Arp2/3 complex in response to Rac1/CED-10 GTPase signaling (Lundquist et al., 2001; Severson et al., 2002; Sawa et al., 2003; Patel et al., 2008; see sections 1.2.1 and 1.2.2). Embryos that are mutant for *gex-2*, *gex-3* or *ced-10* display severe defects in epidermal cell migration and result in Gex (gut on the exterior) phenotypes leaving the internal content of the embryo exposed (Soto et al., 2002; Patel et al., 2008; Quinn et al., 2008). These studies emphasize the importance of regulating F-actin for leading cell migration during ventral enclosure.

In a second step, more posterior-oriented ventral epidermal cells (pocket cells) become wedge-shaped and extend toward the ventral midline (Chisholm and Hardin, 2005). Pocket cells do not form extensive protrusive tips, but instead actin filaments (cables) accumulate along their free edges, thereby forming a ring that runs around the tips of cells to form a ventral pocket. Thus, it has been proposed that a supra-cellular actomyosin 'purse string' pulls the cells together by a drawstring or zipper analogous to dorsal closure in *Drosophila* (Kiehart et al., 2000; see section 1.3).

As contralateral epidermal cells meet at the ventral midline, they must properly adhere (and subsequently fuse) to resist contractile forces during later developmental stages (Costa et al.

5
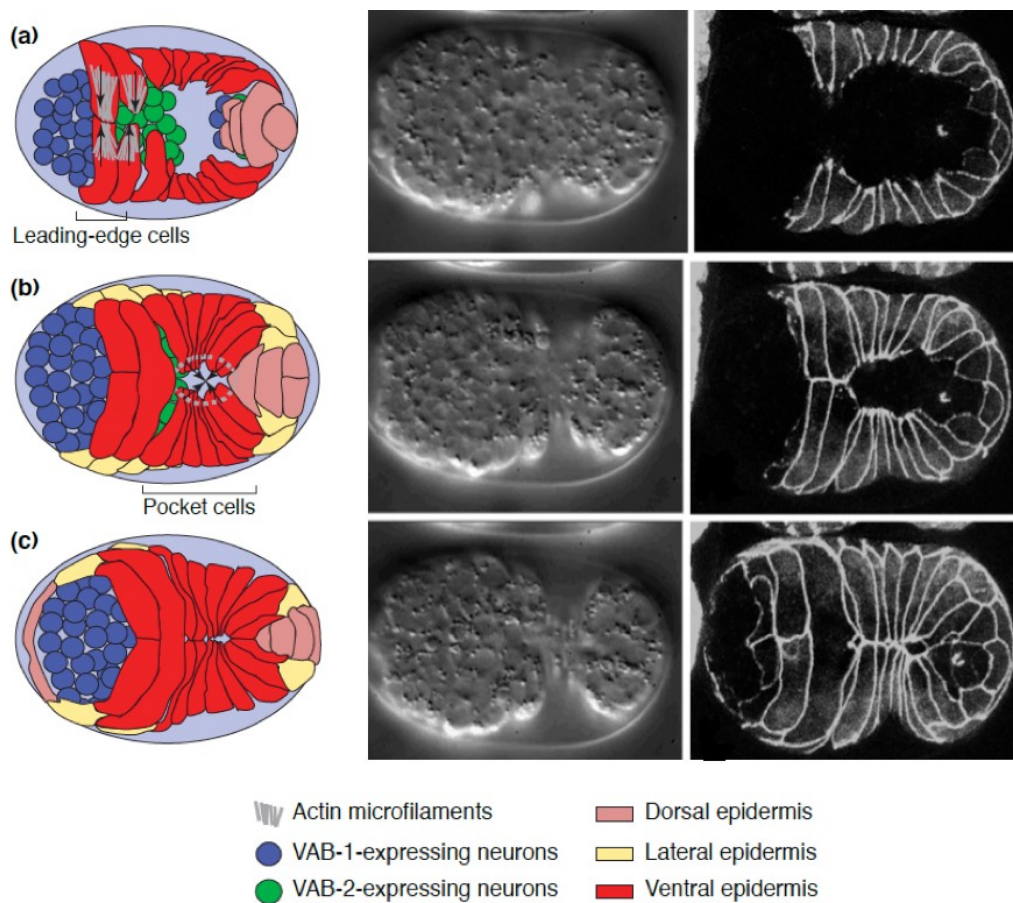
Figure 3. Ventral enclosure during *C. elegans* embryogenesis. Cartoon images are shown for the different stages of ventral enclosure, along with DIC images (middle) and DLG-1:GFP (epidermal adherens junction marker) fluorescence micrographs (right). In the cartoons, ventral epidermal cells are shown in red, seam cells in yellow and dorsal cells in pink. (a) Ventral enclosure is initiated on the anterior (left) side of the embryo by two pairs of leading cells that migrate toward the ventral midline via actin-rich protrusions (arrows, grey lines) using signals from the underlying neurons (blue and green circles). (b) In a second step, more posterior-positioned (right) pocket cells migrate to close the ventral pocket. Ventral pocket closure likely is mediated by a purse string-like mechanism reminiscent of wound healing (arrows, dotted grey line). (c) Once the ventral epidermal cells meet and are aligned at the ventral midline, they adhere with their contralateral partners through the formation of adherens junctions. Scale bar = 5 μm. Figures adapted from Chin-Sang and Chisholm, 2000 (cartoon images), and Chisholm and Hardin, 2005 (DIC and DLG-1:GFP images).

1998; Raich et al., 1999). Embryos with mutations in core components of the most apical part of the junction, the catenin-cadherin complex (CCC), often rupture, likely due to increased pressure on improperly adhered ventral cells, or hatch with abnormal body morphologies due to an uneven distribution of pulling forces across the epithelium (Costa et al., 1998; Pettitt et al., 2003). The CCC depends on the proper localization and function of a more subapical complex, the DLG-1/AJM-1 complex (DAC), which causes loss of localized HMP-1/E-cadherin when compromised (Köppen et al., 2001; Segbert et al., 2004; see section 1.2.5). Taken together, these findings support the idea that junction integrity is required for ventral enclosure (Chin-Sang and Chisholm, 2000; Simske and Hardin, 2001; Chisholm and Hardin, 2005). Interestingly, loss of either the CCC or the DAC does not cause tissues to fall apart, likely because maternal gene products persist until after ventral enclosure (Costa et al., 1998; Raich et al., 1999; Simske and Hardin, 2001). However, there also is some redundancy between the two complexes, because embryos lacking components of both complexes cannot complete embryogenesis (Firestein and Rongo, 2001).

1.1.2 Neuroblasts and their role in epidermal morphogenesis

Neuroblasts, which are neuronal precursors, lie under the epidermal cells and provide chemical and/or mechanical cues to mediate pocket closure during ventral enclosure (**Figures 2 and 3**). Ephrins sort anterior and posterior neuroblasts, and are required for ventral enclosure. VAB-1 (ephrin receptor)-expressing neuroblasts are located at the anterior and posterior of the embryo, while VAB-2 (ephrin ligand)-expressing neuroblasts are found in the center of the embryo (**Figure 3**; Chin-Sang et al., 1999; Wang et al., 1999). Although *vab-1* and *vab-2* mutants both exhibit ventral enclosure defects, it is not clear if phenotypes are caused by mispositioned neuroblasts or due to failure of the epidermal cells to respond to guidance cues (Chin-Sang et al.,

1999). Another study found that a specific subset of neuroblasts form a bridge to guide the overlying pocket cells to the ventral midline (Ikegami et al., 2012). Bridge formation requires the neuroblasts to form cellular extensions, which likely depends on plexin/semaphorin and ephrin signaling, because in embryos lacking functional PLX-2 or MAB-20/semaphorin-2a, the semaphorin ligand, protrusions fail to form from the neuroblasts preventing bridge formation (Ikegami et al., 2012, **Figure 4**). Also, VAB-1 depletion prevents the five pairs of PLX-2/plexin-expressing neuroblasts from being in their correct position causing ventral enclosure defects (Ikegami et al., 2012).

Axon guidance cues that regulate the actin cytoskeleton also have been shown to contribute to ventral enclosure (Ghenea et al., 2005). UNC-40, the netrin receptor, may facilitate the transport of inactive CED-10/Rac1 to endosomes where it is activated (Bernadskaya et al., 2012). Thereafter, CED-10/Rac1 may be recruited to the plasma membrane in a SAX-3/Robo (receptor)-dependent manner to activate the WAVE/SCAR complex for Arp2/3-mediated actin nucleation (Bernadskaya et al., 2012). In support of this hypothesis, loss of UNC-40 causes changes in CED-10 and WVE-1 localization, which leads to a decrease in F-actin levels in the ventral epidermal cells and embryos display the Gex phenotype (Shekarabi and Kennedy, 2002; Shekarabi et al., 2005; Bernadskaya et al., 2012). Also, in *sax-3* mutants, less CED-10 is recruited to the ventral epidermal cell membrane, and embryos have a reduction in WVE-1 and F-actin in those cells (Gitai et al., 2003; Shekarabi et al., 2005; Bernadskaya et al., 2012). In conclusion, these findings suggest that the underlying neuroblasts provide chemical cues for ventral epidermal cell migration, and help regulate ventral enclosure in a non-autonomous manner. However, it is not known if neuroblasts also provide mechanical cues.
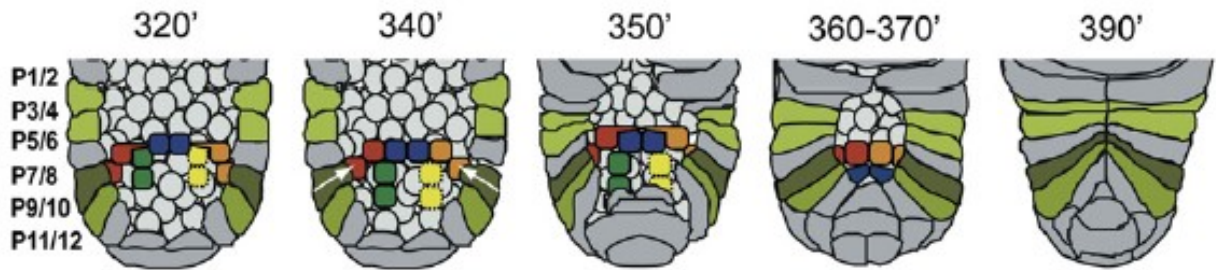
Figure 4. Schematic overview of pocket bridge formation during *C. elegans* ventral enclosure. Epidermal pocket closure is indicated in minutes after the first cleavage. Five pairs of PLX-2-expressing neuroblasts (red, green, blue, yellow and orange) span across the open ventral pocket to form a bridge. Plexin cells of the same color are sisters (daughters from the preceding cell division). Laterally oriented sisters (red and orange) form protrusions (at 320 and 350 minutes) that overlap with neighboring sisters (blue). Neuroblast bridge formation enables the overlying pocket cells P9/10 to migrate toward the ventral midline. Figure adapted from Ikegami et al., 2012.

1.1.3 Elongation

After ventral enclosure is complete, the embryo is transformed into a vermiform shape by a process called elongation (Piekny et al., 2003; Chisholm and Hardin, 2005). To increase the embryo's length by 4-fold, elongation predominantly occurs along the anterior-posterior axis with forces also being exerted dorsal-ventrally (**Figure 5**; Priess and Hirsch, 1986; Piekny et al., 2000; Martin et al., 2014). The epidermal cells undergo dramatic changes in shape, which is achieved by actomyosin-based contractions. Actin filaments form circumferential bundles in the seam cells that constrict to squeeze them from cuboidal to cylindrical in shape (Priess and Hirsch, 1986). High levels of active myosin in the lateral (seam) cells and low levels of active myosin in the dorsal and ventral epidermal cells permit these extensive shape changes to occur (Wissmann et al., 1997; Piekny et al., 2003). However, a recent study showed that higher myosin activity also likely occurs in the anterior dorsal cells to uniquely drive constriction of the head (Martin et al., 2014).

The main regulator of myosin contractility during elongation is the small GTPase RhoA/RHO-1. RHO-1-GTP activates LET-502/ROCK, which in turn triggers contraction by phosphorylating MLC-4 (non-muscle myosin light chain, RLC; see section 1.2.1). LET-502 is highly expressed in the seam cells and loss-of-function or gain-of-function mutants display elongation phenotypes where the epidermal cells fail to change shape, likely due to a reduction in myosin activity (Wissmann et al., 1997; Piekny et al., 2000). In contrast, MEL-11, myosin phosphatase regulatory subunit, leads to dephosphorylation of MLC-4, which renders myosin inactive. MEL-11 is highly expressed in dorsal and ventral epidermal cells, and *mel-11* mutant embryos rupture likely due to hyper-elongation and constriction of the seam cells (**Figure 5**; Wissmann et al., 1997; Wissmann et al., 1999). Strikingly, *mel-11*; *let-502* double mutants develop almost normally, supporting that they have opposing functions, and that contractility can
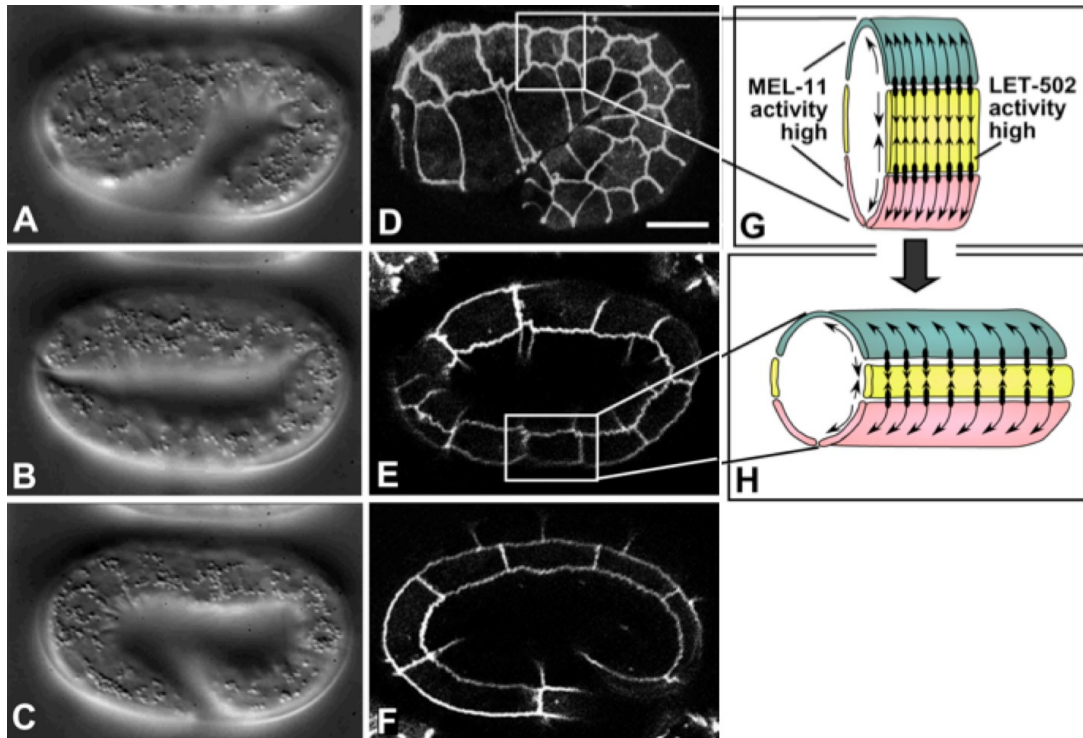
Figure 5. Elongation during *C. elegans* embryogenesis. Cartoon schematics (right) along with DIC images (left), and DLG-1:GFP (epidermal adherens junction marker) fluorescence micrographs (middle) show the different stages of elongation from a comma/bean shape (A, D and G) to two-fold (B, E and H) and three-fold (C and F). In the cartoon schematics, ventral epidermal cells are shown in pink, seam (lateral epidermal) cells are in yellow and dorsal epidermal cells are in green. High levels of LET-502/Rho kinase in the seam cells induce myosin contractility to mediate circumferential cell constriction to change the cells from cuboidal to cylindrical in shape. This also requires high levels of MEL-11/Myosin phosphatase in the dorsal and ventral epidermal cells, to downregulate myosin activity for their relaxation and pliability. Scale bar = 5 μm. Figure adapted from Chisholm and Hardin, 2005.

be controlled via a redundant pathway in their absence (Piekny et al., 2000; Wissmann et al., 1997; Wissmann et al., 1999). Recent studies showed that elongation of the head also depends on other Rho GTPases. While LET-502/ROCK appears to control both the width of the head and the tail during elongation, PIX-1, a Cdc42/Rac-specific activator (GEF), and PAK-1, a Cdc42/Rac-specific effector, control the width of the head. In line with this idea, PIX-1:GFP forms a gradient along the anterior-posterior axis, which is notably increased in dorsal-anterior cells compared to dorsal-posterior cells (Martin et al., 2014). In summary, these findings suggest that a balance of both contraction and relaxation in seam versus dorsal/ventral epidermal cells along the anterior-posterior axis is the key to successful elongation.

In addition, during later stages of elongation, the developing muscles provide mechanotransduction signals to further change epidermal cell shape. Mutants that lack muscle activity or that have impaired attachment of muscle cells to the extracellular matrix (e.g. loss of integrin-based attachments) fail to develop beyond the 2-fold stage and arrest with Pat (paralyzed arrest at twofold) phenotypes (Hresko et al., 1994; Williams and Waterston, 1994). This suggests that tension-induced mechanosignaling in response to contractions also is needed for epidermal morphogenesis (Zhang et al., 2011).

1.2 Cytoskeleton regulators

1.2.1 Rho GTPases

The precise spatiotemporal regulation of F-actin and myosin is crucial to mediate cell shape changes, division, migration and adhesion for tissue morphogenesis. The master regulators of actin cytoskeleton dynamics are the small Rho GTPases, which include RhoA, Rac1 and Cdc42. Rho GTPases are molecular switches that undergo conformational changes depending on

their nucleotide-bound state, which is regulated by guanine nucleotide exchange factors (GEFs) and guanine nucleotide activating proteins (GAPs). While GEFs activate Rho GTPases by promoting the exchange of GDP to GTP, GAPs inactivate them by promoting the hydrolysis of GTP to GDP (reviewed in Bos et al., 2007). Upon activation, the various Rho GTPases regulate different aspects of the actin cytoskeleton. For example, RhoA-GTP recruits effectors such as mDia1 that promote the formation of long, unbranched F-actin, while Rac and/or Cdc42-GTP recruit components of the Arp2/3 pathway to promote the formation of short, branched F-actin.

RhoA-GTP forms stable F-actin that is bound by non-muscle myosin II (hereafter referred to as myosin) to regulate migration and cell shape changes. In migrating cells, RhoA is activated by GEF-H1 to form stress fibers, composed of bundles of F-actin, in the cell rear (Nalbant et al., 2009; Tojkander et al., 2012). Stress fibers also associate with the extracellular matrix via focal adhesions, and when myosin constricts the fibers, this generates rearward forces that propel the cell forward (reviewed in Akhshi et al., 2013). During cell shape change events such as cytokinesis, where the mother cell pinches into two daughters, RhoA-GTP directs the formation of an actomyosin contractile ring that ingresses to physically separate the daughter cells (Glotzer, 2001; Piekny et al., 2005). RhoA is activated by the GEF Ect2 at the equatorial cortex, which is recruited to the plane of division via binding to a complex that regulates the mitotic spindle (Yüce et al., 2005). Another cell shape change event that requires active RhoA is elongation during epidermal morphogenesis in *C. elegans* embryos (Wissmann et al., 1997; Piekny et al., 2000; Fotopoulos et al., 2013; see section 1.1.3). RhoA/RHO-1 is kept inactive in dorsal and ventral epidermal cells likely via its GAP *rga-2*, and is activated in the lateral/seam epidermal cells, possibly through *rhgf-2* and other yet unknown GEFs, to change them from a cuboidal to a cylindrical shape, which helps transform the embryo into the vermiform larva (Chisholm and Hardin, 2005; Chan et al., 2015).

Rac1 and Cdc42 regulate the nucleation of short, branched F-actin, which is important to regulate cell extensions for migration, alter elastic properties/pliability of membranes for cytokinesis, or to polarize cells during development. For example, during cytokinesis, Rac is inactivated via the centralspindlin component CYK-4 at the equatorial cortex making the cortex more pliable to allow for RhoA-driven furrow ingression (Bastos et al., 2012; Davies and Canman, 2012). In migrating cells, Rac and Cdc42 are active at the leading edge to form filopodia and lamellipodia (ruffling membranes) to extend the front of migrating cells in response to environmental cues (Ridley, 2011). While Cdc42-GTP regulates the WASp (Wiskott-Aldrich syndrome protein) complex, Rac1-GTP regulates the WAVE (WASp-family verprolin homology proteins)/SCAR (suppressor of cAMP receptor) complex, leading to the nucleation of short, branched F-actin via Arp2/3 (Chesarone and Goode, 2009; Champellone and Welch, 2010; see section 1.2.2). As described earlier, in *C. elegans*, Rac1/CED-10 regulates the WAVE/SCAR complex to regulate ventral epidermal cell migration for ventral enclosure during epidermal morphogenesis (Soto et al., 2002; see section 1.1.1).

1.2.2 Actin

Different Rho GTPases regulate the nucleation of long, unbranched, or short, branched F-actin (filamentous actin). Long, unbranched filaments form in response to active RhoA, which binds to the GTPase binding domain (GBD) of formin (mDia1) and induces a conformational change to relieve autoinhibition. This change frees the FH2 domain of formin for dimerization, and the neighboring FH1 domains then associate with profilin-actin to polymerize actin filaments from their barbed end in an ATP-dependent manner (Higashida et al., 2004; Goode and Eck, 2007). The branching of actin filaments is achieved by the activity of Arp2/3, a seven-subunit complex that serves as a template for monomeric actin. The subunit Arp2 associates with a pre-

existing (mother) strand of F-actin and the subunit Arp3 allows for the addition of monomeric actin to build a daughter strand at an angle of 70° (Amann and Pollard, 2001; Goley and Welch, 2006). The Arp2/3 complex requires activation by nucleation-promoting factors (NPF; Welch and Mullins, 2002) such as WASp (Wiskott-Aldrich syndrome protein) and WAVE (WASp-family verprolin homology proteins)/SCAR (suppressor of cAMP receptor), which are regulated by Cdc42 and Rac1, respectively as described earlier (see section 1.2.1). These GTPases bind to the GBD domain of WASp and WAVE/SCAR to release their autoinhibitory state and displace motifs that allow them to bind to Arp2/3 to mediate actin branching (Goley and Welch, 2006). The stability of actin filaments is further regulated by specific kinases that inhibit cofilin, a factor that promotes F-actin disassembly. For example, LIM kinase (LIMK) phosphorylates and negatively regulates cofilin (Edwards et al., 1999). Both ROCK, which is activated by RhoA-GTP, and p21-activated kinase (PAK), which is activated by Cdc42-GTP and Rac1-GTP, regulate LIMK to control cofilin and F-actin stability (**Figure 6**; Arber et al., 1998; Edwards et al., 1999).

1.2.3 Myosin

Non-muscle myosin II (myosin) motors associate with actin filaments, and can crosslink or slide them past one another to generate force. Myosin is formed from a hexamer consisting of one pair of heavy chains (MHCs), one pair of essential light chains (ELCs) and one pair of regulatory light chains (RLCs). The heavy chains have coiled-coil regions that permit multimerization, as well as a catalytic motor head domain in their N-terminus with highly conserved actin and ATP-binding sites. The ELCs and RLCs wind around the 'neck' region of the heavy chains, and phosphorylation of the RLCs is required for motor activity (**Figure 7**; reviewed in Sweeney and Houdusse, 2010). Myosin II's RLCs are phosphorylated on residues
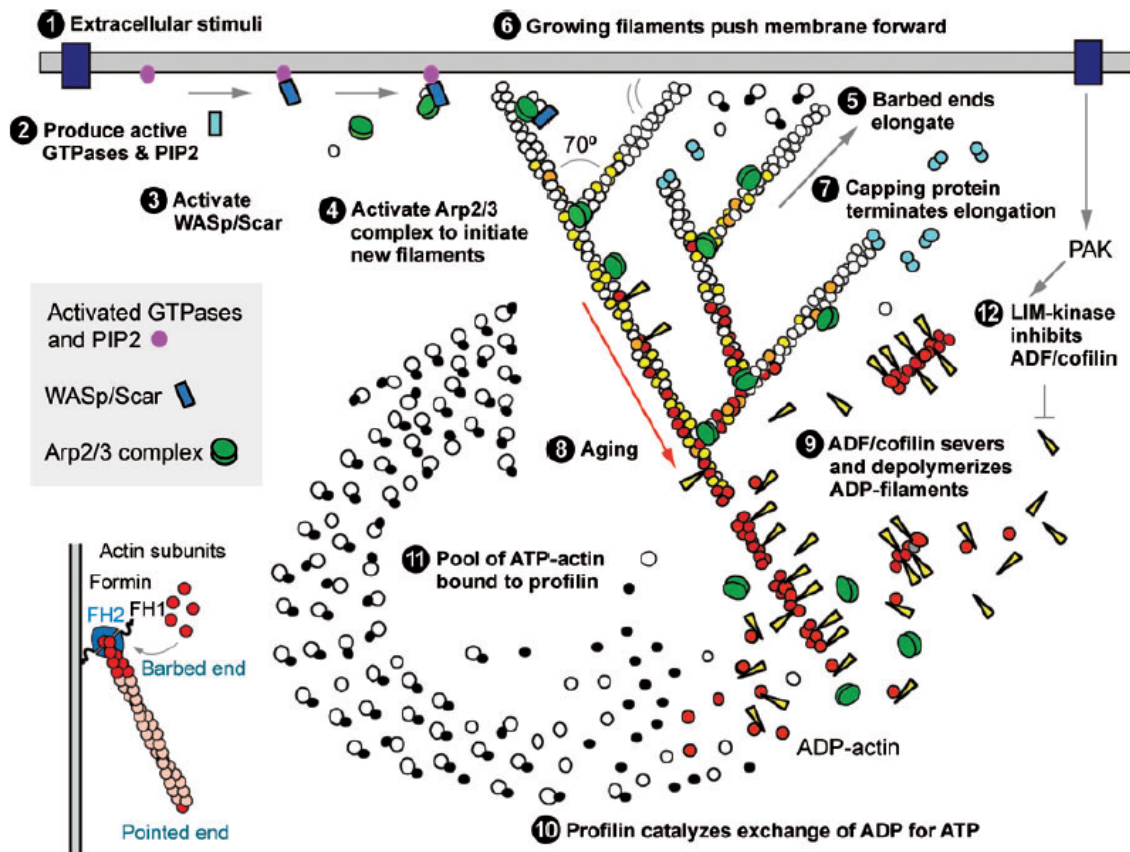
Figure 6. F-actin formation in lamellipodia/filopodia. The cartoon schematic depicts how F-actin is regulated in response to stimuli. (1) An external stimulus is translated into changes in F-actin by (2) triggering Rho GTPase activity, (3) promoting WASp or WAVE/SCAR function, and (4) bringing together the Arp2/3 complex with monomeric actin. (5) The addition of monomeric actin to the barbed end of actin filaments (6) facilitates their growth to push out the membrane (7) until actin-capping proteins terminate this process. (12) Rho GTPase-induced activation of kinases such as PAK or ROCK promote LIMK activation to prevent (9) actin depolymerization via the inhibition of cofilin. The dimerized FH2 domains of formins take on donut-like structures that surround the barbed end of actin filaments. The FH1 domains of formins tether profilin-actin to the barbed end, thereby elongating the filament (bottom left). Figure adapted from Pollard, 2007.
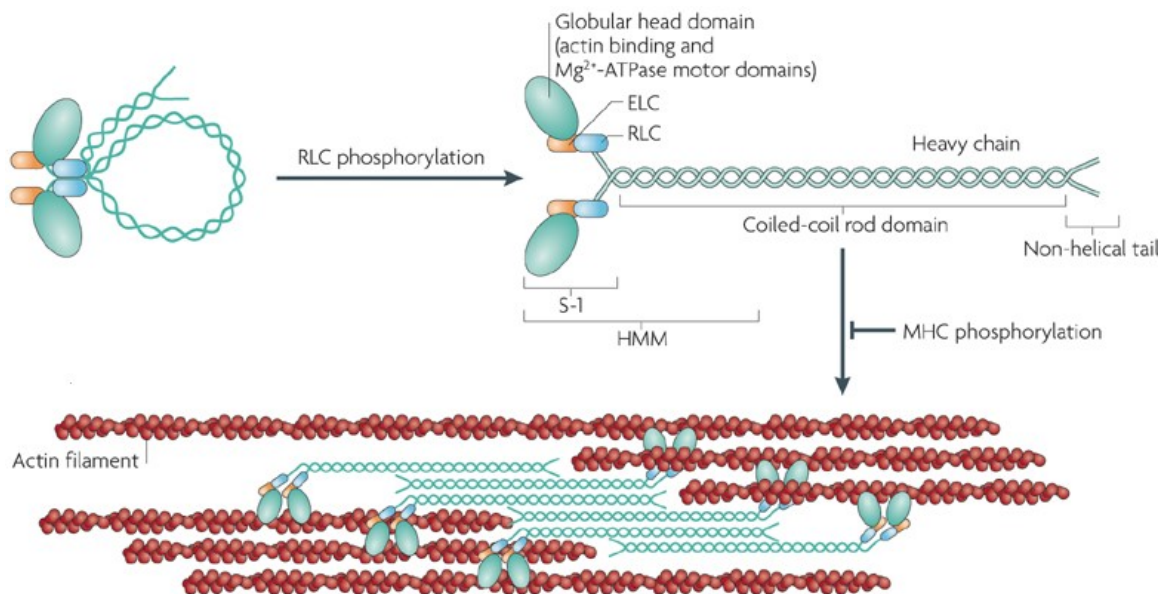
Figure 7. Non-muscle myosin's domain structure and function. Cartoon schematics show how myosin assembles into filaments. When the RLCs are dephosphorylated, myosin is folded (top left), and upon their phosphorylation, myosin unfolds (top right) and is able to form multimeric filaments (bottom). Each of the two heavy chains consists of a globular head motor domain in the N-terminus and a coiled-coil domain including a non-helical tail domain in the C-terminus. The ELCs and the RLCs wind around the heavy chains between the head motor domain and the coiled-coil domain. Myosin molecules assemble into bipolar structures through the interactions of their coiled-coil domain along the heavy chains. Myosin binds to actin filaments via its head motor domains. ATP hydrolysis, which is stimulated by RLC, enables myosin to move actin filaments past each other in an anti-parallel manner (bottom). Figure adapted from Vincente-Manzanares et al., 2009.

Ser19 and/or Thr18 by various kinases including myosin light chain kinase (MLCK), Rho kinase (ROCK) and Citron kinase (Vincente-Manzanares et al., 2009; Yamashiro et al., 2003; Matsumura, 2005). Myosin light-chain phosphatase (MLCP) decreases myosin activity by dephosphorylating RLCs. Interestingly, ROCK can also phosphorylate the regulatory subunit of MLCP to down-regulate MLCP activity, thereby further increasing myosin activity upon its activation (Matsamura and Hartshorne, 2008; Vincente-Manzanares et al., 2009).

The importance of regulating myosin for cell shape changes and cell movements has been demonstrated for different developmental events during *C. elegans* embryogenesis. As described earlier, it is crucial to balance myosin activity during epidermal morphogenesis. While the loss of LET-502/ROCK blocks elongation of the embryo due to failed epidermal cell shape changes, loss of MEL-11/MLCP regulatory subunit causes embryos to rupture due to their hyperconstriction, and embryos lacking both LET-502 and MEL-11 develop almost normally (Wissmann et al. 1997; Piekny et al., 2000; see section 1.1.3). Another developmental process that depends on myosin activity during embryogenesis is gastrulation, where small groups of cells ingress at varying times into a small space, the blastocoel, to establish the three different germ layers (endo-, meso- and ectoderm). Here, myosin accumulates at the apical surface of a subset of cells, which mediates their ingression via apical constriction and reduces their surface area (Nance and Priess, 2002; Lee and Goldstein, 2003). Myosin contractility pulses across the apical surface of the cell, which is ratcheted to transmit the pulsations into a change in cell shape by being tethered to junctions (Terry et al., 2011; Mason et al., 2013). Myosin accumulation in ingressing cells likely depends on apical-basal polarity, because in embryos depleted of the apical polarity proteins PAR-3 and PAR-6, cells take longer to shrink and ingress more slowly (Nance et al., 2003). In addition, the non-canonical Wnt-Frizzled signaling pathway (planar cell polarity pathway), which can signal to Rac1 or RhoA, regulates actomyosin contractility during gastrulation (reviewed in

Schlessinger et al., 2009). In the absence of Wnt signaling, endodermal precursor cells polarize and accumulate apical myosin, but their apical surfaces do not constrict, possibly due to decreased RLC phosphorylation (Morel and Arias, 2004; Lee et al., 2009).

1.2.4 Anillin

Anillin is a key regulator of actomyosin contractility and is a highly conserved protein. While it is best known for its regulation of animal cell cytokinesis (reviewed in Piekny and Maddox, 2010), it also regulates non-mitotic events including cellularization in *Drosophila* embryos, neurite outgrowth in *C. elegans*, and epidermal junctions in *Xenopus* (Field et al., 2005; Reyes et al., 2014; Tian et al., 2015). Anillin binds to F-actin, active myosin, membrane lipids, and microtubules, as well as RhoA and its regulators (reviewed in Piekny and Maddox, 2010; Liu et al., 2012; van Oostende Triplet et al., 2014; **Figure 8A**). Through these interactions, anillin helps define cortical domains to polarize cells, such as maintaining the division plane during cytokinesis (Straight et al., 2005; Piekny and Glotzer, 2008). The *C. elegans* genome has three anillin genes: *ani-1*, *ani-2* and *ani-3,* with ANI-1 sharing the highest overall homology with human and *Drosophila* (scraps) anillin (**Figure 8B;** Maddox et al., 2005; 2007). Although studies demonstrated that the *C. elegans* anillin genes do not appear to be essential for cytokinesis, it is likely that it is impossible to sufficiently deplete ANI-1 via RNAi without preventing a complete block in oogenesis or causing other meiotic phenotypes, which may require a different anillin threshold than needed for cytokinesis in *C. elegans* (Maddox et al., 2007). ANI-2 and ANI-3 are truncated forms that lack the characteristic myosin and actin-binding sites in the N-terminus. While there are no known functions described for *ani-3*, *ani-2* appears to be exclusively required for post-embryonic gonad and oocyte development (Maddox et al., 2005).

Recent studies have begun to shed light on non-cytokinetic functions for anillin during

A
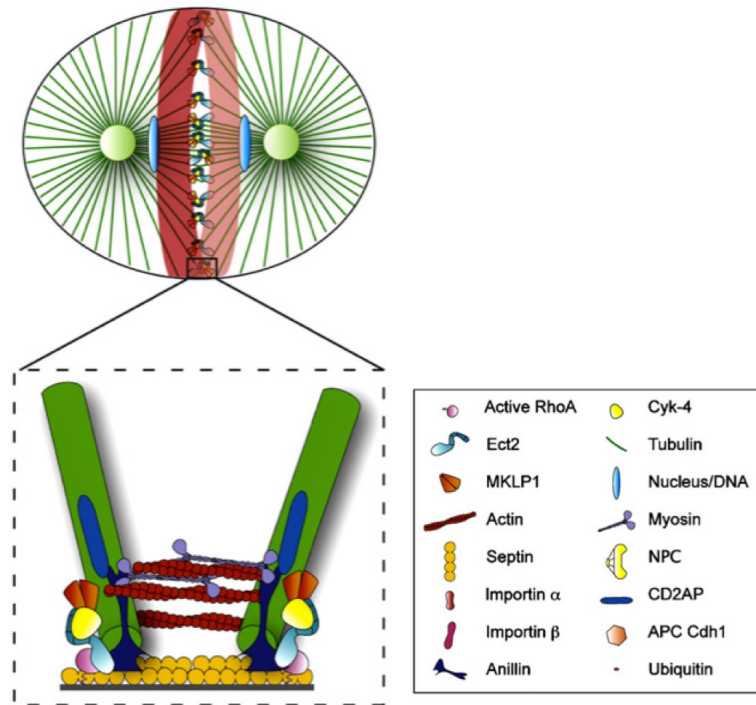
B
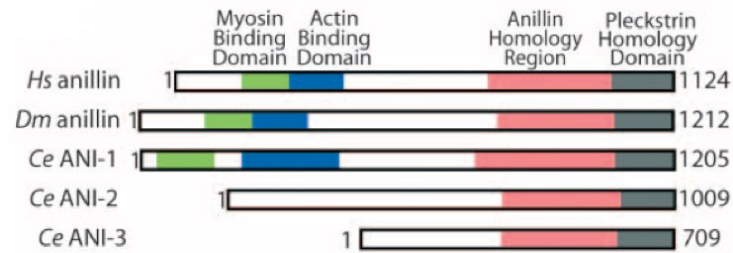
Figure 8. The structure and location of anillin during cytokinesis. (A) A cartoon schematic shows the localization of anillin and its binding partners during mammalian cytokinesis. During anaphase, anillin is recruited to the equatorial cortex by RhoA-GTP where it tethers the contractile ring to the plasma membrane (red ring in the cell). A detailed view depicts anillin at the equatorial cortex with other contractile ring components (hatched box). (B) A cartoon schematic shows anillin's structure in human, *Drosophila* (scraps) and *C. elegans* (isoforms *ani-1*, *ani-2* and *ani-3*). Human anillin, scraps and *ani-1* share high homology in their myosin (green) and actin (blue)-binding domains in the N-terminus, and the Anillin Homology (red) and Pleckstrin Homology (grey) domains in the C-terminus. Figures adapted from Piekny and Maddox, 2010 (A) and Maddox et al., 2005 (B).

development. Although it is sequestered to the nucleus in interphase cells, anillin is often not (entirely) nuclear in developing tissues. For example, studies in *Xenopus* embryos suggest that anillin localizes to cell-cell junctions in interphase cells to regulate junctional integrity, because adherens junctions and tight junctions become disrupted upon anillin knock-down. This likely is due to the ability of anillin to reinforce Rho1 localization (via a feedback loop), and maintain actomyosin at the junction, since they are mislocalized upon anillin depletion (Reyes et al., 2014). Furthermore, recent studies showed that anillin is distributed to the leading edge of Q neuroblasts (precursors of sensory and interneurons) in *C. elegans* L1 larvae, where it mediates growth cone extension and cell migration by stabilizing the F-actin network likely in response to the activities of the novel GTPase RhoG/MIG-2 (Tian et al., 2015). Based on these findings, it may be possible that anillin fulfills additional functions during (embryonic) development that go beyond its role in cytokinesis.

1.2.5 Adherens Junctions

The actin cytoskeleton is crosslinked between neighboring epidermal cells via adhesion/adherens junctions, which help coordinate cell shape changes and migration during tissue morphogenesis (Halbleib and Nelson, 2006; Nichimura and Takeichi, 2009; Harris and Tepass, 2010). In the early *C. elegans* embryo, adherens junction proteins are found at sites of contact between blastomeres. During mid-late embryogenesis, adherens junction proteins localize to a global apical junction in epidermal cells known as the *C. elegans* Adherens Junction (*Ce*AJ), which is a single structure that combines the adhesive and barrier functions of vertebrate adherens and tight junctions (Armenti and Nance, 2012). As described earlier, the *Ce*AJ is comprised of several complexes, including the catenin-cadherin complex (CCC) and the DLG-1 (*Drosophila* Discs Large)/AJM-1(Adherens Junction Marker) complex (DAC; see section 1.1.1).

The CCC is composed of E-cadherin/HMR-1, α-catenin/HMP-1 and β-catenin/HMP-2 and is at the more apical part of the *Ce*AJ. HMR-1 is a transmembrane calcium-dependent glycoprotein, with an extracellular domain that interacts with other HMR-1 proteins and crosslinks adjacent cells. Intracellularly, HMR-1 forms a complex with α-catenin/HMP-1 and β-catenin/HMP-2, both of which directly bind to actin filaments (**Figure 9**; Costa et al., 1998; Kobielak and Fuchs, 2004). The DAC is composed of DLG-1, a PDZ-domain-containing scaffolding protein (**Figure 3**), and AJM-1, a coiled-coil domain protein that has no clear orthologues in *Drosophila* or vertebrates (Köppen et al., 2001; Armenti and Nance, 2012). As described earlier, *C. elegans* embryos lacking E-cadherin or catenin rupture during mid-late embryogenesis, or larvae have abnormal body morphologies due to failed adhesion of neighboring contralateral epidermal cells at the ventral midline during ventral enclosure (Costa et al., 1998; Raich et al., 1999; Labouesse, 2006). Thus, the two complexes within the *Ce*AJ likely are redundant, since loss of either complex causes phenotypes during mid-late embryogenesis, while loss of both blocks development altogether (Firestein and Rongo, 2001). Consistent with this, only cells that drive ventral enclosure fail to attach to each other, while other epidermal cells (*e.g.* seam cells) still adhere and retain their integrity (Costa et al., 1998; Raich et al., 1999). Furthermore, removing DLG-1 or AJM-1 results in a slightly abnormal aggregation of some CCC-associated proteins, while the CCC overall remains its integrity (McMahon et al., 2001).

Most studies have focused on junctions in epithelial cells or their precursors, and cardiomyocytes are one of the few non-epithelial cell types where cell-cell adhesion complexes have been studied (Sheikh et al., 2009). However, different cell types express different cadherins or proteins containing cadherin repeats that uniquely mediate cell-cell adhesion as well as other cellular events, including migration. One of the best-known examples is N-cadherin, which is expressed in neurons. Previous experiments where N and E-cadherin were expressed in cultured

Key

SMA-1/ßH-spectrin

SPC-1/α-spectrin

apical proteins

CRB-1, PAR-3, PAR-6, PKC-3

F-actin

HMR-1A/E-cadherin

JAC-1/p120-catenin

HMP-2/ß-catenin

HMP-1/α-catenin

VAB-9/claudin

DLG-1/Discs Large

AJM-1 (novel)

? LAD-1/L1CAM ?

CLC-1/claudin

LET-413/Scribble

CCC

DAC

CeAJ components
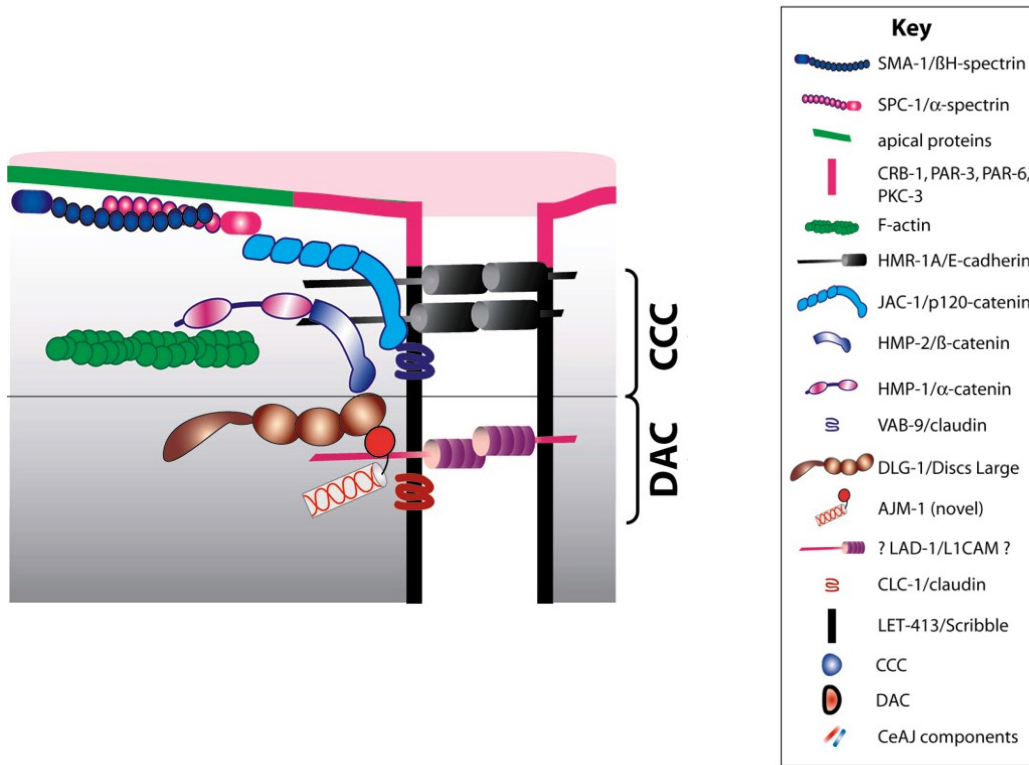
Figure 9. The *C. elegans* adherens junction. A cartoon schematic shows the architecture of the adherens junction found in *C. elegans* epidermal cells. These junctions contain two types of adhesion complexes; the catenin-cadherin (CCC) and the DLG-1/AJM-1 (DAC) complex. The CCC consists of E-cadherin/HMR-1 (black) that links to adjacent plasma membranes via its extracellular face. Intracellularly, E-cadherin/HMR-1 binds to a complex of α-catenin/HMP-1 (pink) and β-catenin/HMP-2 (dark blue), which associates with F-actin (green) and helps tether the cytoskeleton to the junction. The DAC is comprised of L1CAM (light purple), which links adjacent cells via its extracellular face, and associates with AJM-1 (red) and DLG-1 (brown) intracellularly. Figure adapted from Labouesse, 2006.

cells showed that cells expressing N-cadherin grouped together and sorted away from those expressing E-cadherin, and vice versa (Niessen and Gumbiner, 2002). Likewise, proper levels of β-catenin are required for the sorting of cells from the notochord to the somites during mesoderm formation in *Xenopus*, because reduced levels led to sorting in the opposite direction (Reintsch et al., 2005). However, the complexes that catenin and cadherin interact with to mediate changes in the cytoskeleton for various cellular events are not well understood. Another recent study in human glial cells and astrocytes also demonstrated that N-cadherin-mediated adhesion controls cell velocity during collective migration likely via the regulation of focal adhesions. It is assumed that the loss of N-cadherin could contribute to the invasive capacity of tumor astrocytes, because low levels of N-cadherin were frequently associated with increased cell migration while re-expressing N-cadherin restored cell polarity and strongly reduced cell velocity in gliomas (Camand et al., 2012). Similar to mammals, *C. elegans* expresses N-cadherin (reviewed in Tepass et al., 2000). The gene *hmr-1* can be expressed as two different isoforms of cadherin via alternative splicing. While the shorter transcript is translated into the classic E(epidermal)-cadherin (HMR-1A), the longer isoform gives rise to N(neuronal)-cadherin (HMR-1B), which is confined to the nervous system at all developmental stages (White et al., 1986; Broadband and Pettitt, 2002). This finding may raise the idea that neuroblasts and neurons accumulate unique cadherin complexes, which could regulate the actomyosin cytoskeleton to mediate cell shape changes during embryogenesis.

1.3 *Drosophila* dorsal closure – an analogous event to *C. elegans* ventral enclosure

Dorsal closure in *Drosophila* is when dorsal epidermal sheets cover the dorsal surface of the embryo, possibly relying on mechanisms similar to *C. elegans* ventral enclosure. During dorsal closure, a thick actomyosin cable forms along the dorsal edges of the epithelial sheets, which reduces in size as the sheets migrate toward the dorsal midline of the fly embryo where they meet, align (zipper) and subsequently fuse (Kiehart et al., 2000). Interestingly, the aminoserosa, an extraembryonic epidermal tissue that lies directly underneath the epidermal cells, contracts rhythmically to displace the two epithelial sheets in a dorsal-ward direction (**Figure 10**; Jacinto et al., 2002A; Solon et al., 2009).

Several studies suggest that the spatiotemporal regulation of actomyosin in the epithelial cells is crucial to orchestrate closure of the dorsal surface. Embryos mutant for *pebble* (*pbl*), the *Drosophila* ortholog of ECT-2, have less F-actin at the leading edge of the dorsal-most row of epidermal cells (Jankovics et al., 2011). Similarly, mutants for *rho1,* the *Drosophila* ortholog of RhoA, have diminished actomyosin cables at the leading edge of the epithelial cells, suggesting that an actin cable associated with these cells may close in a purse string-like fashion (Martin and Lewis, 1992; Lu and Settleman, 1999; Magie et al., 1999; Jacinto et al., 2002B). Consistent with this model, *zipper* (*zip*; non-muscle myosin II heavy chain in *Drosophila*) mutant embryos fail dorsal closure (Jacinto et al., 2002B). Furthermore, severing the leading edge of the epithelial cells via a laser leads to a ventral-ward (recoiling) movement of epidermal cells in wild-type embryos, which is abolished in *zip* mutants, indicating that the actin cable likely is under myosin-based tension (Franke et al., 2005; Solon et al., 2009).

Interestingly, myosin also is required in the amnioserosal cells, where it localizes to the
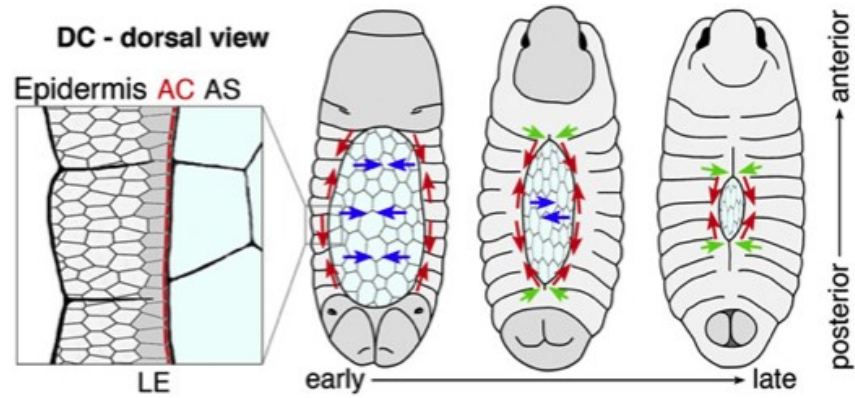
Figure 10. *Drosophila* dorsal closure. Cartoon schematics show a *Drosophila* embryo during dorsal closure. The zoomed in region (box on the left) depicts the leading edge (LE) of the epidermis (left) with the actin cable (AC) and the adjacent amnioserosal cells (right). The colored arrows show the direction of movements and forces produced by the AS cells (blue), the AC (red), and zippering (green) of the epidermal cells. Figure adapted from Solon et al., 2009.

apical surface of cells that shrink as the epithelial sheets come together (Kiehart et al., 2000; Franke et al., 2005). The structural integrity of the amnioserosa is altered in null *zip* mutant embryos, where the cells fail to constrict and remain the same size and shape (Franke et al., 2005). Also, in *pbl* mutants, the amnioserosal cells have fewer rhythmic pulsations of lower amplitude, indicating that myosin contractility is regulated by Rho1-Pbl to drive constriction of the amnioserosal cells for dorsal closure (Jankovics et al., 2011).

1.4 Summary

Tissue morphogenesis and crucial homeostatic events like wound healing depend on coordinated cell shape changes and migration, and misregulation of these processes can promote metastasis, where cancer cells migrate to multiple locations in the body (Schäfer and Werner, 2008; Friedl and Wolf, 2009). Therefore, identifying the key mechanisms that regulate cell shape changes and migration can help elucidate our understanding of development and cancer.

We study *C. elegans* ventral enclosure, which is part of epidermal morphogenesis, as a model to elucidate the mechanisms driving tissue morphogenesis. Our work sheds light on the interplay between different cell types – epidermal and non-epidermal, and how this impacts the actomyosin cytoskeleton. In addition to improving our understanding of epidermal morphogenesis, this work also sheds light on neural development.

The first part of this thesis describes a role for anillin (*ani-1*) and RhoA (*rho-1*) in epidermal morphogenesis during *C. elegans* embryogenesis. We found that anillin is expressed and functions to regulate neuroblast cytokinesis, and may non-autonomously facilitate ventral epidermal cell migration. Moreover, we demonstrated that *rho-1* is required for ventral enclosure and elongation, a later step in epidermal morphogenesis. While downstream effectors of RHO-1

27

that regulate myosin contractility had previously been shown to regulate elongation, our work suggested for the first time that this same pathway could function earlier in epidermal morphogenesis. Indeed, ventral enclosure phenotypes caused by depletion of *ani-1* were alleviated or strengthened by mutants that altered actomyosin contractility. These data suggest that 1) myosin contractility may regulate ventral enclosure and 2) tissue-tissue interactions may regulate ventral enclosure.

The second part of this thesis further characterizes the function of myosin (*nmy-2*) in ventral enclosure. We show that myosin accumulates as foci that form a supra-cellular ring along the junction free edges of the epidermal cells, and forms a dynamic star-like pattern in the neuroblasts during ventral enclosure. We show that the RhoA GEF Ect2 (*ect-2*) functions as an upstream regulator of myosin in both epidermal and neuroblast tissue, and that myosin is required in the neuroblasts for ventral enclosure. We also found that a subset of neuroblasts organizes into a rosette-like pattern, and their surface area decreases as the overlying contralateral neighboring epidermal cells meet. We propose a model where mechanical forces are coordinated, either through junctional proteins or mechanosensing, in both the epidermal cells and neuroblasts for successful ventral enclosure.

Chapter 2. *Caenorhabditis elegans* anillin (*ani-1*) regulates neuroblast cytokinesis and epidermal morphogenesis during embryonic development

2.1 Abstract

The formation of tissues is essential for metazoan development. During *C. elegans* embryogenesis, ventral epidermal cells migrate to encase the ventral surface of the embryo in a layer of epidermis by a process known as ventral enclosure. This process is regulated by guidance cues secreted by the underlying neuroblasts. However, since the cues and their receptors are differentially expressed in multiple cell types, the role of the neuroblasts in ventral enclosure is not fully understood. Furthermore, although F-actin is required for epidermal cell migration, it is not known if non-muscle myosin is also required. Anillin (ANI-1) is an actin and myosin-binding protein that coordinates actin-myosin contractility in the early embryo. Here, we show that ANI-1 localizes to the cleavage furrows of dividing neuroblasts during mid-embryogenesis and is required for their division. Embryos depleted of *ani-1* display a range of ventral enclosure phenotypes, where ventral epidermal cells migrate with similar speeds to control embryos, but contralateral neighbors often fail to meet and are misaligned. The ventral enclosure phenotypes in *ani-1* RNAi embryos suggest that the position or shape of neuroblasts is important for directing ventral epidermal cell migration, although does not rule out an autonomous requirement for *ani-1* in the epidermal cells. Furthermore, we show that *rho-1* and other regulators of non-muscle myosin activity are required for ventral epidermal cell migration. Interestingly, altering non-muscle myosin contractility alleviates or strengthens *ani-1*'s ventral enclosure phenotypes. Our findings suggest that ventral enclosure is a complex process that likely relies on inputs from multiple tissues.

2.2 Introduction

Tissue morphogenesis is crucial for the development of multicellular organisms and requires coordinated cell shape changes and movements. During *C. elegans* embryogenesis, ventral epidermal cells migrate from the dorsal to the ventral side of the embryo to enclose the ventral surface in a layer of epidermal cells by a process called ventral enclosure. These cell movements are actin dependent since embryos carrying mutations in F-actin regulators fail to initiate epidermal migration and cause Gex (gut on the exterior) phenotypes (Soto et al., 2002; Sawa et al., 2003; Patel et al., 2008). Ventral enclosure is initiated by the migration of two pairs of anterior leading cells towards the ventral midline, where they meet and adhere, followed by the migration and adhesion of eight pairs of pocket ventral cells (Williams-Masson et al., 1997; Chin-Sang and Chisholm, 2000; Simske and Hardin, 2001; Chisholm and Hardin, 2005). Ablating or disrupting F-actin within the leading cells inhibits ventral enclosure suggesting that ventral epidermal cells migrate as a 'unit' (Williams-Masson et al., 1997; Raich et al., 1999; Soto et al., 2002; Sawa et al., 2003; Withee et al., 2004; Sheffield et al., 2007; Patel et al., 2008). The internal actin cytoskeletons of neighboring cells are anchored together via adherens junctions, which contain cadherin/catenin complexes (Costa et al., 1998; Raich et al., 1999). Cadherin or catenin mutant embryos rupture, likely due to increased pressure on improperly adhered ventral cells, or hatch with abnormal body morphologies due to an uneven distribution of pulling forces across the epidermal cells (Costa et al., 1998; Raich et al., 1999; Chin-Sang and Chisholm, 2000; Simske and Hardin, 2001; Chisholm and Hardin, 2005).

While F-actin is required for ventral epidermal cell migration, it is not clear if non-muscle myosin is also involved. Some of the ventral pocket cells may close by a purse string-like mechanism analogous to wound healing, a process that requires myosin contractility (Williams-

Masson et al., 1997; Chin-Sang and Chisholm, 2000; Simske and Hardin, 2001; Benink and Bement, 2005; Clark et al., 2009). Myosin contractility also mediates cell shape changes, such as apical constrictions, in dorsal closure of the epidermis in *Drosophila* and gastrulation in *C. elegans* and *Drosophila* (Franke et al., 2005; Roh-Johnson et al., 2012). Furthermore, migrating cells often rely on forces generated by myosin contractility to help propel forward movements. In *C. elegans*, non-muscle myosin and its regulators are encoded by *mlc-4* (regulatory light chain), *nmy-2* (myosin heavy chain), *nmy-1*, *let-502* (Rho kinase) and *mel-11* (regulatory subunit of myosin phosphatase; Guo and Kemphues, 1996; Wissmann et al., 1997; Shelton et al., 1999; Piekny et al., 2003). They are required for multiple contractile events, such as cytokinesis and polarity in the early embryo, and for elongation in later-staged embryos (see below), but their role in ventral enclosure has not been studied.

Neuroblasts (neuron precursors) may act as a substrate for migration of the overlying ventral epidermal cells. Ephrin signaling helps sort specific subsets of neuroblasts into distinct regions of the embryo (e.g. VAB-1 (receptor) and VAB-2 (ligand)-expressing cells) and their positions may be required for proper ventral enclosure (George et al., 1998; Chin-Sang et al., 1999; Chin-Sang et al., 2002; Harrington et al., 2002; Ghenea et al., 2005). The receptors for various cues secreted by the neuroblasts are also expressed in the overlying ventral epidermal cells and could guide their migration (Bernadskaya et al., 2012; Ikegami et al., 2012). In addition, it is not known if the rapidly proliferating neuroblasts also provide mechanical forces. Therefore, the non-autonomous regulation of ventral epidermal cell migration is not fully understood, particularly if the position or shape of neuroblasts is essential for ventral enclosure.

After ventral enclosure, the adjacent lateral epidermal cells undergo actomyosin-mediated shape changes to cause a 4-fold increase in the length of the worm, by a process called elongation (Priess and Hirsh, 1986; Wissmann et al., 1997; Shelton et al., 1999; Piekny et al., 2003;

Chisholm and Hardin, 2005). It is not known if the highly contractile lateral epidermal cells also influence ventral enclosure. While *let-502* mutant embryos fail to elongate, likely due to low levels of actomyosin activity, *mel-11* mutant embryos rupture, likely due to hyper-contractility (Wissmann et al., 1997; Wissmann et al., 1999). Ruptures usually indicate ventral enclosure phenotypes and suggest that the tension exerted in the lateral epidermal cells impacts the integrity of ventral epidermal tissue. Moreover, embryos depleted of *rga-2*/Rho GAP, a negative regulator of RHO-1/RhoA, show body morphology phenotypes consistent with unregulated contraction (Diogon et al., 2007).

Another actomyosin event in the *C. elegans* embryo is cytokinesis, where the formation and ingression of an actin-myosin contractile ring physically separates a cell into two daughter cells at the end of mitosis (Piekny et al., 2005). The ingressing ring pinches in to deform the cortex and can be described as a cell shape change. Mutating or depleting genes that encode structural components of the ring or their regulators, such as *rho-1*, *mlc-4* or *let-502*, cause cytokinesis failure in the early embryo due to unsuccessful contractile ring assembly and ingression (Shelton et al., 1999; Piekny and Mains, 2002; Maddox et al., 2007). In other eukaryotes, active RhoA recruits anillin, a multi-domain protein that organizes actin-myosin contractility, to the contractile ring (Piekny and Maddox, 2010). Anillin has binding sites for active myosin and F-actin and may crosslink the actin-myosin cytoskeleton to the division plane (Piekny and Maddox, 2010). In human or *Drosophila* cells that are depleted of anillin, contractile rings still assemble but they become laterally unstable and cytokinesis fails (Straight et al., 2005; Hickson and O'Farrell, 2008; Piekny and Glotzer, 2008). *C. elegans* have three anillin genes: *ani-1*, *ani-2* and *ani-3*. ANI-1 shares the highest overall conservation with other metazoans and is required for organizing actin-myosin contractility and promoting asymmetric furrow ingression in the early embryo (Maddox et al., 2005; Maddox et al., 2007). *ani-1*-depleted embryos display

32

meiotic defects due to failed polar body extrusion and are sensitized to cytokinesis failure during the first cell division when other cytokinesis regulators are co-depleted or mutated (Maddox et al., 2007; Dorn et al., 2010). Interestingly, *ani-1*-depleted adult worms display body morphology phenotypes consistent with roles for *ani-1* in later stages of development (Maddox et al., 2005). We wanted to determine if *ani-1* functions during mid-late embryogenesis to regulate actomyosin-dependent events.

Here, we describe roles for *ani-1* and non-muscle myosin in ventral enclosure during epidermal morphogenesis. During mid-embryogenesis, AN1-1 is expressed in the neuroblasts and is required for their division. In *ani-1*-depleted embryos, ventral epidermal cells fail to meet and are often misaligned, suggesting that the position or shape of neuroblasts is important for ventral epidermal cell migration. We found that *rho-1* is also required for ventral enclosure, and the migration of ventral epidermal cells is severely delayed in *rho-1* mutants. In support of a requirement for non-muscle myosin contractility in ventral enclosure, embryos mutant for non-muscle myosin regulators display ventral epidermal cell migration defects. Interestingly, the ventral enclosure phenotypes caused by *ani-1* depletion are alleviated or strengthened by mutants that alter actomyosin contractility, supporting the importance of tissue-tissue interaction in regulating ventral enclosure.

2.3 Materials and methods

2.3.1 Strains and alleles

C. elegans strains (var. Bristol) were maintained according to standard protocol (Brenner, 1974). The following strains were obtained from the *Caenorhabditis* Genetics Center (CGC): N2 (wild type), *rho-1 (ok2418)/nT1 [qIs51], dpy-4 (e1166), mlc-4 (or253)/qC1, nmy-1 (sb115), mel-*

11 (it26) unc-4 (e120) sqt-1 (sc13)/mnC1, ajm-1 (ok160); jcEx44 [ajm-1:GFP + pRF4 (rol-6 (su1006)], unc-119 (ed3); tjIs1 [pie-1:GFP:rho-1 + unc-119 (+)], unc-119 (ed3); xnIs96 [pJN455 (hmr-1p:hmr-1:GFP:unc-54 3' UTR) + unc-119 (+)], ltIs44pAA173 [pie-1p-mCherry:PH(PLC1delta1) + unc-119(+)], wgIs102 [ham-1:TY1:EGFP:3xFLAG + unc-119(+)], JJ1136 unc-119 (e2498) III; zuEx24 [(unc-119(+) + hmp-1:gfp)], hmp-1 (zu278)/daf-11 (m84) sma-1 (e30), otIs33 [kal-1::GFP] and rde-1 (e219). The following strains were obtained from P. Mains (University of Calgary): rhgf-2 (sb100) and let-502 (sb118). GFP:ANI-1 was obtained from A. S. Maddox (University of North Carolina Chapel Hill) and *mcIs40 [lin-26p:ABD vab-10:mCherry + myo-2p:GFP] was obtained from M. Labouesse (IGBMC, Strasbourg, France).* The following strains were made for this study: *rho-1 (ok2418)/dpy-4 (e1166), rho-1 (ok2418)/+; jcEx44, let-502 (sb118); jcEx44, mel-11 (it26); jcEx44, nmy-1 (sb115); jcEx44 and ltIs44pAA173; wgIs102. C. elegans* strains were maintained on NGM (Brenner, 1974). All temperature sensitive strains were maintained at 15°C.

2.3.2 Genetic crosses

Broods were scored as described by Mains et al., (1990) to assess genetic interactions. A variation in the protocol consisted of using eight or more L4 hermaphrodites, where each worm was brooded on multiple plates with a minimum of 30 eggs per plate. An average of 800 progeny was recorded per experiment unless sterility was an issue. The temperature sensitive strains, *mel-11*, *let-502* and *rhgf-2* were maintained at 15°C and upshifted to 20°C or 25°C at the L4 stage. Phenotypes were assessed as indicated in the tables. The significance of genetic interactions was determined using the Chi-square test, based on predicted frequencies of genotypes and phenotypes for independently segregating alleles.

2.3.3 RNA interference

RNA-mediated interference (RNAi) was performed using feeding vectors obtained from the RNAi library described in Fraser et al. (2000) and Kamath et al. (2003) and clones specific for *rho-1* (Y51H4A.3) and *ani-1* (Y49E10.19) were used in this study (provided by M. Glotzer, University of Chicago). Eight L4 hermaphrodites were placed onto one RNAi plate, then after ~24 hours (to allow RNAi to become effective), individual worms were transferred to fresh RNAi plates and progeny from these second plates were assessed for phenotypes. The L4440 vector lacking an insert served as a negative control and *rho-1* RNAi was used as a positive control (i.e., 100% lethality and eventual sterility should be observed with efficient RNAi). Furthermore, all RNAi experiments were repeated multiple times and the results were recorded separately.

2.3.4 Immunostaining

N2 embryos were fixed and immunostained for ANI-1. Gravid hermaphrodites were freeze-cracked on polylysine slides, which were placed in -20°C methanol for 15 minutes. They were then washed three times for 10 minutes each with 0.1% TBST (150 mM NaCl, 50 mM Tris HCl pH 7.6 and 0.1% Tween-20). After washing, the slides were incubated with 1:1600 rabbit anti-ANI-1 antibodies (provided by A.S. Maddox, University of North Carolina Chapel Hill) and/or 1:250 mouse anti-Tubulin (DM1A; Sigma) antibodies and/or 1:200 mouse anti-GFP (Roche) antibodies and/or 1:20 mouse MH27 monoclonal antibodies (recognize AJM-1; Developmental Studies Hybridoma Bank) in 5% NDS in 0.1% TBST for two hours at room temperature. After washing three times with 0.1% TBST, slides were incubated with secondary antibodies (1:250 anti-rabbit donkey 488 or 568 antibodies and 1:250 anti-mouse donkey 568 or 488 antibodies; Invitrogen) for one and a half hours at room temperature. They were then washed three times with 0.1% TBST, again with 0.1M Tris HCl pH 8.8, then a drop of pre-warmed

mounting media (5% n-propyl gallate, 50% glycerol, 50 mM Tris pH 9) was added to each slide and coverslips were added and sealed.

2.3.5 Microscopy

Embryos were collected for imaging as described in Sulston et al. (1983). Approximately 10 gravid hermaphrodites were placed into a well of M9 solution in a depression slide and then dissected with a scalpel. Embryos were mouth pipetted onto a slide containing a freshly prepared agarose pad and were grouped together (<10 to avoid oxygen deprivation) using an eyelash. A coverslip was placed on the slide, then more M9 was added to prevent desiccation, and the coverslip was sealed with Vaseline. To assess phenotypes for epidermal morphogenesis by Nomarski (DIC), live embryos were observed by time-lapse every 10 minutes using the 40x or 63x objective on an upright Nikon Optiphot-2 microscope using the Nikon Digital DS-Fi1 camera or on the Leica DMI6000B inverted microscope with a Hamamatsu Orca R2 camera and Volocity acquisition software (PerkinElmer). Z-stacks of 5-10 planes of 0.5 - 1 μm thickness from the surface to medial planes of the embryo were collected using the Piezo Z/ASI stage (MadCityLabs) on the Leica microscope. Live imaging of AJM-1:GFP, HMP-1:GFP, HMR-1:GFP or GFP:RHO-1 embryos was similarly performed on the Leica microscope using the GFP filter (Semrock), but with shorter time intervals (2-5 minutes). Phototoxicity was prevented by closing the aperture to 30% to limit light intensity, and by keeping exposure times below 150 ms (compensated with increasing gain up to 150). AJM-1:GFP, mCherry:PH; HAM-1:GFP and GFP:ANI-1 embryos were imaged using the 60x objective on an inverted Nikon Eclipse Ti microscope outfitted with the Livescan Sweptfield scanner (Nikon), Piezo Z stage (Prior) and the Andor Ixon 897 camera, using Elements 4.0 acquisition software (Nikon). To visualize ventral enclosure and neuroblast division, 0.5 μm Z-stacks of AJM-1:GFP and mCherry:PH; HAM-

1:GFP expressing embryos were observed by time-lapse every 2-3 minutes. Images from fixed embryos were collected as Z-stacks of 0.2 - 0.5 μm through the entire embryo using the Leica DMI6000B inverted microscope and Hamamatsu Orca R2 camera and Volocity acquisition software (PerkinElmer) or using the Leica TCS SP2 confocal microscope with the 63x objective and Leica confocal software (v1.4).

Images were exported as TIFFs and opened with Image J (NIH), where selected planes (used to create maximum intensity Z-stack projections) and time points (for live imaging) were chosen, rotated, cropped and converted into 8-bit images. Some images were deconvolved using Autoquant 3.1. Velocity measurements were performed on the original images from HMR-1:GFP or AJM-1:GFP expressing embryos in Image J (NIH), by measuring the total distance travelled for selected pairs of ventral epidermal cells, and dividing this distance by the total time. For cells that stopped migrating, the velocity was measured for the distance travelled until the cell stopped moving. The velocities for each cell pair from multiple embryos were averaged and the standard deviation was calculated in Excel (Microsoft). All images where copied into Adobe Photoshop and Illustrator to make Figures or used to generate Quicktime (Apple) movies.

2.4 Results

2.4.1 *ani-1* is required during embryogenesis

In early embryos, *C. elegans* anillin (*ani-1*) coordinates actin-myosin contractility for polar body extrusion and asymmetric ingression of the contractile ring during cytokinesis (Maddox et al., 2007; Dorn et al., 2010). In metazoans, actin-myosin contractility mediates cell migration, adhesion and shape changes for the formation of tissues during development. However, *C. elegans ani-1* has not been studied in later stages of embryonic development, and

we determined if *ani-1* is required for actin-myosin events that mediate epidermal morphogenesis. Of the three *C. elegans* anillin isoforms, we chose to study *ani-1*, since *ani-2* is weakly expressed in the embryo and neither *ani-2*, nor *ani-3* have embryonic phenotypes (Maddox et al., 2005; Maddox et al., 2007). N2 hermaphrodites treated with *ani-1* RNAi gave 43% embryonic lethality and 13.4 % Vab (<u>V</u>ariable <u>ab</u>normal <u>b</u>ody morphology) phenotypes, similar to the Humpback phenotypes described for genes that regulate ventral enclosure (Costa et al., 1998). To better assess the embryonic phenotypes, *ani-1* RNAi embryos were imaged throughout development by DIC. A large percentage of embryos (22.2%) displayed 'early' phenotypes (amorphous ball of cells with no obvious structures), likely due to meiotic failures or defects in other early developmental events (Maddox et al., 2007; Dorn et al., 2010). Other embryos displayed defects later in development, including ventral enclosure and elongation (**Figure 11**). An allele of *ani-1, tm5110,* contains a small deletion removing part of the myosin-binding domain, but the remainder of the protein is still expressed (A.S. Maddox, personal communication). The deleted region was previously shown to be non-essential for human anillin function and as expected, homozygous *ani-1 (tm5110)* embryos showed no obvious embryonic phenotypes (**Figure 11**; Piekny and Glotzer, 2008). Furthermore, we also determined that co-depletion of *ani-2* and *ani-1* did not alter the range of the *ani-1* RNAi phenotypes (35% early, 18% early rupture, 10% late rupture and 10% elongation phenotypes; n = 49; $0.2 < p < 0.3$ by Chi-squared analysis). The range of *ani-1* RNAi phenotypes, from early – larval arrest with abnormal body morphology, supports that *ani-1* is required throughout embryogenesis, and may regulate epidermal morphogenesis.

To test for zygotic-specific requirements for *ani-1* and to bypass defects in the early embryo, *rde-1* (RNAi-resistant) hermaphrodites were treated with *ani-1* RNAi and crossed to N2
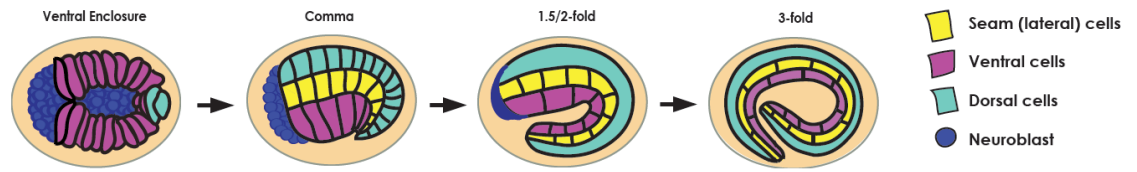
	Ventral Enclosure	Comma	1.5-fold	2-fold	>3-fold	Phenotype
N2						Wild-type 100%
ani-1 (tm5110)						Wild-type 100%
N2						Early Rupture 22.6%
N2						Late Rupture 9.7%
N2						Elongation 16.1%
rde-1 (ne219)						Wild-type 100%
rde-1 (ne219) X N2						Early Rupture 13%
rde-1 (ne219) X N2						Late Rupture 8% *
rde-1 (ne219) X N2						Elongation 16%
	+24 min	+48 min	+96 min	+>120 min		

Figure 11. *ani-1* is required during embryogenesis. On the right, a cartoon schematic shows embryos from the comma stage to the 2/3-fold stage of elongation. The dorsal epidermal cells are in light blue, the lateral (seam) epidermal cells are in yellow, the ventral epidermal cells are in pink and the neuroblast cells are shown in dark blue (see legend). DIC images from time-lapse movies of N2 and *rde-1 (ne219)* embryos treated with L4440 or *ani-1* RNAi (and outcrossed to N2 males, for *rde-1*), and *ani-1 (tm5110)* embryos are shown as indicated. The movies start from ventral enclosure and continue past the 3-fold stage of elongation (times are indicated underneath the images). The proportion of each phenotype is indicated to the right of each set of images (in %). Red arrows point to abnormal body morphologies (Vab). The scale bar is 10 μm. Time-lapse images depicted with an asterisk already appeared in the MSc thesis from Fotopoulos, 2013.

males. This assay permitted maternal ANI-1 to be expressed due to RNAi resistance in the mother, but made zygotically expressed ANI-1 susceptible to RNAi knockdown. A range of 4 to 9 Vab larva were observed on each of the mated plates, giving a total of approximately 17.6% Vab larva (the average brood size per plate was ~35 embryos and only first broods were considered, as the RNAi was titrated out in younger oocytes). The percentage of Vab larva is consistent with what we observed for *ani-1* RNAi, and may reflect zygotic requirements for *ani-1* in epidermal morphogenesis. To further characterize the zygotic *ani-1* RNAi phenotypes, embryos were imaged by DIC. As expected, these embryos displayed phenotypes that likely arose from ventral enclosure and elongation defects (**Figure 11**). The *ani-1* RNAi data shows that *ani-1* is required throughout embryogenesis, and is both maternally and zygotically required for epidermal morphogenesis.

2.4.2 ANI-1 regulates neuroblast cytokinesis during mid-embryogenesis

Our RNAi experiments revealed a potential role for *ani-1* in epidermal morphogenesis. We examined ANI-1's localization during mid-late embryogenesis to determine if its pattern of expression and subcellular localization matches its genetic requirements. GFP:ANI-1 (contains the *pie-1* promoter, which confers maternal expression), localizes to the contractile ring and cortex of dividing cells through the first half of embryogenesis (Maddox et al., 2007). Since this construct does not reflect the zygotic expression of ANI-1, embryos of various stages were fixed and stained with ANI-1 antibodies. Similar to the GFP probe, antibodies revealed ANI-1 localization to contractile rings and cell boundaries in the early embryo (data not shown). However, we noticed that ANI-1 continued to localize to the cortex and cleavage furrows of dividing cells through mid-embryogenesis (data not shown). Hence, to determine the cell types that ANI-1 is expressed in, confocal images were obtained from embryos expressing markers for

the epidermal cells (AJM-1:GFP or ABD (actin binding domain) VAB-10:mCherry) or underlying neuroblasts (neuronal precursors; HAM-1:GFP or KAL-1:GFP) and co-stained for ANI-1 (**Figure 12**; Bülow et al., 2002; Guenther and Garriga, 1996; Hudson et al., 2006; Sarov et al., 2006; Gally et al., 2009; Niu et al., 2011). These images revealed that ANI-1 is strongly expressed in the dividing neuroblasts under the ventral epidermal cells during ventral enclosure (based on Z planes of 0.5 μm thickness; **Figure 13**).

ANI-1's localization to the cleavage furrows of dividing neuroblasts suggests that *ani-1* could be required for their division. Previous studies showed that neuroblasts function as a substrate for the migration of ventral epidermal cells for ventral enclosure (George et al., 1998; Chin-Sang et al., 1999; Chin-Sang et al., 2002; Harrington et al., 2002; Ghenea et al., 2005; Ikegami et al., 2012). If *ani-1* regulates the division of neuroblasts, then it could non-autonomously influence ventral epidermal cell migration, which would explain the epidermal morphogenesis phenotypes in *ani-1* RNAi embryos (**Figure 14**). *ani-1* is not essential for cytokinesis in the early embryo, but anillin homologues are required for cytokinesis in *Drosophila* and human cells (Maddox et al., 2007; Hickson and O'Farrell, 2008; Piekny and Glotzer, 2008). To determine if *ani-1* is required for neuroblast cytokinesis, control or *ani-1* RNAi embryos co-expressing mCherry:PH (PLCdelta1) and HAM-1:GFP were imaged during ventral enclosure (**Figure 14**). The mCherry:PH probe localizes to membranes, while the HAM-1:GFP probe localizes to neuroblast nuclei. In *ani-1* RNAi embryos, the cleavage furrows of several neuroblasts ingressed, but later regressed and cells became multinucleate, unlike cells in control embryos where cytokinesis always completed (**Figure 14**). In addition, some neuroblasts appeared to have odd shapes in comparison to control cells (**Figure 14**). The strong expression of ANI-1 in neuroblasts coupled with its requirement for their division leads us to favor the hypothesis that the epidermal morphogenesis phenotypes in *ani-1*-depleted embryos arise non-
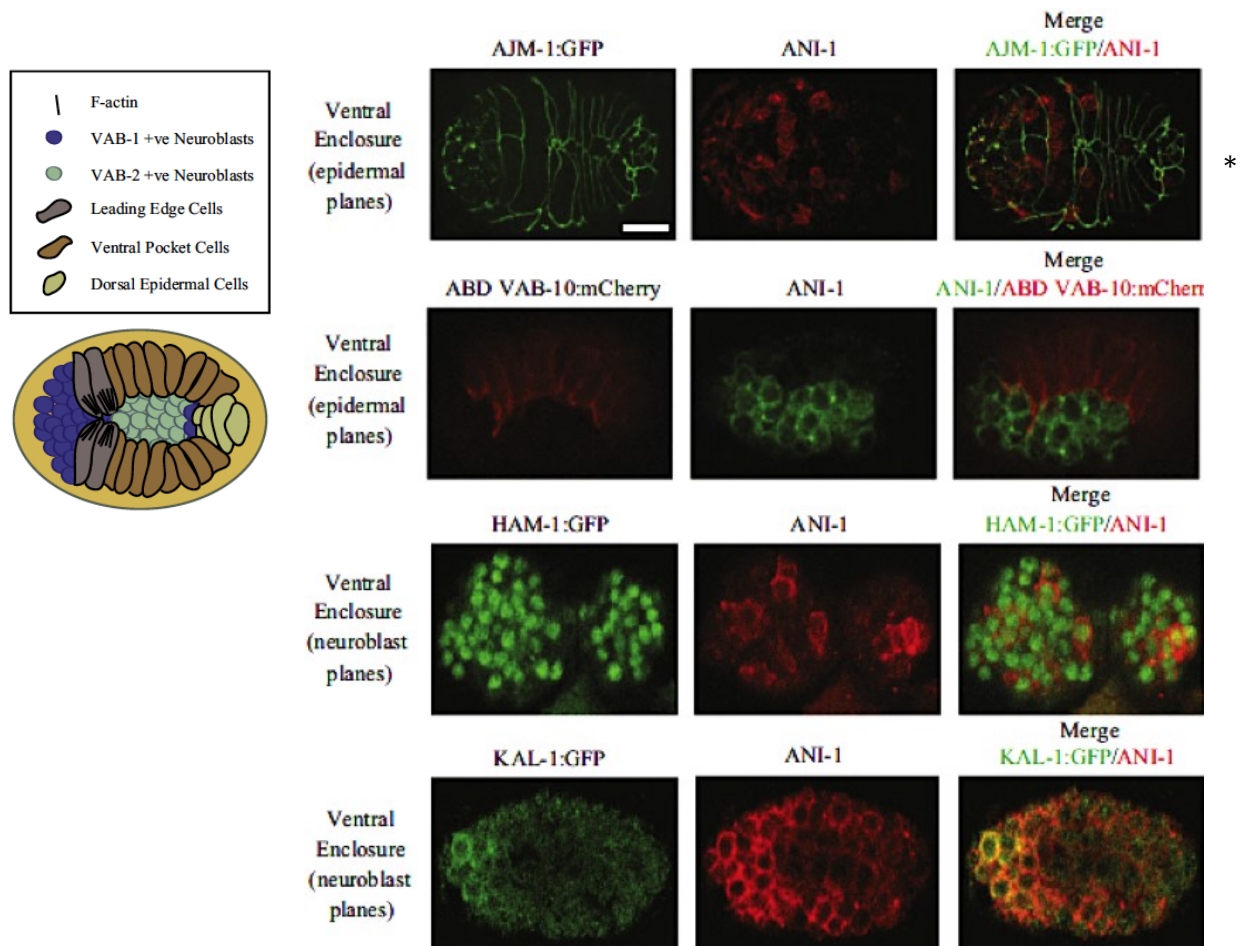
Figure 12. ANI-1 localizes to (ventral) neuroblasts. Confocal images taken near the epidermal planes of fixed embryos co-stained for GFP (green) and ANI-1 (red), or mCherry (red) and ANI-1 (green) as indicated. Shown are an AJM-1:GFP embryo, an ABD (actin binding domain) VAB-10:mCherry embryo, a HAM-1:GFP embryo, and a KAL-1:GFP embryo. A cartoon schematic on the left shows the position and shape of the ventral epidermal cells (light and dark brown) in comparison to the underlying neuroblasts (light and dark blue). The scale bar is 10 μm. The image that is depicted with an asterisk already appeared in the MSc thesis from Fotopoulos, 2013.
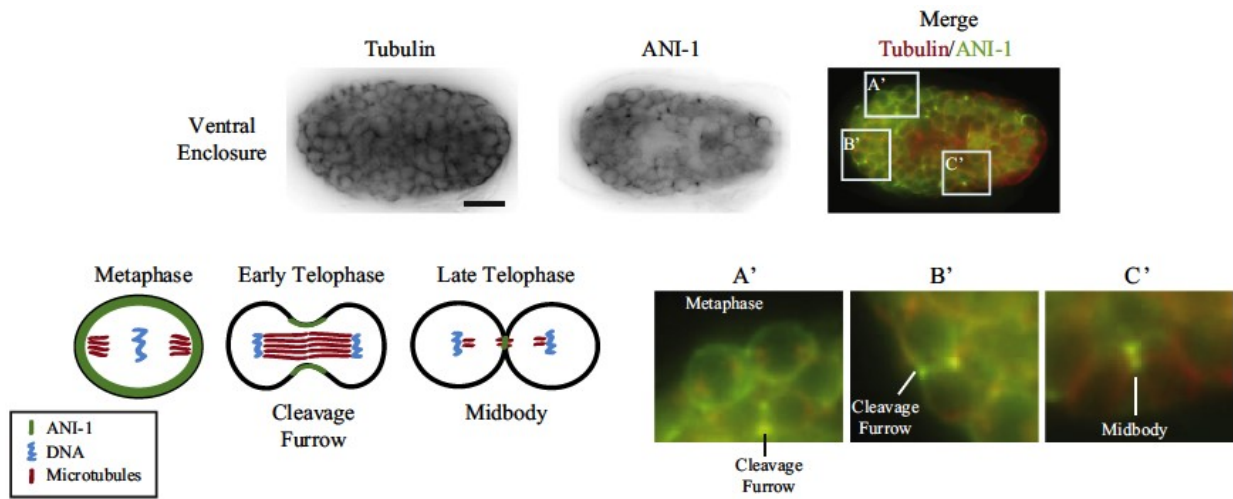
Figure 13. ANI-1 localizes to cleavage furrows of dividing neuroblasts. A fixed embryo just before ventral enclosure was co-stained for Tubulin (red) and ANI-1 (green) to show the cortical enrichment of ANI-1 in dividing cells. Dividing cells are outlined by boxes, and zoomed in regions are shown below (A', B' and C'). Also shown is a cartoon schematic of a dividing cell to show the enrichment of ANI-1 either around the cortex (metaphase), at the furrow (early telophase) or at the midbody (late telophase). The scale bar is 10 μm.
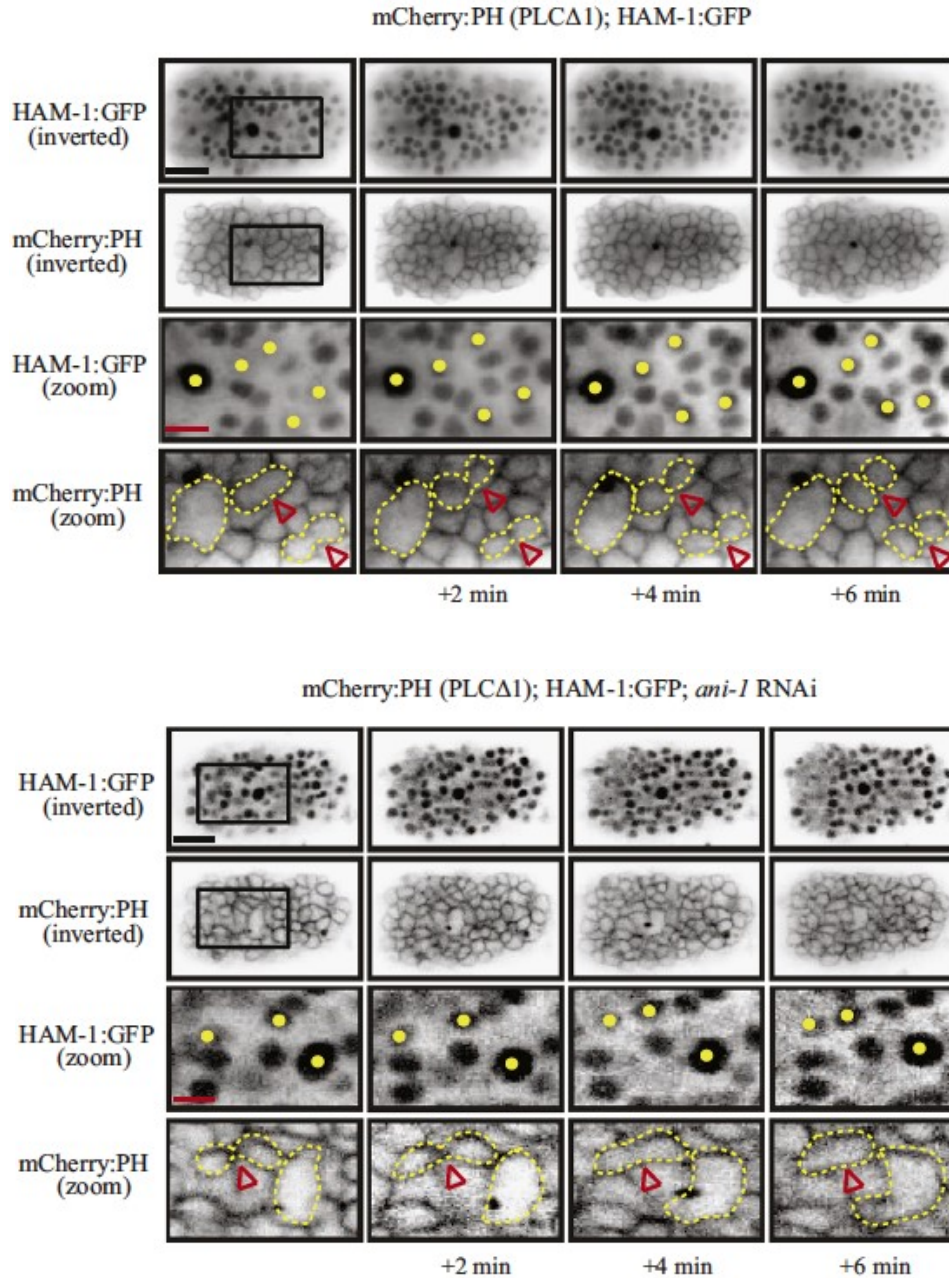
Figure 14. *ani-1* is required for neuroblast cytokinesis. Embryos co-expressing mCherry:PH to visualize membranes and HAM-1:GFP to visualize neuroblast nuclei were treated with *ani-1* RNAi and dividing neuroblasts were imaged every 2 minutes (times are indicated underneath). Unlike cells from control embryos (top panels), where cells successfully divided (yellow dots and dotted lines), cells often failed in the *ani-1* RNAi embryos (bottom panels; yellow dots and dotted lines). The lower sets of images are zoomed in from the outlined boxes above. The scale bars are 10 μm (black) and 3.5 μm (red).

45

autonomously from defects in the number, position or shape of the neuroblasts. However, we cannot rule out an autonomous requirement for *ani-1* in regulating ventral epidermal cell division or migration. Even though we did not detect any ANI-1 in epidermal cells, there could be very low amounts of protein in these cells that are beyond detection via immunofluorescence.

We determined if *ani-1* regulates the division of epidermal cells, since having too few epidermal cells could cause epidermal morphogenesis phenotypes (Hardin et al., 2008). We counted the number of epidermal cells in control and *ani-1*-depleted AJM-1:GFP or HMR-1:GFP embryos. An average of 16 +/- 2 dorsal (n = 21), 19 +/- 1 ventral (n = 17), and 20 +/-1 seam cells (n = 14) were counted for control embryos. *ani-1* RNAi embryos that displayed epidermal morphogenesis phenotypes had similar numbers of epidermal cells [19 +/- 1 dorsal (n = 20), 19 +/- 1 ventral (n = 17) and 20 +/- 1 seam cells (n = 10)]. Therefore, *ani-1* likely is not essential for epidermal cell division; however, this does not rule out an autonomous role for *ani-1* in epidermal cell migration or shape change.

2.4.3 *ani-1* is required for ventral enclosure

Our phenotypic data for *ani-1*-depleted embryos suggests that *ani-1* regulates epidermal morphogenesis. To characterize the morphogenetic phenotypes in *ani-1*-depleted embryos, we performed live imaging using embryos expressing AJM-1:GFP or HMR-1:GFP. Both AJM-1 and HMR-1 mark epidermal cell boundaries, allowing for visualization of the migration and adhesion of epidermal cells during epidermal morphogenesis. First, we verified that the dorsal epidermal surface formed normally in *ani-1* RNAi embryos, since this could also lead to problems later in epidermal morphogenesis (n = 19 *ani-1* RNAi vs. 10 control embryos). Next, we examined ventral enclosure and found that 33% of the *ani-1* RNAi embryos displayed ventral enclosure defects where the ventral cells did not properly migrate and adhere at the ventral midline (vs. 3%

46

of control embryos on L4440, n = 79; **Figure 15**). Based on their ventral enclosure phenotypes, embryos were considered 'early' if the anterior leading cells and/or posterior pocket cells failed to meet at the ventral midline causing internal contents to extrude (cells always migrated and were not truly 'early' in comparison to *gex-2/3* mutant cells that fail to migrate altogether; Soto et al., 2002; **Figure 15**). A ventral enclosure phenotype was considered 'late' when the ventral epidermal cells met at the ventral midline, but the internal contents of the embryo extruded during later stages of embryogenesis or became Vab larvae (**Figure 15**). There was an equal ratio of embryos in the early (53%) and late (47%) phenotypic categories, suggesting that *ani-1* is required for the efficacy of ventral epidermal cell migration to the ventral midline.

To clarify *ani-1*'s role in ventral epidermal cell migration, we measured the velocities of ventral epidermal cell pairs in *ani-1* RNAi embryos and compared them to control cells. The cell pairs are numbered 1 – 9, where 1 represents the first leading edge pair and 9 refers to the last ventral pocket pair (**Figure 16A**). Although contralateral ventral epidermal cell pairs failed to meet in some embryos, the velocity of cell migration was only mildly slower in comparison to control embryos, and was not slower in embryos with 'early' vs. 'late' ventral enclosure phenotypes (**Figure 16A**). However, contralateral cell pairs were often misaligned in *ani-1* RNAi embryos (61.1%; n = 18). To determine if there are delays prior to the onset of ventral epidermal cell migration in *ani-1*-depleted embryos, we also measured the developmental timing of embryos from the 8-cell stage to the onset and end of ventral enclosure (**Figure 16B**). There was a slight delay for *ani-1* RNAi embryos to reach the onset of ventral enclosure in comparison to control embryos (**Figure 16B**). Additionally, unlike control embryos, *ani-1* RNAi embryos remained at the onset of ventral enclosure for ~6 minutes before progressing through ventral enclosure (**Figure 16B**). The mild delay in ventral epidermal cell migration and their misalignment in *ani-1* RNAi embryos suggests that *ani-1* is not essential for ventral epidermal
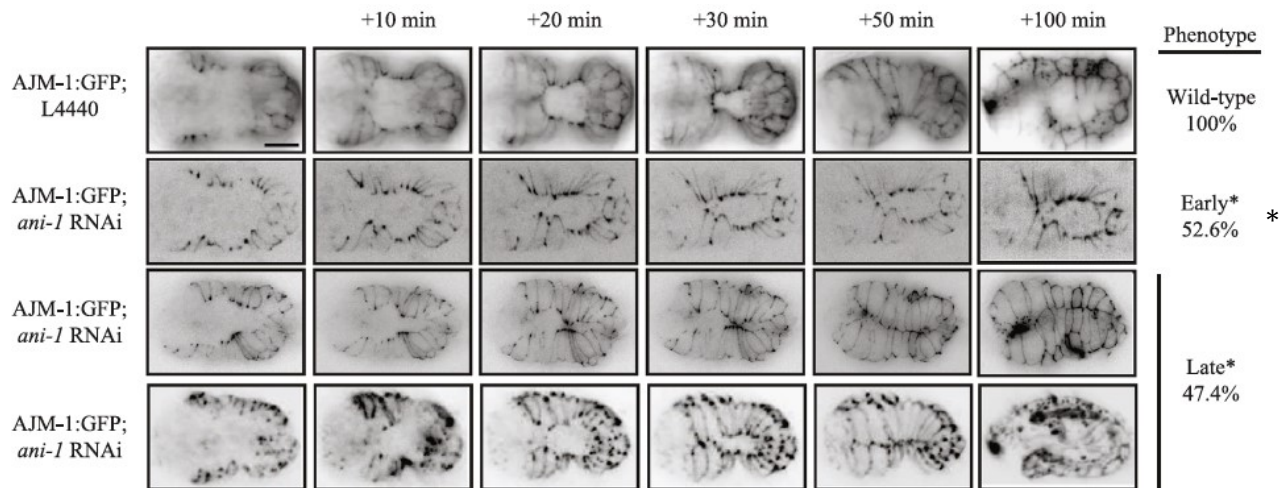
Figure 15. *ani-1* is required for ventral enclosure. Inverted projections of Z-stacks near the ventral surface show the ventral epidermal cells from AJM-1:GFP and AJM-1:GFP; *ani-1* RNAi embryos as indicated. The proportion of each phenotype is indicated to the right of each set of images (*early and *late are normalized to proportion of embryos with rupture phenotypes). The scale bar is 10 μm. The early *ani-1* RNAi embryo that is depicted with a second asterisk already appeared in the MSc thesis from Fotopoulos, 2013.

A

B

*p = 0.035; **p = 0.003
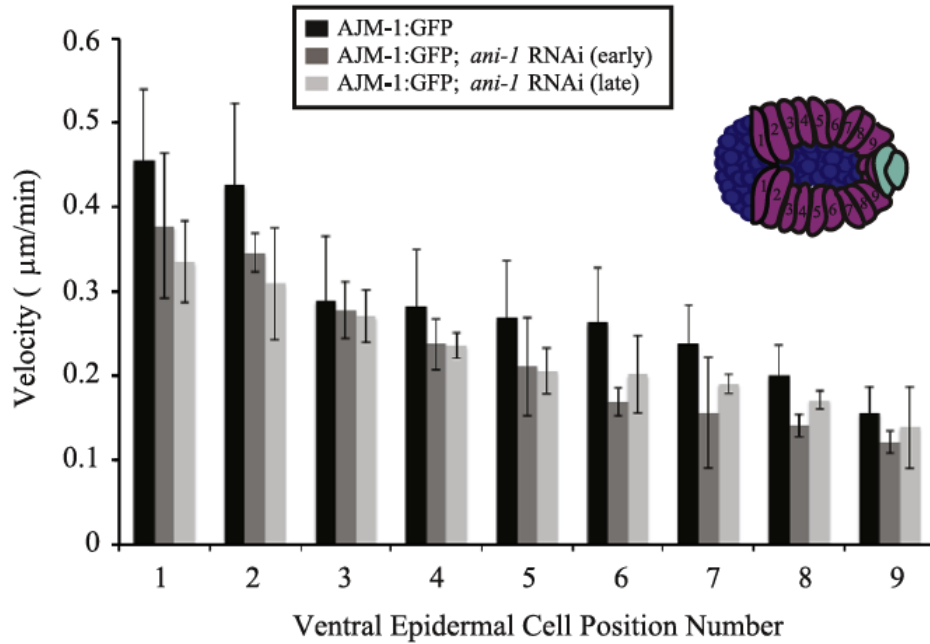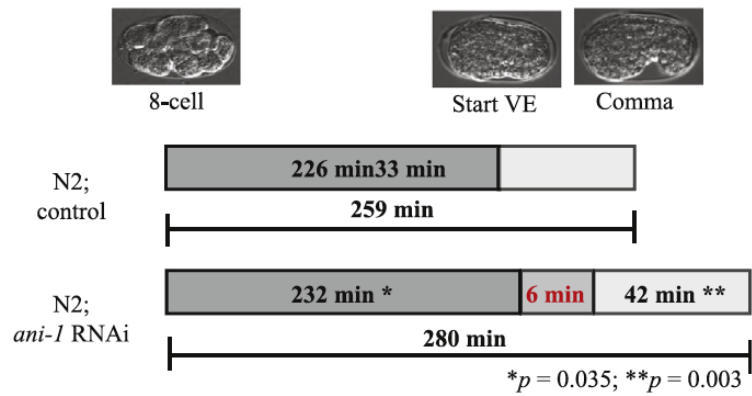
C
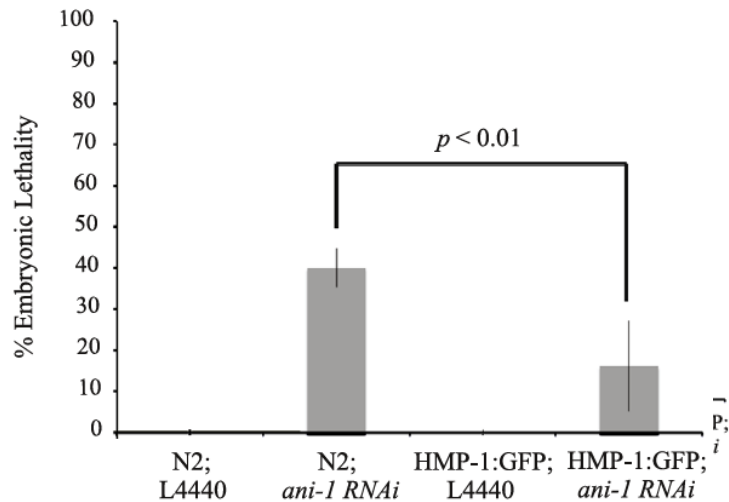
Figure 16. *ani-1* influences ventral epidermal cell migration. A) A graph shows the average velocity of each pair of ventral epidermal cells (from 1-9 as indicated in the cartoon above). The standard deviation for each set is also shown. The black bars show measurements from control cells, the dark grey bars show velocities of cells from *ani-1* RNAi embryos that have early ventral enclosure phenotypes and the light grey bars show velocities from *ani-1* RNAi embryos that have late ventral enclosure phenotypes (n = 3 -15 per cell pair). B) A timeline shows the average time (in minutes) for control (N2) embryos and *ani-1* RNAi embryos to develop from the 8-cell stage to the onset of ventral enclosure, and until the onset of elongation. Also shown is the probability for the difference in time for each segment, calculated by student t tests. C) A graph shows the suppression of *ani-1* RNAi embryonic lethality from the over-expression of □-catenin (HMP-1). The percent lethality is shown for N2 and HMP-1:GFP embryos treated with L4440, and for N2 and HMP-1:GFP embryos treated with *ani-1* RNAi. The lethality is significantly reduced in the HMP-1:GFP; *ani-1* RNAi embryos compared to N2; *ani-1* RNAi embryos (*p* <0.01; Chi-squared test).

cell migration per se, but rather modulates their migration to make them more efficient and to permit proper pairing of contralateral neighbors.

Adhesion junctions contain complexes of cadherin and catenin, and mutations in either of these components cause Vab phenotypes. Thus, we determined if *ani-1* genetically interacts with ☐☐catenin. Although embryonic lethality is enhanced in heterozygous *hmp-1* (α-catenin) mutant embryos treated with *ani-1* RNAi (*ani-1 RNAi* = 39.8% lethality; *hmp-1 (zu278)/daf-11 (m84) sma-1 (e30)* = 24.8% lethality, *hmp-1 (zu278)/daf-11 (m84) sma-1 (e30); ani-1 RNAi* = 82.9% lethality; $p < 0.001$ by Chi-squared analysis), embryos over-expressing HMP-1:GFP partially suppressed *ani-1* embryonic lethality (**Figure 16C**). While it is difficult to interpret data based on over-expression, the suppression of *ani-1* RNAi phenotypes by HMP-1:GFP may reflect the interplay between neuroblast and epidermal cells during ventral enclosure, or could point toward a more autonomous function for *ani-1* in ventral epidermal cells.

2.4.4 *rho-1* is required for ventral enclosure and elongation

ANI-1 regulates neuroblast cell division and is required for ventral enclosure. RHO-1 is required for cytokinesis in the early embryo and could be required for neuroblast cell division (Loria et al., 2012). However, as an upstream regulator of actomyosin contractility, RHO-1 also could directly mediate the migration of ventral epidermal cells. Furthermore, we expect RHO-1 to be involved in other morphogenetic events including elongation, which requires actomyosin contractility to drive lateral epidermal cell shape changes to form the long, thin worm shape. To study *rho-1*'s functions throughout embryogenesis, we performed loss of function experiments. However, we could not use *rho-1* RNAi due to *rho-1*'s requirement for cytokinesis in the early embryo. Recently, a deletion allele of *rho-1*, *ok2418*, was made by the *C. elegans* Gene Knockout Consortium and comprises a 2091 bp deletion, which deletes amino acids 53-192. The truncated

protein (1-52 amino acids) would not be able to function biochemically as it requires structure more C-terminal to this, and this allele is considered to be a null (Dvorsky and Ahmadian, 2004). Heterozygous *rho-1 (ok2418)/dpy-4* hermaphrodites segregated 76% wt or Dpy worms (used as a marker), 15.1% arrested embryos and 8.9% Lumpy Dumpy (Lpy Dpy) larva (data shown in MSc thesis Fotopoulos, 2013). We previously described similar Lpy Dpy phenotypes for *let-502* (Rho kinase) alleles. For example, partially elongated Lpy Dpy larva arrest at L1 for antimorphic *let-502* alleles that decrease maternal contribution and eliminate zygotic function (Piekny et al., 2000).

To better assess the *rho-1* phenotypes, mutant embryos were imaged by DIC. The majority of *rho-1 (ok2418)* embryos arrested at the 2-fold stage of embryonic development or hatched as elongation-defective L1 larva (80%). In addition, a small proportion of *rho-1* embryos displayed phenotypes before (15%) or during ventral enclosure (5%; n = 98; data shown in MSc thesis Fotopoulos, 2013). We also determined if zygotic-specific *rho-1* RNAi phenocopies the *ok2418* allele. Similar to the experiments described earlier for *ani-1*, we performed *rho-1* RNAi in *rde-1* hermaphrodites, then outcrossed these worms to wild-type males and visualized the phenotypes of the progeny. We found that 59% of the embryos displayed 2-fold arrest or hatched as Lpy Dpy larva, and 41% of the embryos arrested prior to, or during, ventral enclosure (n = 38; data shown in MSc thesis Fotopoulos, 2013). To further examine *rho-1*'s phenotypes, we imaged *rho-1 (ok2418);* AJM-1:GFP embryos. Similar to what was observed with DIC, the majority of these embryos (80%) failed to elongate past the 2-fold stage and seam cells did not fully lengthen (data shown in MSc thesis Chen, 2013). However, a fraction of embryos showed ventral enclosure phenotypes, where the ventral epidermal cells failed to migrate to the ventral midline and the ventral pocket cells remained more laterally positioned, causing the embryo to arrest with a Gex phenotype (14%; n = 7; **Figure 17A**). Unlike *ani-1* RNAi embryos, the migration of

52
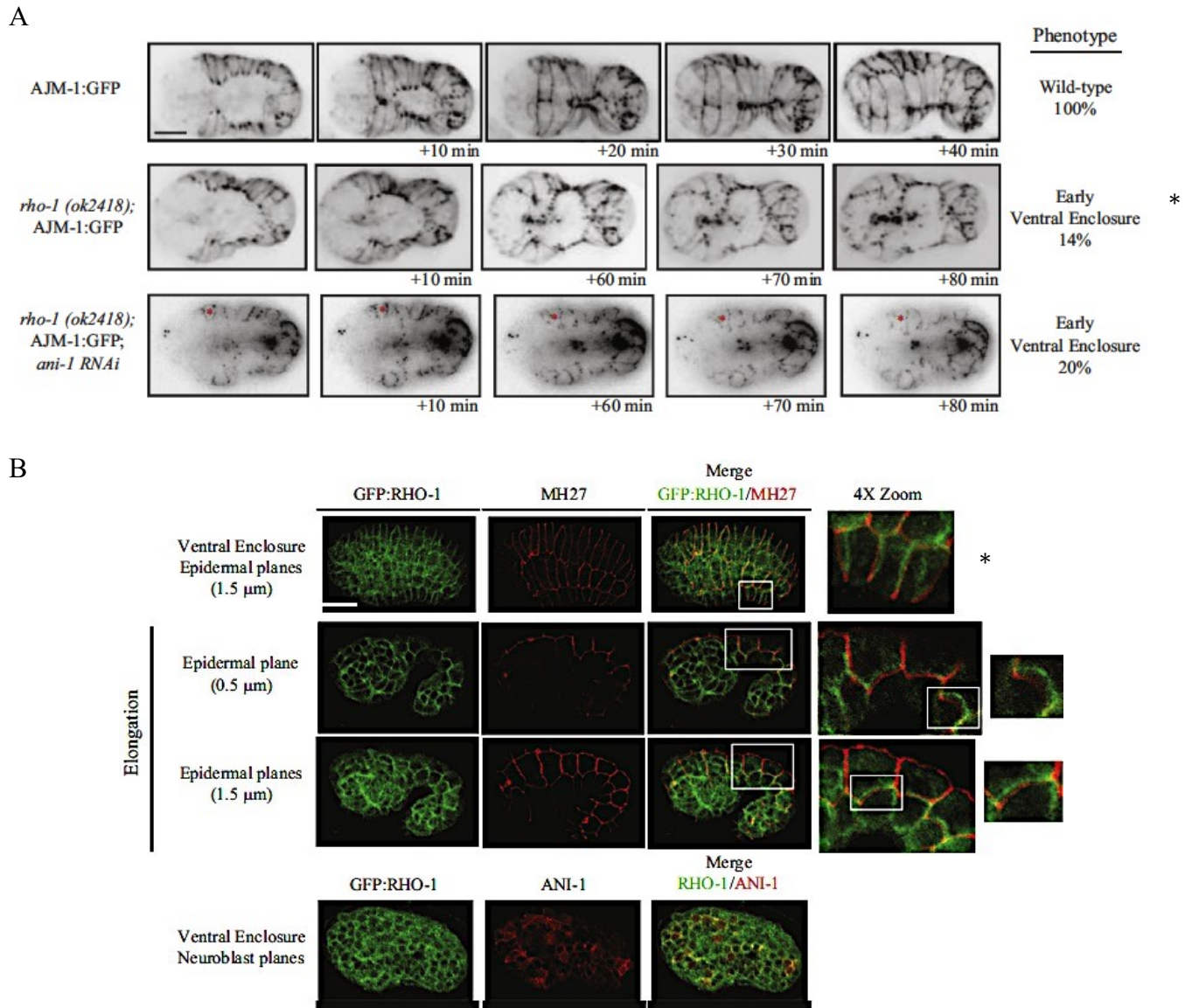
Figure 17. *rho-1* is required for ventral enclosure and localizes to epidermal cell boundaries. A) Time-lapse images of AJM-1:GFP-expressing control, *rho-1 (ok2418)* and *rho-1 (ok2418); ani-1* RNAi embryos during ventral enclosure. The number of embryos that display each phenotype is shown to the right of each set of images (in %). B) Confocal images of fixed GFP:RHO-1 embryos co-stained for GFP (green) and MH27 (AJM-1; red) show RHO-1 localization at the boundaries of epidermal cells during ventral enclosure (top panel) or elongation (middle panels). The z-plane thickness of each image is shown to the left. Boxes outline areas that were zoomed in to better visualize the co-staining of RHO-1 at the epidermal cell boundary. Also shown is a confocal image of a GFP:RHO-1-expressing embryo fixed and co-stained for GFP (green) and ANI-1 (red). The scale bar is 10 μm. Images depicted with an asterisk already appeared in the MSc thesis from Chen, 2014.

ventral epidermal cells appeared severely delayed, suggesting that *rho-1* is required for their migration. Therefore, *rho-1* has multiple functions during epidermal morphogenesis; to mediate the migration of ventral epidermal cells during ventral enclosure, and to regulate lateral epidermal cell shape changes for elongation.

Next, we examined the localization of RHO-1 during mid-embryogenesis. The genetic requirement for *rho-1* in ventral enclosure suggests that it should be enriched in the ventral epidermal cells or in the neuroblasts. Furthermore, as a potential regulator of elongation, RHO-1 should be expressed in the lateral epidermal cells. In live embryos, GFP:RHO-1, driven by the maternal *pie-1* promoter, localized to the boundaries of all epidermal cells during ventral enclosure and early stages of elongation (data shown in MSc thesis Fotopoulos, 2013). RHO-1 was also enriched at the boundaries of dorsal cells undergoing intercalation (data shown in MSc thesis Fotopoulos, 2013). In fixed embryos co-stained for AJM-1 (via MH27 antibodies), confocal images revealed that RHO-1's localization at epidermal cell boundaries is more basolateral in comparison to AJM-1, which localizes sub-apical to the cadherin/catenin complex at adherens junctions (**Figure 17B**). Co-staining fixed embryos for ANI-1 also showed that RHO-1 is expressed in the majority of neuroblasts, unlike ANI-1, which appears to be restricted to a subset of cells (**Figure 17B**).

RHO-1's localization to lateral epidermal cell boundaries matches its requirement for elongation, and the ability of maternal RHO-1 to persist through early elongation suggests that there could be overlapping redundancies with zygotic RHO-1. Genetic crosses were performed using strains carrying *rho-1 (ok2418)* with worms carrying mutations in components of the elongation pathway, including *mlc-4* (non-muscle myosin light chain), *let-502* (Rho kinase), *mel-11* (myosin phosphatase) and *rhgf-2* (a GEF for RHO-1; P.E. Mains, personal communication; Lin et al., 2012). Although the severity of elongation phenotypes changed depending on the

nature of the allele being tested (maternal vs. zygotic), the genetic interactions between *rho-1* and the elongation pathway components showed that *rho-1* likely functions as an upstream component of this pathway (data shown in MSc thesis Fotopoulos, 2013).

The expression of RHO-1 in both the neuroblasts and epidermal cells makes it difficult to assign tissue-specific requirements for *rho-1* in ventral enclosure. Furthermore, it is not known where zygotic RHO-1 is expressed, which could be upregulated in specific subsets of epidermal cells and neuroblasts. The ventral enclosure phenotype for *rho-1* mutants was quite different than what was observed for *ani-1*-depleted embryos, and we favor the hypothesis that *rho-1* might be required in the ventral epidermal cells for at least part of their migration.

2.4.5 *ani-1* RNAi ventral enclosure phenotypes are enhanced or suppressed by altering myosin contractility

The ventral enclosure phenotype in *rho-1* mutant embryos supports a role for non-muscle myosin in mediating the migration of ventral epidermal cells. However, actomyosin contractility also controls constriction of the lateral epidermal cells and it is not clear how these neighboring cells may affect ventral enclosure. For example, it was proposed that *mel-11* mutant embryos rupture due to an increase in myosin contractility in the lateral epidermal cells, which places too much pressure on the embryo (**Figure 18A**; Wissmann et al., 1999). Supporting either of these potential roles for myosin, immunostaining revealed that NMY-1 is localized to epidermal cell boundaries, and is enriched in the lateral seam cells (**Figure 18B**). To further study the requirement for myosin activity in ventral enclosure, we determined the proportion of epidermal morphogenesis phenotypes in AJM-1:GFP-expressing embryos mutant for *let-502*/Rho kinase or *mel-11*/myosin phosphatase at 25°C (**Figure 19A**). Embryos were placed into one of several categories based on their phenotypes, which includes 'early' rupture due to failure of the ventral
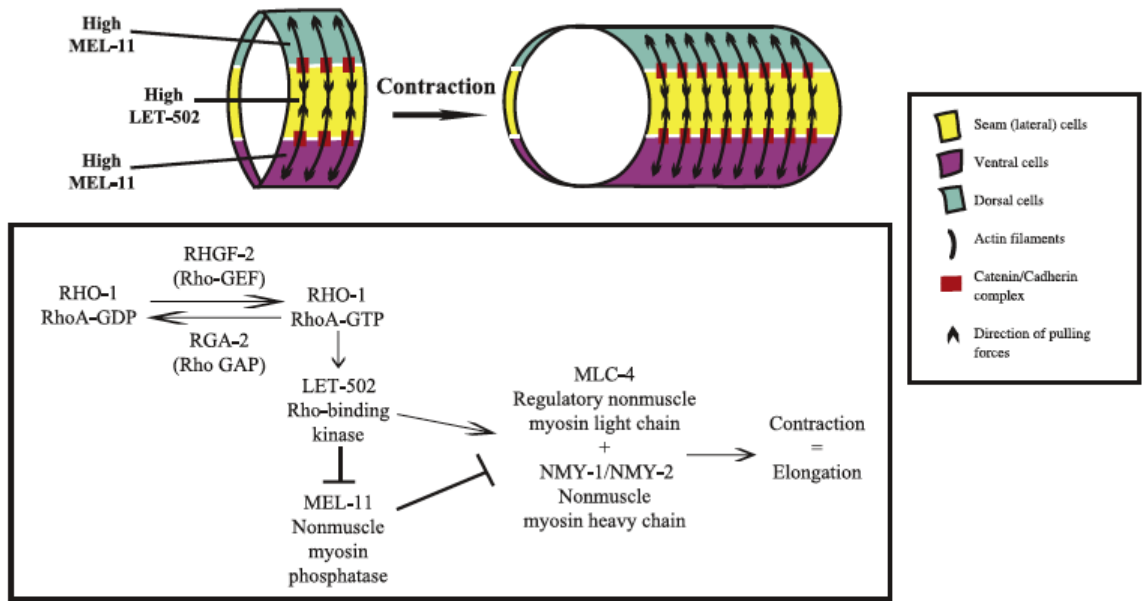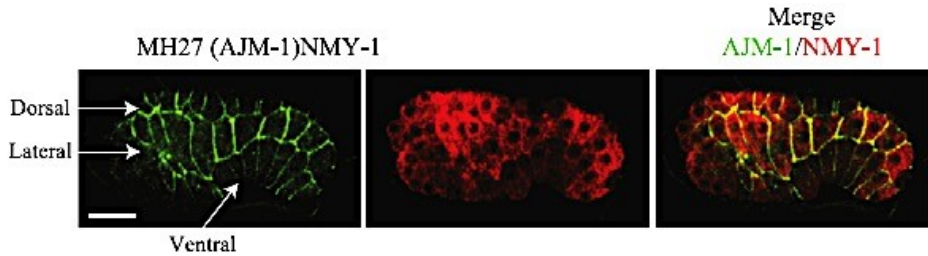
Figure 18. The Rho pathway regulates myosin contractility. A) A cartoon schematic shows the expression levels of LET-502 and MEL-11 in the dorsal, seam and ventral cells and how the forces generated on actin filaments in the seam cells likely drive cell shape change and elongation. These filaments are connected to neighboring epidermal cells by adhesion junction complexes, including the cadherin/catenin complex. Part of the actomyosin contractile pathway is also shown. B) A confocal image of a fixed, wild-type (N2) embryo at the comma stage co-stained for MH27 (for AJM-1; green) and NMY-1 (red). White arrows point to the different epidermal cell types as indicated. The scale bar is 10 μm.

A
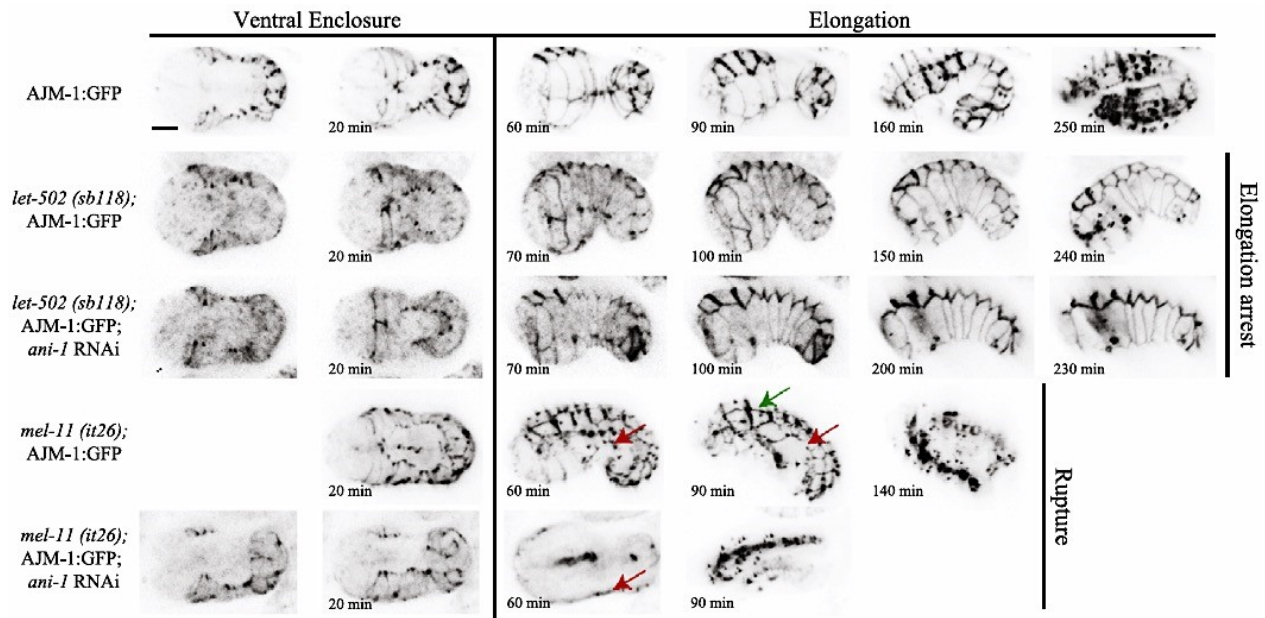
B
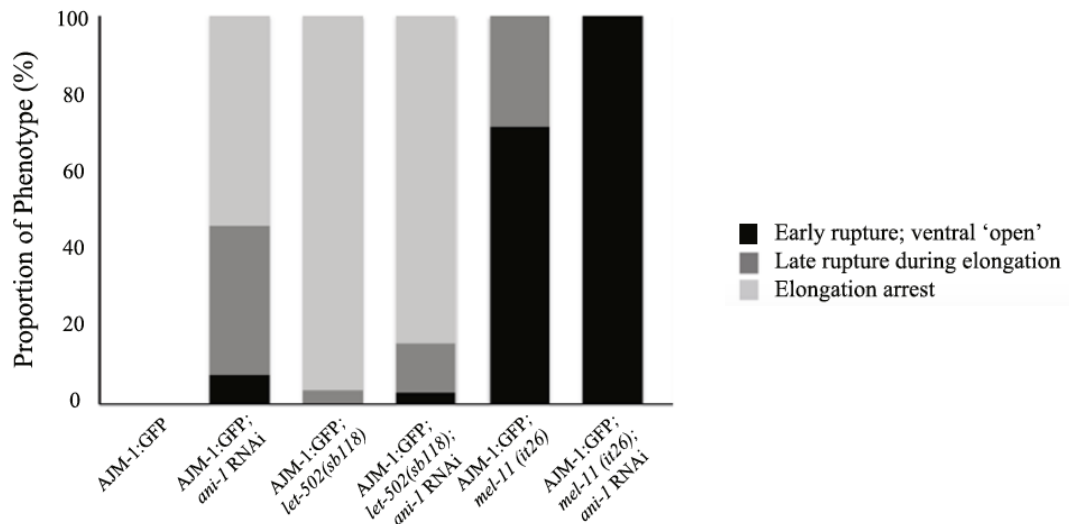
Figure 19. Actomyosin contractility influences ventral enclosure. A) Images from time-lapse movies of AJM-1:GFP-expressing embryos mutant for *let-502* or *mel-11,* and with co-depletion of *ani-1,* are shown from ventral enclosure and through part of elongation (time points are shown underneath the images). The red arrows point to ventral epidermal cells that failed to meet and remain open in elongation. The green arrow points to prematurely constricted lateral epidermal cells. The scale bar is 10 μm. B) A graph shows the relative proportion of each phenotype (in %). As indicated, early rupture is shown by the black bars, late rupture by the dark gray bars and elongation arrest by the light gray bars.

57

epidermal cells to meet at the ventral midline, 'late' rupture if the ventral epidermal cells met, but the embryos ruptured during elongation, and elongation phenotypes (**Figure 19A**). As expected, control AJM-1:GFP embryos did not show any phenotypes (n = 13). Interestingly, both *let-502 (sb118)*; AJM-1:GFP (n = 28) and *mel-11 (it26)*; AJM-1:GFP (n = 14) embryos showed ventral enclosure phenotypes. In particular, *let-502 (sb118)* embryos had a slight, but significant delay in the migration of ventral epidermal cells (54 +/- 7 vs. 42 +/- 3 minutes for control embryos; $p = 0.0065$), as well as 3% late rupture, and 97% elongation-defective phenotypes. Interestingly, ventral epidermal cells failed to meet altogether in 71% of *mel-11 (it26)* embryos, which ruptured at the onset of elongation (see red arrows in **Figure 19A**). As shown in Figure 19A (green arrow), when comparing similar time points in elongation, the shape of the lateral epidermal cells appeared more constricted in *mel-11* mutant embryos in comparison to control embryos. The failed ventral enclosure phenotype in *mel-11* mutant embryos with prematurely constricted lateral epidermal cells, suggests that the constriction of lateral epidermal cells influences the efficacy of ventral enclosure.

Next, we used *ani-1* RNAi to perturb ventral enclosure and determined the effect of altering non-muscle myosin contractility on *ani-1*'s ventral enclosure phenotypes. Not surprisingly, embryos mutant for *let-502* or *mel-11* and treated with *ani-1* RNAi showed strengthened or enhanced lethality, where the observed lethality exceeded predicted additive lethality rates, as determined by Chi-squared analysis ($p < 0.05$) (*rho-1, nmy-1, mlc-4, rhgf-2* and *let-502; mel-11* were also tested; data shown in MSc thesis Fotopoulos, 2013). For example, *rho-1 (ok2418)/dpy-4*; *ani-1* RNAi displayed hatching rates of 13.9% vs. 73.4% for *rho-1 (ok2418)/dpy-4;* L4440 and 53.2% for *ani-1* RNAi, and the expected additive hatching rates were 26.6% (data shown in MSc thesis Fotopoulos, 2013). Next, we assessed the phenotypes of AJM-1:GFP-expressing embryos mutant for *let-502* or *mel-11*, and treated with *ani-1* RNAi. AJM-

1:GFP; *ani-1* RNAi embryos showed a range of phenotypes including delayed ventral enclosure, early rupture (14%), late rupture (43%) and Vab (43%; n = 7). This experiment was filmed at 25°C vs. earlier experiments, which were filmed at 20°C and the change in temperature could explain the increase in *ani-1*'s late rupture phenotypes in comparison to early rupture (**Figure 15**). AJM-1:GFP-expressing *let-502; ani-1* RNAi mutant embryos showed a decrease in rupture phenotypes compared to AJM-1:GFP; *ani-1* RNAi embryos (**Figure 19B**). For example, *let-502;* AJM-1:GFP; *ani-1* RNAi embryos displayed a total of 16% rupture phenotypes (n = 32) vs. 46% for AJM-1:GFP; *ani-1* RNAi ($p < 0.001$ by Chi-squared analysis; **Figure 19B**). The remaining embryos showed strong elongation defects (**Figure 19B**). Conversely, *mel-11;* AJM-1:GFP; *ani-1* RNAi embryos showed an increase in the proportion of early rupture phenotypes (100%; n= 9) in comparison to *ani-1* RNAi (8%) or *mel-11 (it26)* (71%) on its own ($p < 0.05$ by Chi-squared analysis; **Figure 19B**). The ability of non-muscle myosin mutants to alleviate or strengthen *ani-1*'s ventral enclosure phenotypes could arise due to a direct requirement for non-muscle myosin contractility within the ventral epidermal cells for their migration. Alternatively, the lack of lateral epidermal cell constriction in the *let-502* mutant embryos, or their premature constriction in *mel-11* mutant embryos could cause a change in pressure exerted by the lateral epidermal cells, which could affect ventral enclosure.

To shed light on how the myosin pathway might influence the *ani-1* ventral enclosure phenotypes, we assayed the phenotypes of *rho-1 (ok2418); ani-1* RNAi embryos. Since the migration of ventral epidermal cells is severely delayed in *rho-1* mutant embryos, we wanted to determine if this delay rescues the misalignment of ventral epidermal cells in *ani-1* RNAi embryos. Rupture was not suppressed in *rho-1 (ok2418); ani-1* RNAi embryos (imaged by DIC; the double mutant embryos displayed 42% early, 21% early rupture, 11% late rupture and 26% elongation phenotypes; n = 19; $0.1 < p < 0.2$ by Chi-squared analysis). Since *rho-1* mutant

59

embryos show a strong delay or failure in ventral epidermal cell migration, this could impede their ability to be suppressed by weak contractility in the lateral epidermal cells. Next, we imaged *rho-1 (ok2418); ani-1* RNAi embryos expressing AJM-1:GFP. The double mutant embryos displayed ventral enclosure phenotypes consistent with both *rho-1 (ok2418)* and *ani-1* RNAi; ventral epidermal cell migration was severely delayed, and contralateral cells were misaligned (20% and n = 10; **Figure 17A**). The phenotype of the double mutant supports the hypothesis that *rho-1* and *ani-1* may differentially affect the migration of ventral epidermal cells.

2.5 Discussion

The *C. elegans* embryo is covered in epidermal tissue by a process called ventral enclosure, where ventral epidermal cells migrate to enclose the ventral surface of the embryo. The embryo is then lengthened into the long, thin worm shape by actomyosin constrictions that occur within the lateral epidermal cells. Both ventral enclosure and elongation require epidermal cells to undergo extensive shape changes, migration and adhesion. We show that *ani-1* (*C. elegans* anillin), which coordinates actomyosin contractility in the early embryo, regulates neuroblast cytokinesis during mid-late embryogenesis and is required for ventral enclosure. In addition, we describe a role for *rho-1* (*C. elegans* RhoA) in regulating both ventral enclosure and elongation. Furthermore we show that actomyosin contractility must be carefully controlled to permit ventral enclosure to occur properly. Interestingly, at least some of this requirement for myosin may come from the neighboring lateral epidermal cells, which constrict during elongation and may generate tension that affects the efficacy of ventral enclosure. These studies shed light on how multiple tissues may work together to regulate tissue formation in vivo.

2.5.1 *ani-1* is required for neuroblast cell division

Anillin is a scaffold for actin and myosin, and helps organize actin-myosin contractility during cytokinesis and meiotic polar body extrusion (Maddox et al., 2005; Maddox et al., 2007; Dorn et al., 2010). We found that *ani-1* is required for neuroblast cytokinesis and possibly for maintaining their shape (**Figures 12-14**). Neuroblasts may function as a substrate for the migration of ventral epidermal cells, by secreting guidance cues and/or by providing a mechanical surface, and changes in their position, number or shape could make them a less effective substrate (George et al., 1998; Chin-Sang et al., 1999; Chin-Sang et al., 2002; Harrington et al., 2002; Ghenea et al., 2005). For example, cell proliferation can alter the overall mechanical properties of a tissue (Zhang et al., 2012). Furthermore, at least two sets of neuroblasts sort from each other (VAB-1 and VAB-2-expressing cells) and their position is essential for ventral enclosure to occur properly (George et al., 1998; Chin-Sang et al., 1999; Chin-Sang et al., 2002; Ghenea et al., 2005). It would be interesting to determine which subset of neuroblasts ANI-1 is enriched in, and how this affects migration of the overlying ventral epidermal cells.

It is interesting that *ani-1* is required for neuroblast cytokinesis when it is not essential for cytokinesis in the early embryo. Anillin homologues are essential for cytokinesis in other organisms and cell types including *Drosophila* spermatocytes, S2 cells and cultured mammalian cells (Straight et al., 2005; Hickson and O'Farrell, 2008; Piekny and Glotzer, 2008; Goldbach et al., 2010). Neuroblasts are much smaller in comparison to the first cell in the early embryo, and the pathways and their relative contributions to cytokinesis may differ depending on cell size or other structural features of the cell (Tse et al., 2011).

2.5.2 *ani-1* is required for ventral enclosure

Even though *ani-1* is required for neuroblast cell division, its embryonic phenotypes are consistent with a requirement for *ani-1* in epidermal morphogenesis. In particular, *ani-1* RNAi embryos displayed ventral enclosure defects where the ventral epidermal cells migrated, but failed to reach the midline and/or were misaligned (**Figures 11 and 15**). These embryos ruptured or developed into Vab larvae, possibly because their adherens junctions were not formed as strongly as in control embryos. Based on the strong expression of ANI-1 in the neuroblasts, we favor a model where *ani-1* functions non-autonomously to mediate the migration of ventral epidermal cells (**Figure 12**). However, our data does not rule out an autonomous role for *ani-1* within the ventral epidermal cells. Since ventral epidermal cells migrated at rates only mildly slower in *ani-1* RNAi vs. control embryos, we hypothesize that *ani-1* is not required for migration and the pathways that regulate the formation of branched F-actin filaments, such as Rac (*ced-10*), Arp2/3 (*arx-2/3*), WAVE/SCAR regulators (*gex-2* and *gex-3*) and WASP (*wsp-1*), remain functional (Williams-Masson et al., 1997; Soto et al., 2002; Patel et al., 2008; **Figure 16A**). Interestingly, *ani-1*'s embryonic lethality was suppressed by the over-expression of □-catenin (**Figure 16C**). This protein is a component of adherens junctions that binds to intracellular F-actin and helps crosslink the apical cortex with neighboring cells (Costa et al., 1998; Raich et al., 1999; Chisholm and Hardin, 2005; Maiden et al., 2013). Although preliminary, one way to interpret the suppression data is that over-expressing □-catenin strengthens F-actin at junctions or crosslinks more intracellular F-actin, overcoming the misalignments caused by *ani-1* depletion. Alternatively, both □-catenin and ANI-1 could regulate similar pools of intracellular F-actin, and the over-expression of one could partially compensate for loss of the other.

2.5.3 *rho-1* and roles for actomyosin contractility in ventral enclosure

The role of actomyosin contractility and mechanical input from neighboring tissues is emerging as a theme in tissue morphogenesis in metazoans (Zhang et al., 2010; Zhang et al., 2011; Pohl et al., 2012; Roh-Johnson et al., 2012; Zhang and Labouesse, 2012). For example, oscillating actomyosin contractility coupled with ratchet mechanisms is essential for establishing and maintaining cell shape changes, particularly apical constrictions during gastrulation (Roh-Johnson et al., 2012). Within the context of a tissue, these shape changes and movements also are aided by the formation of supracellular structures in neighboring cells, and mechanical inputs from neighboring tissues (Pohl et al., 2012; Zhang et al., 2010; Zhang and Labouesse, 2012). The actomyosin purse string that forms around the ventral pocket cells could be considered a supracellular structure, which may coordinate apical constrictions within a subset of cells to close the ventral pocket. This supracellular structure likely is *rho-1*-dependent, and the 'ventral open' phenotype of *rho-1* mutant or RNAi embryos supports a requirement for actomyosin in ventral enclosure (**Figure 17A**). Interestingly, we saw similar 'ventral open' phenotypes in *ect-2* mutant embryos, suggesting that RHO-1 is active to mediate ventral enclosure (Chen and Piekny, unpublished observations). However, it is not clear if the RHO-1 pathway mediates purse string closure of the ventral epidermal cells, or if it regulates ventral epidermal cell migration. For example, we observed a strong delay in ventral epidermal cell migration in *rho-1* mutant embryos, and a mild delay in *let-502* (Rho-binding kinase) mutant embryos. Thus, an alternative model is that *rho-1* mediates ventral epidermal cell migration by regulating substrate adhesion and generating forward propulsion movements, similar to other eukaryotic cells.

We found that *rho-1* also regulates the constriction of lateral epidermal cells (data shown in MSc thesis Fotopoulos, 2013). As shown in Figure 19, we observed alleviation or strengthening of ventral enclosure phenotypes using mutants that alter actomyosin contractility

(e.g. *let-502* and *mel-11*; Wissmann et al., 1997; Wissmann et al., 1999; Piekny et al., 2000; Piekny et al., 2003; Diogon et al., 2007; Gally et al., 2009). Although actomyosin contractility may be required within the ventral epidermal cells, this does not explain why the rupture phenotypes in *ani-1* RNAi embryos are suppressed in *let-502* mutant embryos. Furthermore, *rho-1; ani-1* mutant embryos had both delays in ventral epidermal cell migration and misalignment of contralateral neighbors (**Figure 17A**). Therefore, we favor the hypothesis that mechanical inputs from the lateral epidermal cells may be important for ventral enclosure (Zhang et al., 2012). The majority of *mel-11* mutant embryos had ventral open phenotypes similar to *rho-1*, where ventral epidermal cells failed to meet at the ventral midline (**Figure 19**). However, unlike *rho-1* mutant embryos, the lateral epidermal cells of *mel-11* mutant embryos constricted prematurely in comparison to control embryos, indicating that the constriction of lateral epidermal cells must be carefully regulated to permit closure of the ventral epidermal cells. Although we did not test for tension in this experiment, we hypothesize that hyperconstriction of the lateral epidermal cells in the *mel-11* mutant embryos generates high tension with the neighboring ventral epidermal cells, and prevents them from closing properly. If lateral epidermal cell constriction and tension is low, as in the *let-502* mutant embryos, this may have the opposite effect and suppress rupture in embryos that have mild ventral enclosure defects.

Chapter 3. Myosin contractility regulates
neuroblast and epidermal morphogenesis

3.1 Abstract

Tissue morphogenesis is highly complex, since it involves multiple cell types and the coordination of mechanical forces between cells. As a simple metazoan, *C. elegans* is a good model to study tissue morphogenesis. During epidermal morphogenesis, epidermal cells migrate to cover the belly of the embryo using cues from the underlying neuroblasts. Part of this process, called ventral enclosure, involves the accumulation of F-actin into a supracellular ring along the margins of the epidermal cells. Although this ring was proposed to close by non-muscle myosin contractility, myosin has not been studied in ventral enclosure. Furthermore, it was not known if additional mechanical forces also contribute to this process. We analyzed the localization and genetic requirement of myosin to determine its function in ventral enclosure. We found that myosin localizes to foci that form a supracellular ring-like structure in the epidermal cells, supporting the model that myosin may constrict the F-actin ring. Consistent with this model, myosin activity is required for ring closure, and the accumulation of foci to form the ring depends on upstream regulators of myosin activity. Surprisingly, myosin also is required in the neuroblasts, where it localizes to dynamic foci that appear to form intercellular networks. We observed that a subset of neuroblasts organize into a rosette-like pattern and decrease their surface area as the epidermal cells constrict, which fails to occur in mutants with altered neuroblast cell shape or contractility. We propose that contractility in the neuroblasts may be coordinated with constriction of the supracellular actin-myosin ring in the overlying epidermal

cells. The coordination of myosin-dependent events and forces between different cell types could be a common theme for promoting epidermal morphogenesis in metazoans.

3.2 Introduction

Epidermal morphogenesis is essential for metazoan development. However, the complexity of vertebrate tissues has made it challenging to study how mechanical forces are coordinated for their development, particularly since multiple cell types often are involved. For example, many studies have been done '*ex vivo*', and it is not clear how these findings apply to tissues formed in their native environments (Heisenberg and Bellaïche, 2013). *Caenorhabditis elegans* epidermal morphogenesis is an ideal model to study tissue morphogenesis, since the epidermis is formed from a relatively small number of cells in comparison to other organisms. In addition, this small nematode is amenable to microscopy and genetics, and previous studies have revealed the precise order and timing of events during embryonic development.

We study ventral enclosure, when ventral epidermal cells cover the belly of the embryo using cues from underlying neuroblasts (neuronal precursors; Chisholm and Hardin, 2005). This process begins with the migration of two pairs of anterior-positioned ventral epidermal cells toward the ventral midline, followed by the migration of more posterior-positioned ventral epidermal cells (Williams-Masson et al., 1997; Chisholm and Hardin, 2005). As the posterior cells approach the ventral midline, they form a pocket that is lined by F-actin cables, which was hypothesized to close by myosin contractility (Williams-Masson et al., 1997). However, despite this hypothesis, myosin has not been studied in ventral enclosure. Ventral epidermal cell migration also relies on cues from the neuroblasts. Mutations in genes that affect neuroblast sorting and position, or their division and shape, cause ventral enclosure phenotypes, possibly

because the epidermal cells cannot receive short-range cues (George et al., 1998; Chin-Sang et al., 1999; Chisholm and Hardin, 2005; Ghenea et al., 2005; Patel et al., 2008; Giurumescu et al., 2012; Fotopoulos et al., 2013). In support of this model, a recent study showed that a subset of pocket epidermal cells relies on the formation of a neuroblast bridge to migrate successfully (Ikegami et al., 2010).

Non-muscle myosin contractility generates intracellular and extracellular forces via actin-myosin networks for several developmental events (Heisenberg and Bellaïche, 2013). Non-muscle myosin conformation and activity is stimulated by regulatory light chain (MRLC) phosphorylation by Rho-binding kinase (ROCK; LET-502 in *C. elegans*), and is negatively regulated by myosin phosphatase (Wissmann et al., 1997; Matsumura, 2005; Matsumura and Hartshorne, 2008). ROCK also can phosphorylate and inhibit the regulatory subunit of myosin phosphatase (MEL-11 in *C. elegans* to promote myosin activity; Wissmann et al., 1997). Myosin and its regulators are required for multiple events throughout *C. elegans* embryogenesis, including cytokinesis, gastrulation and epidermal morphogenesis (Wissmann et al., 1997; Shelton et al., 1999; Piekny et al., 2000; Piekny and Mains, 2002; Piekny et al., 2003; Diogon et al., 2007; Gally et al., 2009; Pohl et al., 2012; Roh-Johnson et al., 2012; Davies et al., 2014). During cytokinesis, an actin-myosin ring constricts the cell to form two daughters (Piekny et al., 2005). In *Drosophila* and *C. elegans* gastrulation, the apical constriction of mesodermal cells coordinates their ingression. Pulsatile centripetal flows of actin-myosin are translated into apical constrictions, which is controlled via a supracellular myosin network (Martin et al., 2010; Pohl et al., 2012; Roh-Johnson et al., 2012). The changes that occur in cell shape in response to pulsatile myosin flows likely depend on the frequency and amplitude of the actin-myosin network, the coupling of this network to junctions, which acts as a clutch and transmits forces, and the stabilization of periodic changes in shape via a molecular ratchet (Heisenberg and Bellaïche,

67

2013). During *Drosophila* embryogenesis, closure of the dorsal epidermis requires the coordinated adhesion, extension and migration of rows of epidermal cells toward the dorsal midline, as well the underlying amnioserosal cells (Jacinto et al., 2002A; Franke et al., 2005). In the amnioserosal cells, pulsatile apical actin-myosin contractility is transformed into stable, apical constrictions, which contributes to dorsal closure (Solon et al., 2009). In addition, actin-myosin cables form along the edges of the most proximal row of epidermal cells, which constricts to zipper the sheet together (Young et al., 1993; Kiehart et al., 2000; Bloor and Kiehart, 2002; Jacinto et al., 2002B). Although myosin has not yet been studied in ventral enclosure, the ring formed around the ventral pocket shares some striking similarities to the ring mediating dorsal closure. Furthermore, it is not clear how or if mechanical feedback contributes to epidermal morphogenesis, since the accumulation of myosin in epithelial cells could be triggered by myosin-mediated mechanical tension (Kee and Robinson, 2008).

The upstream regulators of non-muscle myosin contractility are controlled by the small GTPase RhoA, which is regulated by guanine nucleotide exchange factors (GEFs). During cytokinesis, the highly conserved GEF Ect2 generates active RhoA for contractile ring formation in *C. elegans*, *Drosophila* and mammalian cells (Miki et al., 1993; Tatsumoto et al., 1999; Kimura et al., 2000; Piekny and Mains, 2002; Somers and Saint, 2003; Piekny et al., 2005; Loria et al., 2012; Davies et al., 2014). During later stages of *Drosophila* embryogenesis, the Ect2 homologue, Pbl, and DRhoGEF2 (another RhoA GEF) regulate RhoA activity for the constriction of the actomyosin cables during dorsal closure (Young et al., 1993; Lu and Settleman, 1999; Kiehart et al., 2000; Bloor and Kiehart, 2002; Jacinto et al., 2002B, Azevedo et al., 2011). However, Ect2 also controls cell migration by regulating a different GTPase, Rac. For example, in *C. elegans*, zygotic ECT-2 regulates Rac for the migration of epidermal P cells, a subset of vulva precursor cells (Morita et al., 2005). In *Drosophila*, Pbl regulates cell migration

during gastrulation to mediate mesoderm spreading over the ectoderm (Schumacher et al., 2004; Smallhorn et al., 2004; van Impel et al., 2009). Furthermore, in interphase cancer cells, Ect2 activates Rac for tumor cell migration (Justilien and Fields, 2009; Fields and Justilien, 2010]. Therefore, studying myosin contractility during development has been complicated by the different functions of its upstream regulators. We recently found that the *C. elegans* RhoA homologue, *rho-1,* is required for ventral enclosure, supporting the idea that myosin contractility could be a crucial part of this process (Fotopoulos et al., 2013). However, we did not know how RHO-1 was regulated, or the cellular processes that myosin regulates for ventral enclosure. As described earlier, an obvious function for myosin would be to constrict the F-actin ring formed around the posterior epidermal cells, but myosin also could contribute additional mechanical forces.

We found that myosin is required for ventral enclosure, where it localizes to foci in epidermal cells and neuroblasts. In epidermal cells, the foci form a ring around the ventral pocket that highly resembles the previously described F-actin ring (Williams-Masson et al., 1997). Myosin contractility is required for ventral enclosure, because mutations in myosin or in its upstream regulators, or inhibiting myosin activity with the drug Blebbistatin (Straight et al., 2003), caused ventral enclosure phenotypes. Furthermore, the accumulation of myosin foci in both epidermal cells and neuroblasts is dependent on these regulators. Interestingly, a tissue-specific rescue assay revealed that myosin is required in the neuroblasts for ventral enclosure. In support of this finding, we observed that a subset of neuroblasts organizes into a rosette-like pattern, and their surface area decreases as the overlying epidermal cells constrict. We propose a model where mechanical forces in both the epidermal cells and neuroblasts are coordinated for successful ventral enclosure. Consistent with this model, altering neuroblast shape or decreasing myosin activity prevents neuroblasts from shrinking, and causes ventral enclosure phenotypes.

3.3 Materials and methods

3.3.1 Strains and alleles

C. elegans stocks were maintained on NGM plates with *E. coli* (OP-50) according to standard protocol (Brenner, 1974). The following strains were obtained from the *Caenorhabditis* Genetics Center (CGC): N2 (wild-type*), nmy-2 (ne1490) I, ect-2 (ax751) II, mlc-4 (or253)/qC1 dpy-19 (e1259) glp-1 (q339) III, unc-119 (ed3) III; tjIs1 [pie-1*::GFP::*rho-*1 + unc-119(+)]*, ajm-1 (ok160)* X; jcEx44, *rho-1 (ok2418)/nT1 [qIs51]) I, mcIs46 [dlg-1::RFP + unc-119]*, *ltIs44pAA173 [pie-1p-mCherry::PH(PLC1delta1) + unc-119(+)]*, and *lin-15B (n744); uIs57 [unc-119p::YFP + unc-119p::sid-1 + mec6p::mec6]*. The following strains were obtained from colleagues: *let-502 (sb118)* from P. Mains (U. Calgary), *unc-4 (e120) ect-2 (zh8) II* from A. Hajnal (U. Zurich), *ect-2 (gk44) II; unc-119 (ed3) III; xnIs162 [ect-2::GFP + unc-119(+)]* from J. Nance (Skirball Institute), *nmy-2 (cp7 [nmy-2::gfp + LoxP unc-119(+) LoxP]) I* from B. Goldstein (UNC), and *pRI.20 Pplx-2::GFP* (transcriptional reporter) from J. Culotti (U. Toronto). The following strains were made for this study: *nmy-2 (ne1490);* AJM-1:GFP, *let-502 (sb118);* AJM-1:GFP, *let-502 (sb118); ect-2 (ax751);* AJM-1:GFP, *ect-2 (ax751);* AJM-1:GFP, *ect-2 (zh8);* AJM-1:GFP, *ect-2 (ax751)*; *rho-1 (ok2418)/+, ect-2 (ax751)*; *mlc-4 (or253)/+, let-502 (sb118); ect-2 (ax751)*, NMY-2:GFP; *ect-2 (ax751),* NMY-2:GFP; *ect-2 (zh8), ect-2 (zh8)*; *rho-1 (ok2418)/+,* NMY-2:GFP; DLG-1:RFP, NMY-2:GFP; mCherry:PH, NMY-2:GFP; mCherry:PH; *ect-2 (ax751)*, and *ect-2 (ax751); Pplx-2:GFP*. All strains were maintained at 15˚C except for fluorescent strains, which were kept at 20˚C.

3.3.2 Genetic crosses and RNA interference

Genetic crosses were performed using standard protocols and Chi-square analyses were used to assess genetic interactions (Mains et al., 1990). For crosses using *ts* strains, such as *ect-2 (ax751)*, *let-502 (sb118)* and *nmy-2 (ne1490)* crosses were performed at 20°C, and the L1's (*let-502* - zygotic) or L2's (*ect-2* - maternal) were upshifted as L4 stage hermaphrodites to 25°C to assess lethality of the F2 or F3 generation at restrictive temperature. RNA-mediated interference was performed as previously described (Fotopoulos et al., 2013), and clones specific for *ani-1* (Y49E10.19), *let-502* (C10H11.9; both provided by M. Glotzer, U. Chicago), *ani-2* (K10B2.5) and *nmy-2* RNAi (F20G4; both provided by J. C. Labbé, IRIC Montreal) were used in this study.

3.3.3 Immunostaining

Embryos were fixed and immunostained as previously described (Fotopoulos et al., 2013). Embryos were stained with 1:100 rabbit anti-GFP antibodies (provided by M. Glotzer, U. Chicago), 1:10 mouse MH27 antibodies (anti-AJM-1; Developmental Studies Hybridoma Bank), and 1:1600 rabbit anti-ANI antibodies (provided by A.S. Maddox, UNC; Maddox et al., 2005) and 1:250 anti-rabbit Alexa 488 and anti-mouse Alexa 568 secondary antibodies (Invitrogen). Slides were stored at -20˚C.

3.3.4 Microscopy

Imaging was performed on embryos collected using established protocols (Sulston et al., 1983; Wernike et al., 2014). DIC imaging was performed on the LEICA DMI6000B microscope using the 40X 1.25 NA objective, capturing z-stacks of 2 µm thickness every 10 minutes for 7 hours using a Hamamatsu Orca R2 camera, piezo Z/ASI stage (MadCityLab), and Volocity acquisition software (PerkinElmer). Embryos expressing AJM-1:GFP were imaged with the same

microscope, but z-stacks of 1 μm thickness from the ventral surface were acquired with fluorescence using the GFP filter (Semrock) every 12 minutes. To prevent phototoxicity, the aperture was closed to 17%, and exposure times were <300 ms, using gain (up to 100). Fixed embryos were imaged with the 63X 1.4 NA objective and collecting z-stacks of 0.3 μm thickness. Strains expressing GFP, RFP or mCherry also were imaged using the 60X 1.4 NA or 100X 1.45 NA objective on an inverted Nikon Eclipse Ti microscope outfitted with the Livescan Sweptfield scanner (Nikon), piezo Z stage (Prior) and the Andor Ixon 897 camera, with Elements 4.0 acquisition software (Nikon), dual GFP/mCherry filter (Chroma) and the 488 and 561 lasers (set between 10-25% power). Z-stacks of 0.5 μm thickness were collected from the ventral surface every 10 minutes. All imaging was performed at room temperature, or at 25°C using chambers (IBIDI or TOKAI HIT model INU-TIZ-F1) on the Leica DMI6000B or Sweptfield microscope, respectively. TIRF imaging was performed using an inverted Nikon Ti-E microscope outfitted with a NI-DAQ piezo Z stage (National Instruments), an Evolve (EMCCD) camera, with Elements 4.0 acquisition software (Nikon), filters for 488 and 561 laser diodes, and a 100X CFI Apo TIRF objective. Images were collected every 10 seconds with a z thickness of 0.2 μm and laser power at 15%. Images were exported as TIFFs and opened in Image J (NIH Image) to create z-stack projections, perform image rotation and to crop desired regions. All images were converted to 8-bit format and used to make figures in Illustrator (Adobe).

3.3.5 Image analysis

To examine the localization of NMY-2:GFP in embryos, the original image files were deconvolved using AutoQuant X3 (MediaCybernetics). All measurements were performed in Image J (NIH Image) or Fiji. Kymographs were performed in Fiji along a line drawn in the ventral pocket of TIRF images from NMY-2:GFP embryos during ventral enclosure. A second

line was drawn in the anterior of the embryo for comparison. To measure velocity, the distance that each epidermal cell pair moved from ventral enclosure onset to closure was determined in pixels, then converted to μm and divided by time (in minutes). The velocities for each cell pair were averaged together. To measure the decrease in ventral pocket area from the time when the leading edge cells meet until adhesion of the pocket cells at the ventral midline, the surface was determined in pixels, then converted to $μm^2$ and divided by the time (in minutes). To measure myosin enrichment, regions enriched with NMY-2:GFP signal were chosen over different time points (or at one time point for area), then the average intensity and area in pixels was determined. We also measured an ROI in other regions of the embryo to create a ratio of myosin enrichment vs. background intensity to control for variations in imaging conditions. The total intensity of NMY-2:GFP along the edges of epidermal cells and in neuroblasts was determined by outlining the edges of epidermal cells using the red channel (DLG-1:RFP), then measuring the total intensity from the green channel (NMY-2:GFP). Any GFP signal that did not overlap with the epidermal cells was determined to be neuroblast-specific. Values for all measurements and calculations were averaged together and graphed using Excel (Microsoft). Standard deviations were calculated for all measurements, and the *p* values were calculated using the student t test or by a one-way ANOVA.

3.4 Results

3.4.1 Non-muscle myosin localizes as foci in epidermal cells and neuroblasts during ventral enclosure

We wanted to determine if non-muscle myosin is required for ventral enclosure. First, we characterized the localization of myosin during this process. To do this, we imaged embryos

expressing GFP-tagged NMY-2 (non-muscle myosin heavy chain), with GFP integrated at the gene locus by CRISPR/Cas9 genome editing (Dickinson et al., 2013). NMY-2 localizes as foci, which form an intercellular ring-like pattern around the ventral pocket (**Figure 20A**). Co-staining fixed embryos with antibodies that recognize epidermal adherens junctions (MH27), revealed that some of the foci overlap with junctions, while other foci localize along the junction-free edges of the epidermal cells (**Figure 21A**). Co-staining fixed embryos with antibodies specific for ANI-1 (*C. elegans* anillin; Maddox et al., 2005), which is enriched in neuroblasts (Fotopoulos et al., 2013), revealed that the epidermal NMY-2 foci appear to align with ANI-1 positive neuroblasts, while other foci may be in the neuroblasts (**Figure 20B**). Images from a NMY-2:GFP; mCherry:PH embryo (myosin is in green, while PH is in red and outlines all cell membranes) show how myosin changes with time during ventral enclosure (**Figure 21B**). The ring appears to close from anterior to posterior, reminiscent of the zippering reported for epidermal cells during *Drosophila* dorsal closure (Jacinto et al., 2002A), and foci appear to accumulate in both the epidermal cells and neuroblasts. The accumulation of foci in both tissues suggests that myosin may be associated with contractile events in multiple cell types during ventral enclosure.

As a potential regulator of RhoA and myosin contractility, we also examined the localization of the GEF, ECT-2, during ventral enclosure. Using an ECT-2:GFP strain driven by the *ect-2* promoter, we generated a rescued *ect-2 (ax751);* ECT-2:GFP strain that displays <5% embryonic lethality (n>200; Chan and Nance, 2013). In these embryos, ECT-2 localized to cell boundaries throughout embryogenesis, including the boundaries of epidermal cells and neuroblasts, and although not as obvious as myosin, ECT-2 foci accumulated to a ring-like pattern around the ventral pocket (**Figure 20C**). Co-staining fixed ECT-2:GFP embryos with MH27 antibodies verified that ECT-2 is at the boundaries of epidermal cells during ventral enclosure (data already shown in MSc thesis Chen, 2014). The similar localization patterns of
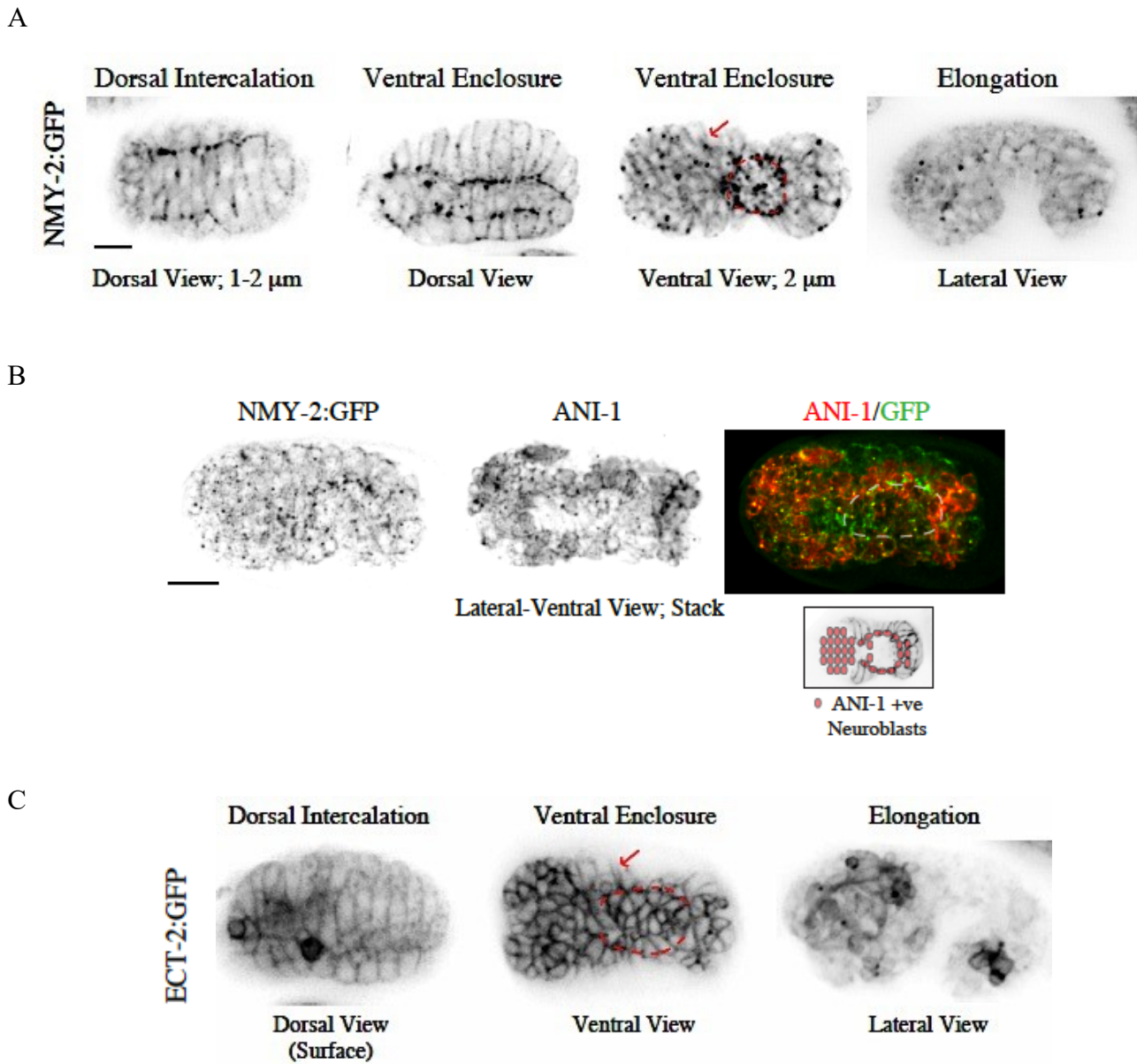
Figure 20. Non-muscle myosin, ANI-1 and ECT-2 are localized in the ventral pocket. A) Z-stack projections of live NMY-2:GFP embryos are shown during dorsal intercalation, ventral enclosure and the 1.5-fold stage of elongation. The red arrow points to the ventral epidermal cells. The red dotted line outlines the ventral pocket. B) Confocal image of a fixed NMY-2:GFP embryo co-stained for ANI-1 shows the position of ANI-1-positive neuroblasts relative to the NMY-2 foci. The inset shows a cartoon representation of these neuroblasts. The white dotted line outlines the ventral pocket. C) Images from live ECT-2:GFP embryos during embryogenesis. The red arrow points to ventral epidermal cells and the red dotted line outlines the ventral pocket. The scale bar is 10 μm.
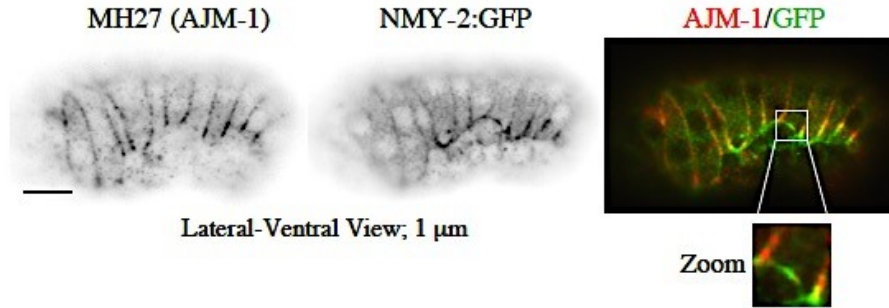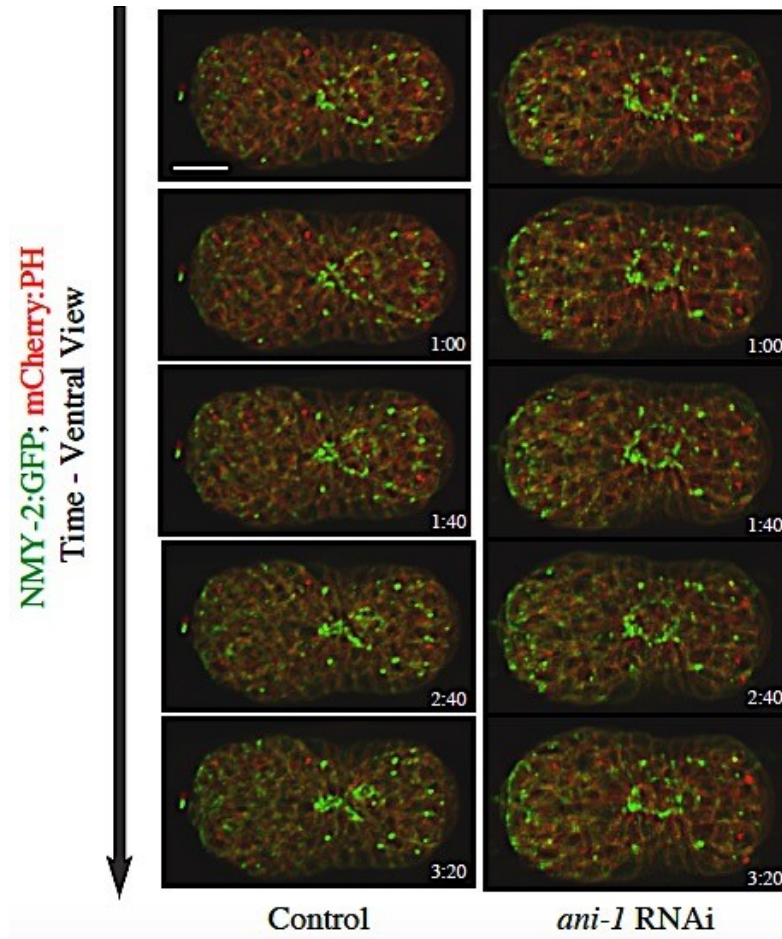
Figure 21. Non-muscle myosin foci form a supra-cellular structure during ventral enclosure. A) A fixed NMY-2:GFP embryo co-stained for GFP and MH27 (AJM-1 – adherens junction protein) is shown during ventral enclosure. A zoomed in region shows the junction-free edge of the epidermal cell. B) Z-stack projections (depth of 6 μm) of NMY-2:GFP; mCherry:PH control and *ani-1* RNAi embryos are shown after deconvolution over time (11<n<13). The scale bar is 10 μm.

ECT-2 and myosin during ventral enclosure suggest that myosin could be contractile at these locations.

We also wanted to characterize the dynamics of myosin foci during ventral enclosure. We followed foci within the epidermal cells and neuroblasts by performing TIRF (total internal reflection fluorescence) microscopy on embryos that co-express NMY-2:GFP and the actin-binding domain from VAB-10 tagged with mCherry driven by an epidermal-specific promoter (**Figure 22A**). We observed foci moving toward and coalescing at the leading edges of the ventral epidermal cells as they migrated toward the midline (**Figure 22A**). When imaging focal planes favoring the neuroblasts, we observed the assembly of dynamic foci into large networks as ventral epidermal cells approached the midline (**Figure 22A**). Kymographs of TIRF images from similarly staged control embryos showed the appearance of several myosin foci of high intensity, which either pulsed or left the focal plane and appeared to flow toward the midline (**Figure 22B**). Myosin foci in other regions of the embryo also appeared to pulse or leave the focal plane, but did not flow (**Figure 22B**). In contrast, myosin foci in *ani-1* RNAi treated embryos appeared static with fewer pulses and flows (**Figure 22B**). Our data suggests that the myosin foci are highly dynamic, and display intercellular patterns during ventral enclosure – as a ring around the pocket, and as star-like networks in the neuroblasts.

3.4.2 Non-muscle myosin contractility is required for *C. elegans* ventral enclosure

Next, we determined if myosin and its upstream regulators are required for ventral enclosure. To do this, we used ts alleles of myosin *nmy-2 (ne1490)* and *ect-2 (ax751)*, since RNAi to either gene causes cytokinesis and polarity defects (Guo and Kemphues, 1996; Zonies et al., 2010; Loria et al., 2012; Davies et al., 2014). At 20°C, both mutants display moderate lethality (*nmy-2* – 62%; *ect-2* – 32%), which increases to 95% at 25°C (**Table 1**). Both mutants

A

B
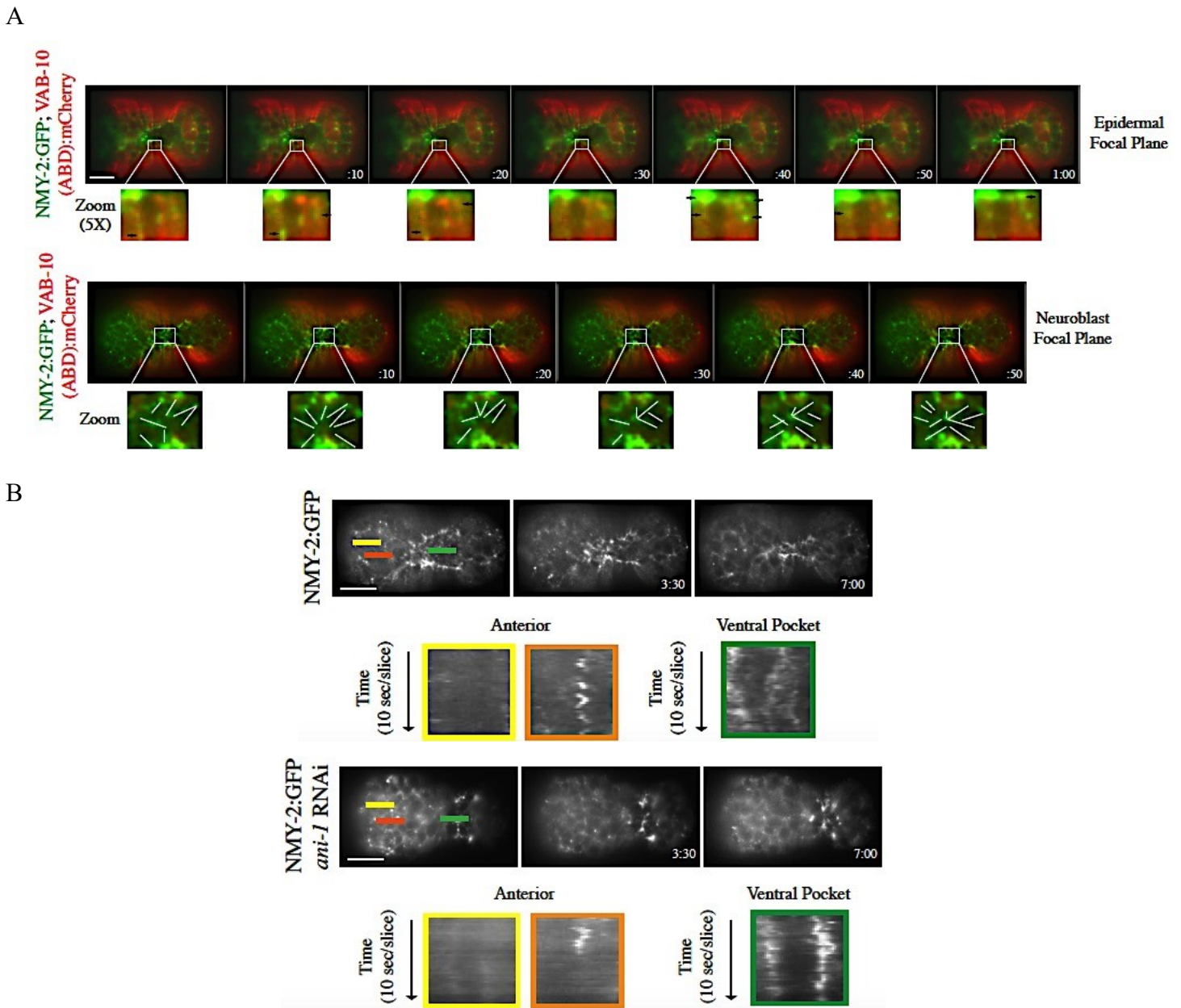
Figure 22. Non-muscle myosin localizes as networks of foci in epidermal cells and neuroblasts during ventral enclosure. A) TIRF images of different NMY-2:GFP; VAB-10 (ABD):mCherry embryos at epidermal (top panels) or neuroblast (bottom panels) focal planes are shown during ventral enclosure. The outlined boxes show regions that were zoomed in to highlight the change in NMY-2:GFP foci over time. B) TIRF images of an NMY-2:GFP control and *ani-1* RNAi embryo are shown during ventral enclosure. The kymograph on the far left corresponds to the yellow line drawn in the anterior of the embryo where there are few foci. The kymograph in the middle is from the orange line drawn in the anterior of the embryo where there are some foci, while the kymograph on the right corresponds to the green line drawn in the ventral pocket. The time is indicated to the left of each kymograph. The scale bar is 10 μm.

78

Table 1. *nmy-2 and ect-2* **are required for embryonic development.**

Genotype	Temperature (ºC)	Embryonic Lethal%^
N2 [#]	20	0
N2 [#]	25	0
nmy-2 (ne1490) [¶]	20	62
nmy-2 (ne1490) [¶]	25	95
ect-2(ax751) [#]	20	32*
ect-2(ax751) [#]	25	95
ect-2(ax751) X N2 males [#]	20	23*
ect-2(ax751) X N2 males [#]	25	89
unc-4 ect-2(zh8) [#]	20	31
ect-2 RNAi [#]	20	100
N2; *nmy-2* RNAi	20	100
N2; *ani-2* RNAi	20	0**
lin-15B(n744) X; uIs57	20	0
lin-15B(n744) X; uIs57; nmy-2 RNAi	20	38***
lin-15B(n744) X; uIs57; ani-2 RNAi	20	0

^ Sample size is 100<n<300.
* Highly variable with a range of 20-50% embryonic lethality.
** Partial sterility with 9 eggs/hermaphrodite.
*** Highly variable with a range of 10-73% embryonic lethality.

[#] Contributions made by Yun Chen
[¶] Contributions made by Karina Mastronardi

have a spectrum of phenotypes that we categorized as 1) early (*nmy-2* – 42%; *ect-2* - 16%), before the onset of ventral enclosure, 2) rupture (*nmy-2* – 42%; *ect-2* - 37%), where the embryos fail to complete ventral enclosure causing internal contents to extrude out of the embryo, 3) delay (*nmy-2* – 6.5%; *ect-2* – 15%), where embryos complete ventral enclosure, but take >10-50 minutes longer in comparison to wild-type embryos, and 4) elongation defects (*nmy-2* – 6.5%; *ect-2* – 5%), where embryos hatch into larvae with abnormal body morphologies (**Table 2**). Consistent with the ts nature of the allele, *ect-2* mutant embryos have a higher percentage of early phenotypes at 25˚C (**Table 2**). A gain-of-function *ect-2* allele, *zh8*, also displays embryonic lethality (31%; **Table 1**), with a proportion of embryos rupturing due to failed ventral enclosure (13%; **Table 1**; Canevascini et al., 2005). This data shows that both *nmy-2* and its upstream regulator, *ect-2*, are required for ventral enclosure. To further characterize ventral enclosure phenotypes in *nmy-2* and *ect-2* mutant embryos, we created strains expressing AJM-1:GFP to visualize epidermal cell movements. In some of the *nmy-2* and *ect-2* mutant embryos, ventral epidermal cells failed to complete migration, while in others, their migration appeared to be slower in comparison to control embryos (**Figure 23A**). Indeed, the average decrease in ventral pocket area until the epidermal cells meet at the ventral midline was drastically decreased in both *ect-2* (1.8 μm^2/min) and *nmy-2* (2.21 μm^2/min) mutant embryos compared to control embryos (4.28 μm^2/min; **Figure 23B**). We performed more detailed measurements of individual cell velocities for *ect-2* mutant embryos, and found that although the two most anterior leading cell pairs migrated faster in comparison to the posterior ventral pocket cells in control embryos (average of 0.43 µm/min vs. 0.23 µm/min), in *ect-2* mutant embryos, the velocity of every cell pair was delayed (data already shown in MSc thesis Chen, 2014). These data suggest that myosin and *ect-2* are not required for migration per se, but are required to mediate the efficient migration of epidermal cells for ventral enclosure.

80

Table 2. Non-muscle myosin and its upstream regulators are required for ventral enclosure.

Genotype	Temp (ºC)	Phenotype Analysis*			
		Early (%)	Rupture (%)	VE Delay** (%)	Elongation Defect^ (%)
nmy-2(ne1490)	22	42	42	6.5	6.5
nmy-2(ne1490)	25	59	34	7	7
ect-2(ax751) [#]	22	16	37	15	5
ect-2(ax751) [#]	25	44	39	0	0
unc-4 ect-2(zh8) [¶]	22	23	13	0	0
rho-1(ok2418)/+ [¶]	22	5	5	0	16
ect-2(ax751); rho-1(ok2418)/+ [#]	22	32	7	18	11
unc-4 ect-2(zh8); rho-1 (ok2418)/+ [#]	22	25	5	50	20
mlc-4(or253)/qC1 [#]	22	0	8	13	29
ect-2(ax751); mlc-4(or253)/+ [#]	22	20	25	25	11
let-502(sb118) [#]	25	28^^	0	39	72
let-502 RNAi	22	43^^	12	19	12
let-502(sb118); ect-2(ax751) [#]	25	73	21	6	0
lin-15B(n744) X; uIs57; nmy-2 RNAi	22	16	16	48	0

*Based on DIC imaging performed at room temperature (~22ºC) or at 25ºC using a chamber; sample size is 15<n<50.

**The embryos with delays in VE (>60 min) hatch as wild-type larva or display elongation defects, and are counted separately from embryos that rupture.

^Embryos may not hatch.

^^Dorsal-specific epidermal phenotypes were observed and included in this category (6% for *sb118* and 12% for RNAi).

[#] Contributions made by Yun Chen

[¶] Contributions made by Karina Mastronardi
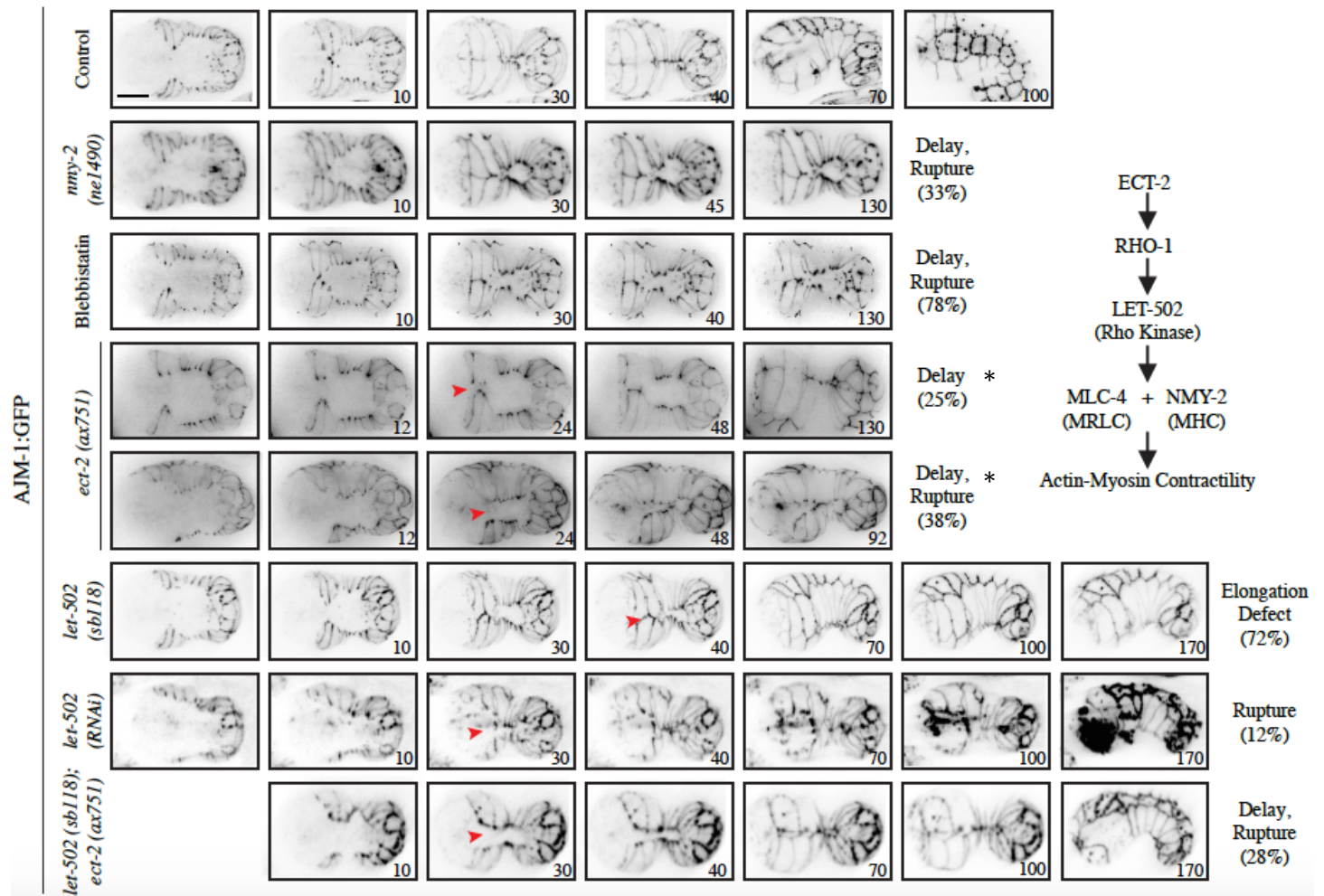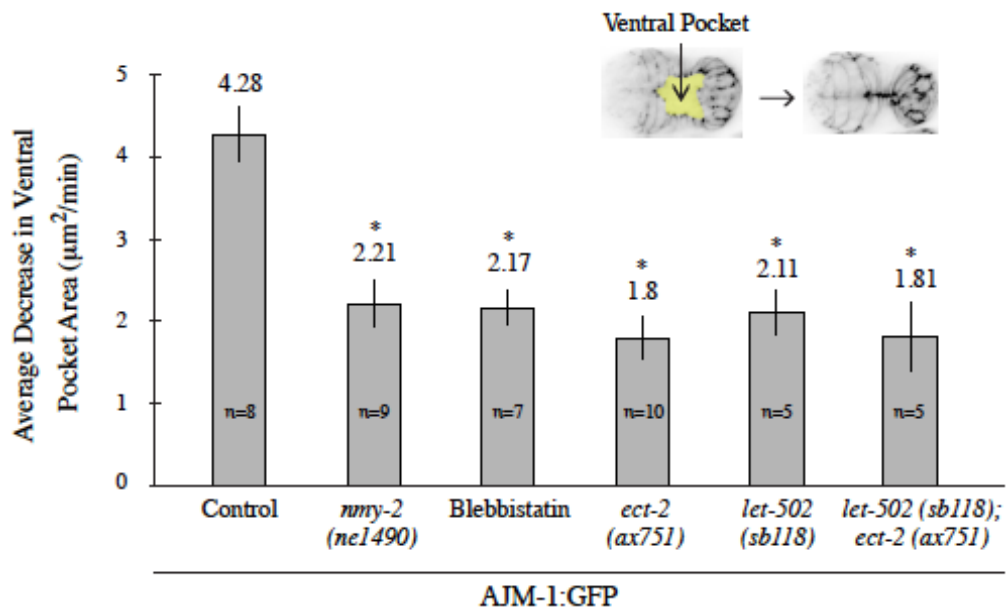
Figure 23. Non-muscle myosin activity regulates ventral enclosure. A) Time-lapse images of embryos expressing AJM-1:GFP are shown during ventral enclosure for control, *nmy-2 (ne1490),* Blebbistatin (100 µM), *ect-2 (ax751), let-502 (sb118), let-502* (RNAi) and *let-502 (sb118); ect-2 (ax751)* mutant embryos as indicated (7<n<26). Red arrows point to the ventral epidermal cells. Phenotypes are indicated on the right. The scale bar is 10 µm. B) A graph shows the average decrease in ventral pocket area (in μm^2/min) for control, *nmy-2,* Blebbistatin, *ect-2, let-502* or *let-502; ect-2* double mutant embryos expressing AJM-1:GFP (7<n<12). The bars show standard deviation, and * indicates *p*<0.001 vs. control by the student t-test. Images depicted with an asterisk already appeared in the MSc thesis Chen, 2014.

Our data indicates that myosin contractility is required for ventral enclosure, and we determined if mutations in other components of the pathway governing myosin contractility also cause ventral enclosure phenotypes. We previously reported that RhoA *(rho-1)* mutant embryos rupture, while Rho kinase *(let-502)* mutant embryos have delayed ventral enclosure (Fotopoulos et al., 2013). To expand on these previous observations, we examined *mlc-4* (regulatory light chain; *or253*) mutant embryos (Shelton et al., 1999), and observed a small proportion of embryos with rupture (8%) and delay (13%; **Table 2**) phenotypes. We also observed ventral enclosure phenotypes in embryos after strong disruption of Rho kinase by RNAi or after upshift of ts *let-502 (sb118)* embryos to 25°C, including rupture (RNAi - 12%), delay (RNAi - 19%; *sb118 –* 39%), as well as the previously described elongation defects (RNAi - 12%; *sb118 –* 72%; **Table 2**, **Figure 23A**). We also measured the average decrease in ventral pocket area in embryos mutant for Rho kinase (*let-502*), a major regulator of myosin contractility. We found that *let-502 (sb118)* embryos closed about twice as slow as control embryos (2.11 vs. 4.28 μm^2/min, respectively; **Figure 23B**). Consistent with them functioning in the same pathway for myosin contractility, *let-502 (sb118); ect-2 (ax751)* double mutant embryos had similar rates of ventral enclosure (1.81 μm^2/min) compared to the single mutant embryos (**Figure 23B**). Observing ventral enclosure phenotypes in different RhoA pathway mutant embryos supports a role for myosin contractility in ventral enclosure. One caveat to these studies is that myosin contractility is required for cytokinesis and gastrulation, and the ventral enclosure phenotypes could be a consequence of disrupting these earlier events. We do not believe that this is the case, since we used a marker that clearly outlined the epidermal cells (e.g. AJM-1:GFP), and we only considered embryos to have a ventral enclosure-specific phenotype if they had the correct number of epidermal cells that were properly positioned at the onset of ventral enclosure. To further verify this, we counted the number of epidermal cells in *ect-2 (ax751);* AJM-1:GFP embryos, and found that there was no

difference in comparison to control embryos (11.3 ventral cells, 11.7 dorsal cells and 9.8 seam cells vs. 11.4, 11.9 and 9.9 in control embryos, respectively, n=8 per genotype). Finally, we also examined ventral enclosure in embryos treated with the non-muscle myosin inhibitor Blebbistatin (Straight et al., 2003). This highly permeable drug (100 μM) was added to the buffer surrounding embryos just prior to ventral enclosure, and 77.8% (n=9) embryos displayed ventral enclosure phenotypes with delayed rates of closure consistent with what we observed for *nmy-2* ts mutant embryos (2.17 μm^2/min; **Figure 23B**). Therefore, this data suggests that myosin contractility is required for ventral enclosure.

3.4.3 Non-muscle myosin is required in the neuroblasts for ventral enclosure

Next, we determined if there was a correlation between myosin localization and its activity during ventral enclosure. We imaged NMY-2:GFP in embryos with disrupted *ect-2* or *let-502*, and found that embryos with ventral enclosure phenotypes had fewer myosin foci around the ventral pocket in comparison to control embryos (**Figure 24A**). We quantitated the average ratio of NMY-2:GFP at sites of enrichment around the ventral pocket (outlined by the red lines) vs. total intensity in *ect-2* mutant and *let-502* RNAi embryos over several time points (**Figure 25A**). In control embryos, the ratio ranged from 1.45 – 2.01, and peaked when the ventral pocket closed (stage 3; **Figure 25A**). In *ect-2 (ax751)* mutant and *let-502* RNAi embryos, the ratio of NMY-2:GFP was lower, ranging from 1.24 – 1.51 and 1.18 – 1.58, respectively (**Figure 25A**). In gain-of-function *ect-2 (zh8)* embryos, the ratio was similar to control levels (**Figure 25A**), however, myosin was enriched over a broader area (1.12 μm^2 vs. 0.89 μm^2 for control), while *ect-2 (ax751)* and *let-502* RNAi embryos had smaller areas of enrichment (0.63 μm^2 and 0.59 μm^2, respectively; **Figure 25B**). This data shows that *ect-2* and *let-502* are required for the localization of myosin to foci during ventral enclosure, suggesting that these foci are contractile.
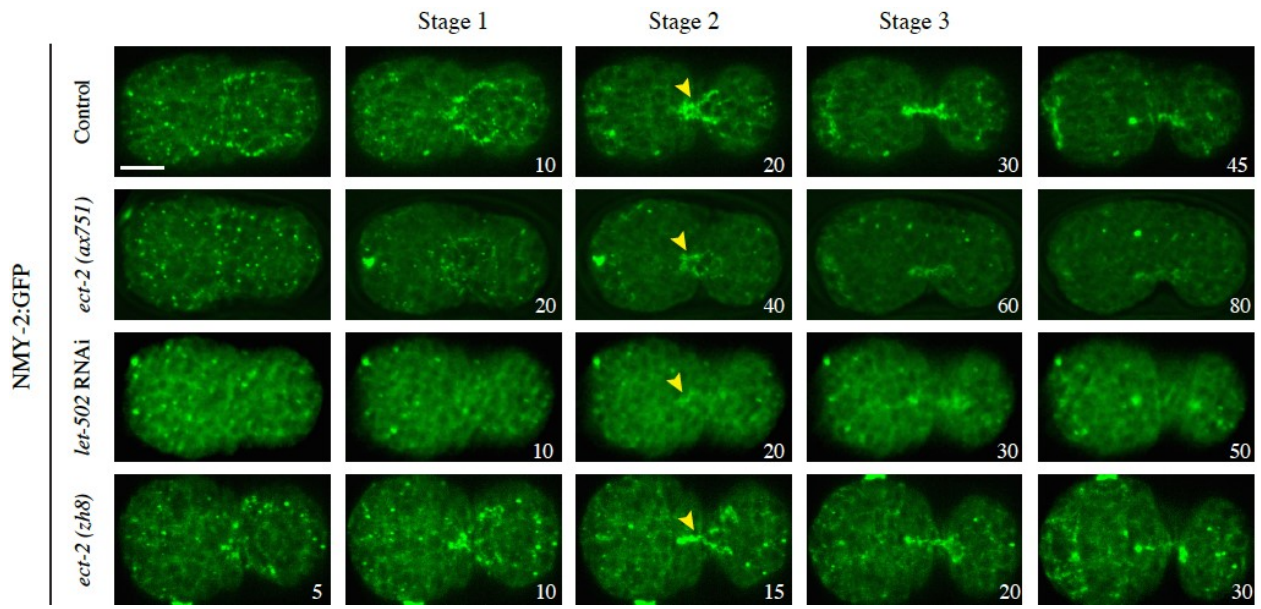
Figure 24. Non-muscle myosin foci are dependent on regulators of myosin contractility during ventral enclosure. Time-lapse images of NMY-2:GFP from control, *ect-2 (ax751* or *zh8)* and *let-502* RNAi embryos are shown during ventral enclosure (7<n<18). The yellow arrows point to sites of myosin accumulation. The scale bar is 10 μm.

A
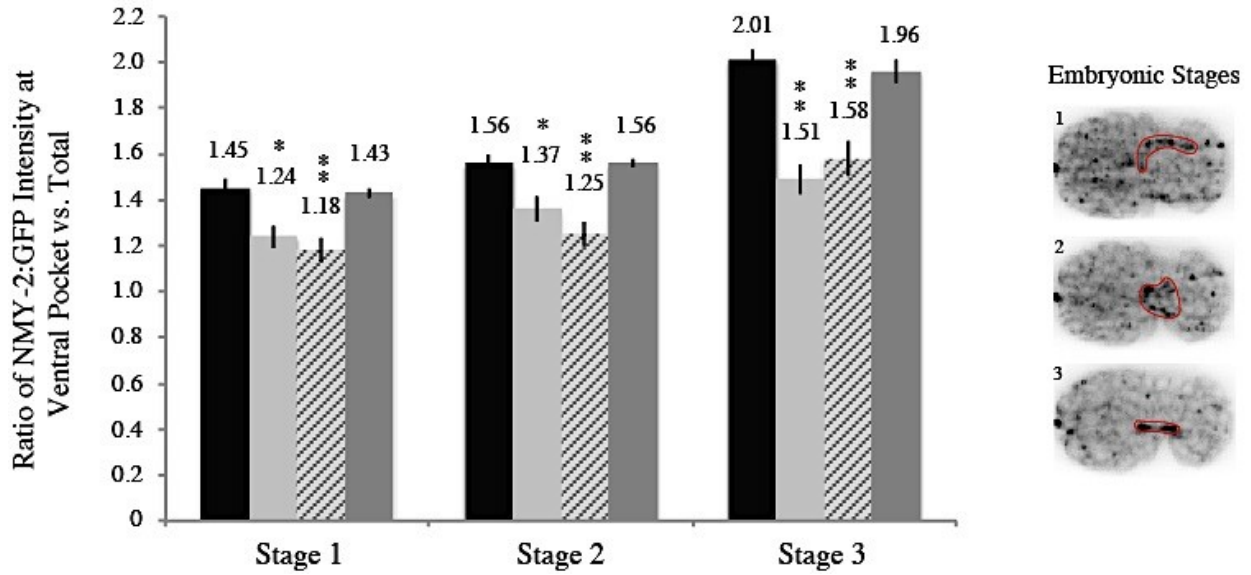
B
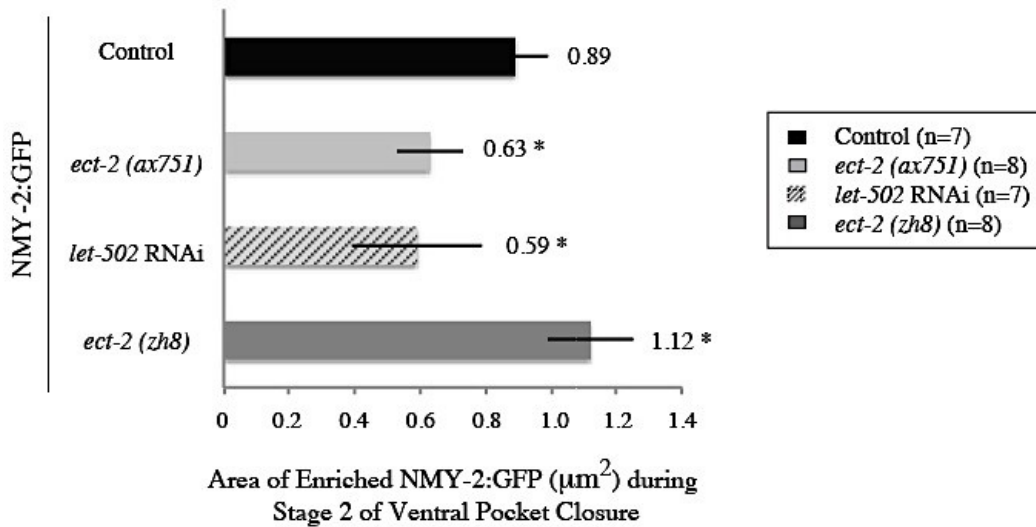
Figure 25. Non-muscle myosin foci accumulate around the ventral pocket as ventral enclosure progresses, which is dependent on regulators of myosin activity. A) A graph shows the average ratio of NMY-2:GFP intensity at, and subsequently in, the ventral pocket vs. total intensity during different stages of ventral enclosure (stage and selected ROI's are outlined in red on the images; $7 < n < 8$). B) A graph shows the area of enriched NMY-2:GFP (in μm^2) during stage 2. Bars show standard deviation, and * indicates $p < 0.05$ vs. control by the student t-test.

We observed the accumulation of myosin to foci in both the epidermal cells and neuroblasts, and we wanted to determine if myosin contractility was more strongly associated with foci in one cell type. To selectively visualize myosin in epidermal cells, we imaged embryos co-expressing NMY-2:GFP and DLG-1:RFP (epidermal junction component; **Figure 26A**). Some foci overlapped with the edges of the ventral epidermal cells (yellow), while other foci were located within the neuroblasts. We then determined if *ect-2* is required for the localization of myosin foci in the two cell types. Indeed, foci appeared to be reduced in both cell types in the *ect-2* mutant embryos, which we verified by measuring the total intensity of myosin foci along the epidermal cells, and in the neuroblasts during closure (**Figure 26B**). The finding that contractile foci accumulate in neuroblasts raises interesting hypotheses about their involvement in ventral enclosure. However, seeing foci in these cells does not necessarily mean that they are essential for ventral enclosure. To determine if myosin has a function in the neuroblasts during ventral enclosure, we monitored neuroblast position. Recent studies showed that a bridge forms from PLX-2 (plexin)-expressing neuroblasts during ventral enclosure, which mediates migration of the overlying ventral epidermal cells (Ikegami et al., 2010). Imaging *ect-2 (ax751)* mutant embryos expressing a GFP transcriptional reporter for *plx-2* revealed that in embryos with ventral enclosure phenotypes, some cells were mispositioned and the bridge failed to form altogether (40%, 8/20) or cells were positioned properly, but took longer to form the bridge (40%, 8/20; **Figure 27A**).

Next, to show that myosin is required in the neuroblasts, we took advantage of a *C. elegans* strain (*lin-15B (n744); uIs57*) that was previously shown to permit RNAi sensitivity selectively in neuronal tissue, while blocking RNAi in other cell types (Calixto et al., 2010). Interestingly, when this strain, *lin-15B (n744); uIs57*, was treated with *nmy-2* RNAi, embryos displayed 38% lethality compared to control embryos (**Table 1**). We saw a range of phenotypes
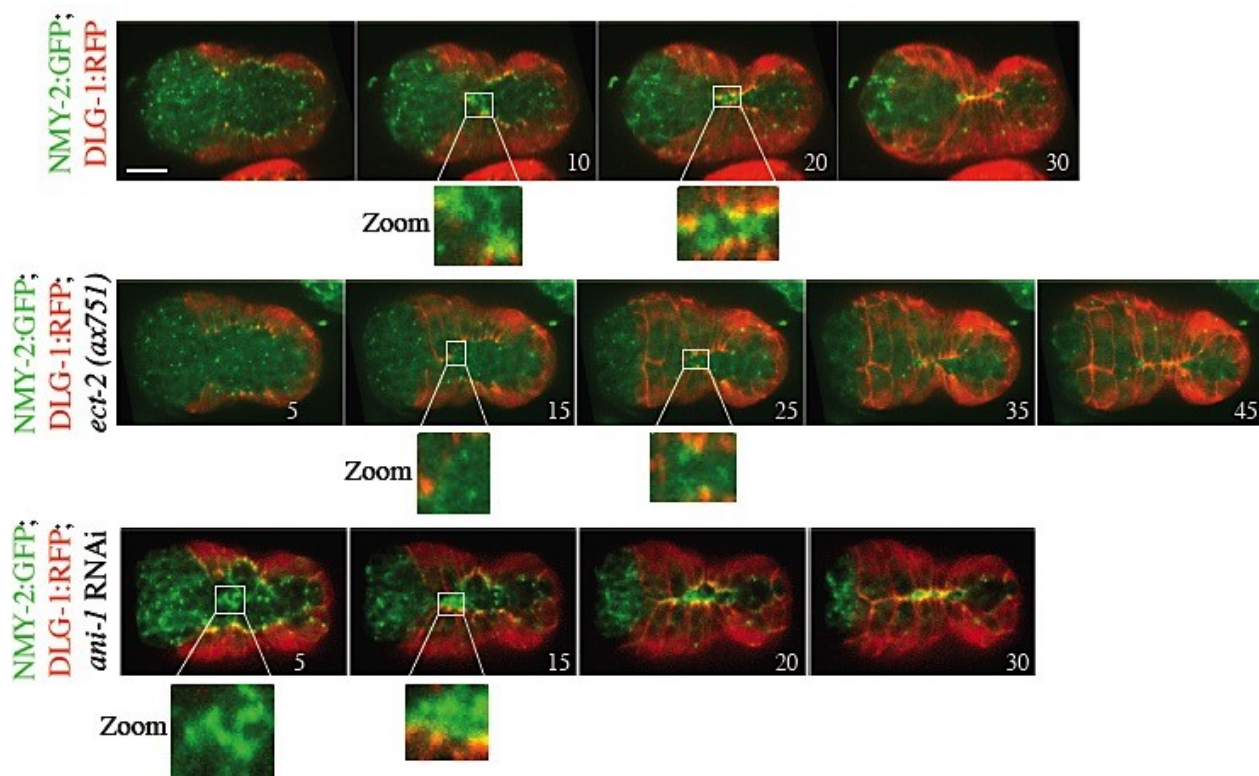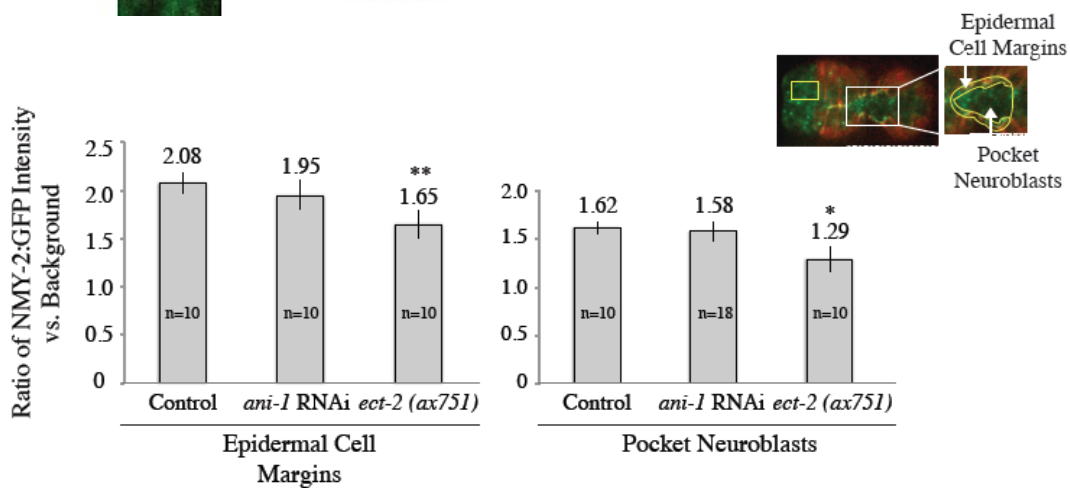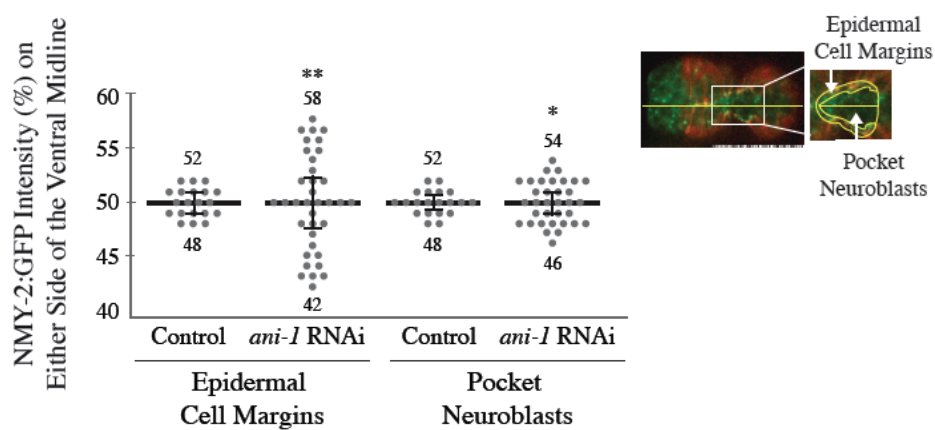
Figure 26. Non-muscle myosin foci in both epidermal cells and neuroblasts are dependent on regulators of myosin activity. A) Images of NMY-2:GFP; DLG-1:RFP from control, *ect-2 (ax751)* and *ani-1* RNAi embryos are shown during ventral enclosure (10<n<18). The insets show zoomed in regions. B) The bar graphs show the ratio of NMY-2:GFP intensity for the ventral epidermal cell edges and the pocket neuroblasts for control, *ani-1* RNAi and *ect-2 (ax751)* embryos as indicated in the image. C) The graph shows NMY-2:GFP distribution on either side of the ventral midline in control versus *ani-1* RNAi embryos as indicated in the image. ** indicates $p<0.01$, and * indicates $p<0.05$ for the average vs. control by the student t test (B) or for the distribution of data vs. control by a one-way ANOVA (C). The scale bar is 10 μm.

A
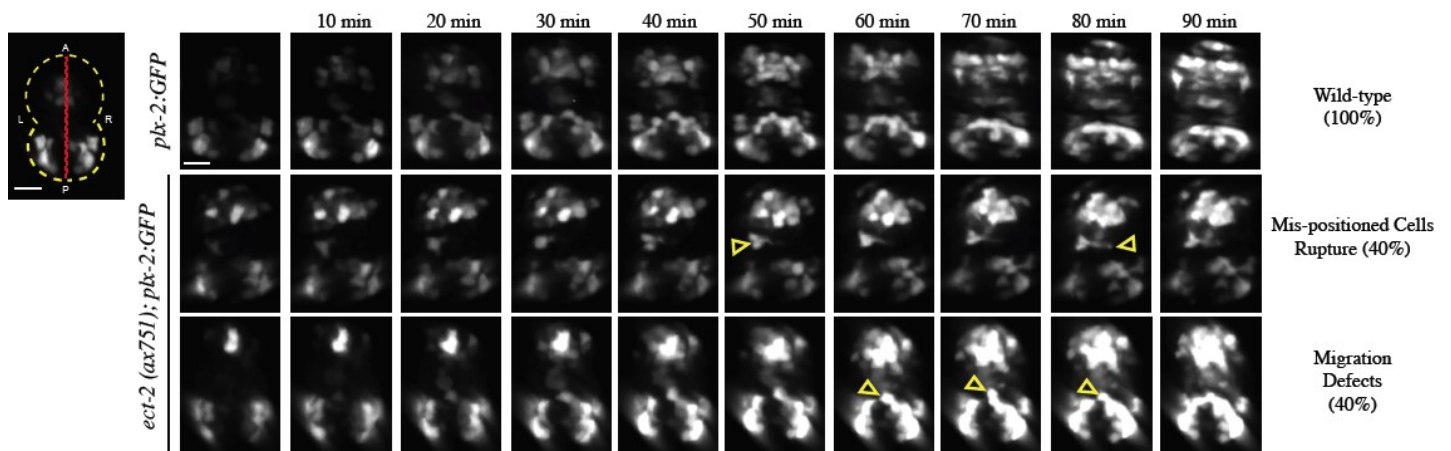
B
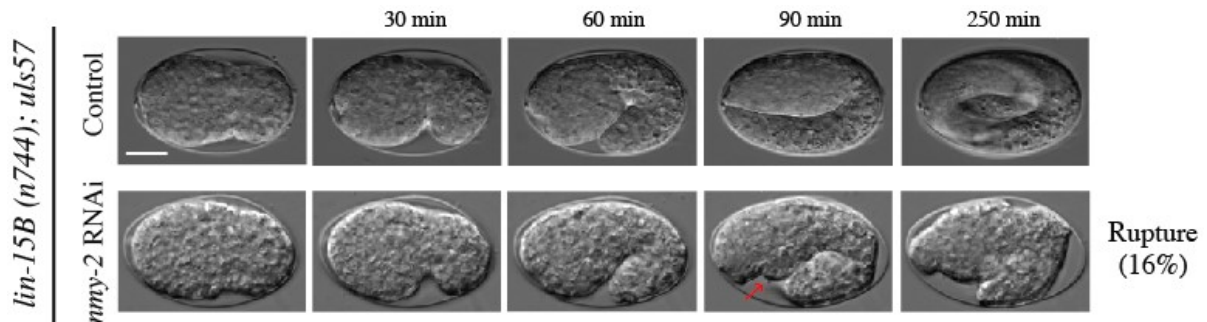
Figure 27. Non-muscle myosin activity is required for neuroblast migration, and non-muscle myosin is required in the neuroblasts for ventral enclosure. A) Images from *plx-2:GFP*-expressing control and *ect-2 (ax751)* embryos are shown prior to, and during ventral enclosure. The image on the left shows the outline of the embryo and the orientation of anterior (A), posterior (P), left (L) and right (R). The open yellow arrow points to mis-positioned cells. The proportion of phenotypes is shown on the right. B) DIC time-lapses of *lin-15B (n744); uIs57* control and *nmy-2* RNAi embryos are shown during ventral enclosure (9<n<25). The phenotype is indicated on the right. The red arrow points to the initial site of rupture. The scale bar is 10 μm.

that aligned with our previously described categories for *nmy-2* and *ect-2* mutants, including 16% early, before the onset of ventral enclosure, and 16% rupture, where the embryos failed to complete ventral enclosure causing internal contents to extrude out of the embryo (**Figure 27B**; **Table 2**). Furthermore, we observed a delay of >10-50 minutes in 47% of the embryos that completed ventral enclosure in comparison to wild-type embryos (n=25; **Table 2**). Together, this data shows that myosin is required in the neuroblasts for ventral enclosure.

3.4.4 Neuroblasts in the ventral pocket re-organize and shrink during ventral enclosure

To further study myosin in the neuroblasts during ventral enclosure, we determined how its localization changes with cell shape. We previously reported that ANI-1 (anillin) is expressed predominantly in neuroblasts and is required for neuroblast cytokinesis (Fotopoulos et al., 2013; Wernike et al., 2014). We imaged NMY-2:GFP; mCherry:PH or DLG-1:RFP embryos treated with *ani-1* RNAi, and monitored changes in the localization of myosin foci in epidermal cells and neuroblasts (**Figures 21B and 22A**). Myosin foci were more asymmetrically distributed around the ventral pocket in anillin-depleted embryos, and were found at different locations within cells (e.g. surface or bottom, data not shown) in comparison to control embryos (**Figures 21B**). When we measured the ratio of myosin intensity in the epidermal cells or neuroblasts, it was not significantly different in comparison to control embryos (**Figure 26B**). However, when we measured the distribution of myosin foci on either side of a central axis running through the length of the embryo, we found that myosin was more variably localized in both the epidermal cells and neuroblasts in anillin-depleted embryos (**Figure 26C**). Therefore, altering neuroblast shape does not affect the localization of myosin to foci, but does alter the organization of these foci. Strikingly, myosin foci in the epidermal cells appear to change in response to changing neuroblast shape.

Next, we imaged NMY-2:GFP; mCherry:PH embryos to visualize neuroblast organization during ventral enclosure. A subset of neuroblasts that lie in the open pocket underneath the closing posterior epidermal cells appeared to form a pattern. This subset of cells formed into columns, then subsequently formed into a rosette-like pattern with at least 5 cells sharing a common vertex (**Figure 28**). We also found that the surface area of several neuroblasts within this area decreased by an average of 8.6%/min as the overlying epidermal cells constricted (n=10 cells from 3 embryos). Altering neuroblast cell shape by treating embryos with *ani-1* RNAi caused the neuroblasts to appear more disorganized, and some of the cells took longer to decrease their surface area in comparison to control embryos (3.4%/min, n=13 cells from 4 embryos; **Figures 28 and 29A**). In *ect-2 (ax751)* embryos with delayed ventral enclosure, the neuroblasts appeared to form a rosette-like pattern, but their surface area failed to change (1.4%/min, n=12 cells from 4 embryos; **Figures 28 and 29A**). Therefore, myosin contractility is required to shrink neuroblasts during ventral enclosure.

3.5 Discussion

Here, we show that non-muscle myosin is required for ventral enclosure during *C. elegans* epidermal morphogenesis, when the ventral epidermal cells migrate to cover the belly of the embryo. Myosin localizes to foci that form a ring around the ventral epidermal cells, in a pattern similar to the previously described F-actin ring (Williams-Masson et al., 1997). We also observed the accumulation of myosin foci to intercellular networks in the underlying neuroblasts, which are known for their role in providing chemical cues to regulate epidermal cell migration (George et al., 1998; Chin-Sang et al., 1999; Chisholm and Hardin, 2005; Ghenea et al., 2005; Patel et al., 2008; Giurumescu et al., 201). We found that the accumulation of foci in both the
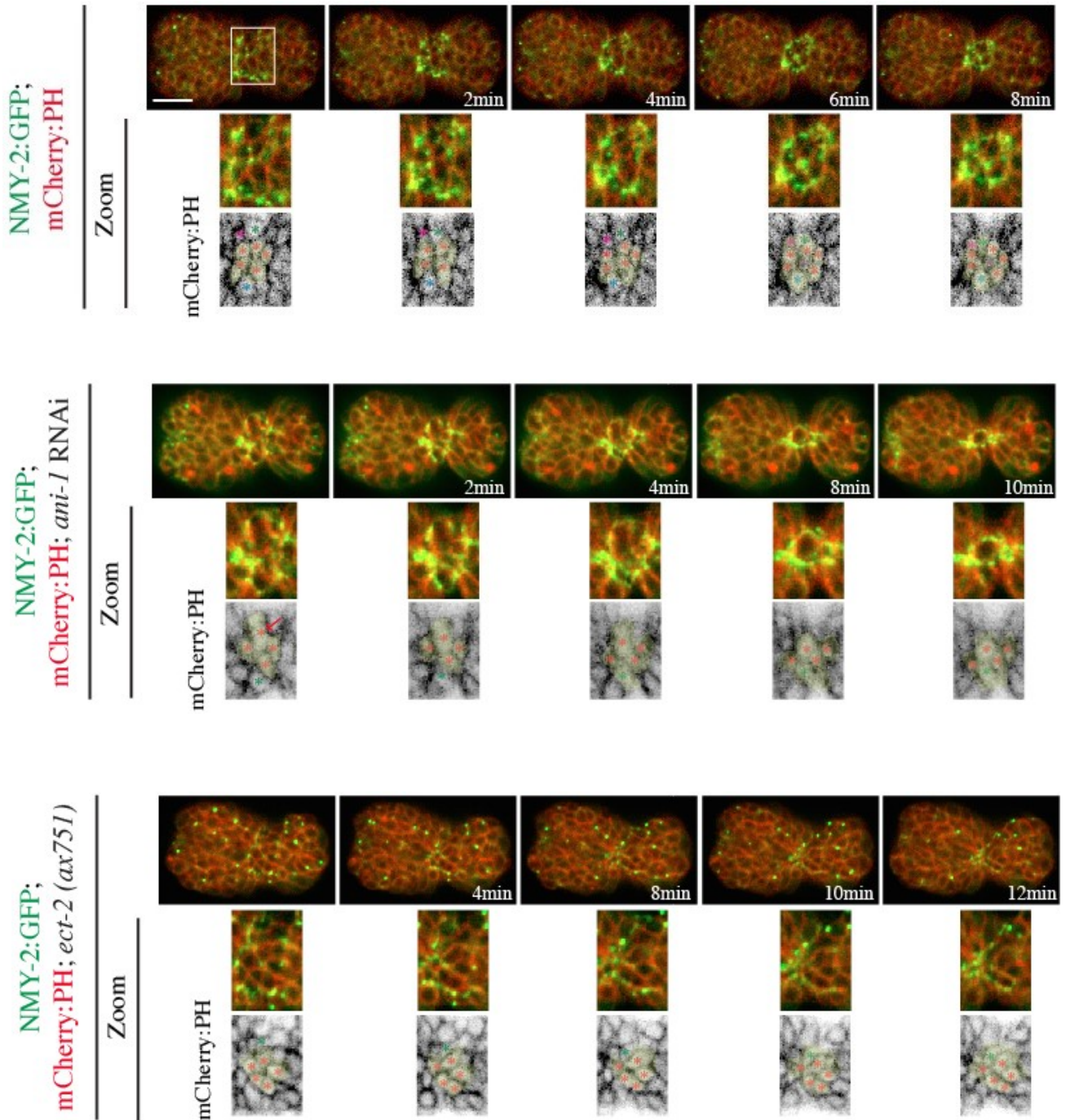
Figure 28. Neuroblasts arrange into rosette-like patterns during ventral enclosure. Images of NMY-2:GFP; mCherry:PH from control, *ani-1* RNAi and *ect-2 (ax751)* embryos are shown during ventral enclosure (9<n<11). Neuroblasts transiently form rosette-like patterns, with myosin enriched at a central vertex. The cells assembling into these patterns are highlighted in light yellow in the boxes showing zoomed in regions of the ventral pocket. The scale bar is 10 μm.

A
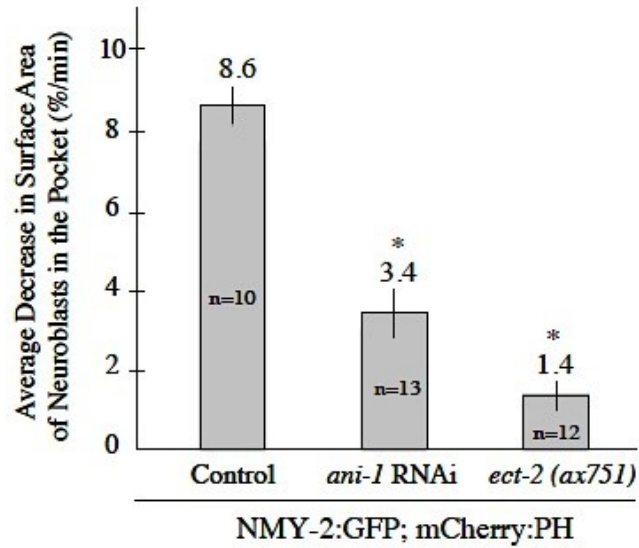
B
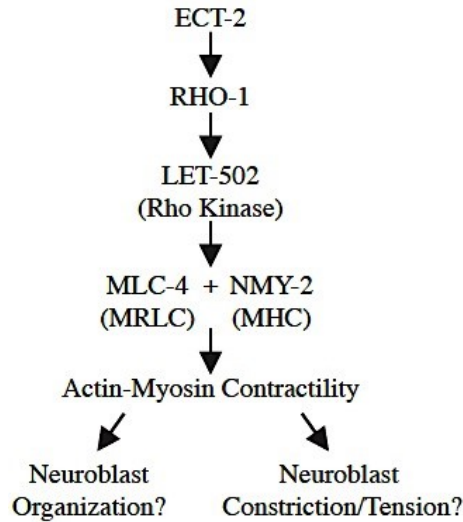
Figure 29. Neuroblasts shrink in surface area during ventral enclosure. A) A graph shows the average decrease (%/min) in the exposed surface area of neuroblasts in NMY-2:GFP; mCherry:PH control, *ani-1* RNAi and *ect-2 (ax751)* embryos (10<n(cells)<13 derived from n(embryos)=3-4/treatment). Bars show standard deviation, and * indicates $p<0.001$ vs. control by the student t-test. B) The molecular pathway regulating actin-myosin contractility in the neuroblasts is shown. This pathway could influence neuroblast organization, neuroblast constriction, or generate tension, all of which could contribute to ventral enclosure.

epidermal cells and neuroblasts were dependent on upstream regulators of myosin contractility. Interestingly, myosin is required in the neuroblasts for ventral enclosure, and a subset of these cells decrease their surface area as the overlying epidermal cells close. In *Drosophila*, mesodermal cells are interconnected via junctions to an extensive actin-myosin network with pulsatile contractility, which helps shrink the surface area of cells (Heisenberg and Bellaïche, 2013). We saw that the myosin foci in both neuroblasts and epidermal cells localize to patterns that appear to be dynamic and interconnected. In the neuroblasts, we observed the appearance of bright myosin foci within the pocket, which either pulsed or left the focal plane, and appeared to flow. The actin-myosin network in neuroblasts may either help constrict the neuroblasts, re-organize them, and/or generate tension (**Figure 29B**). Consistent with any of these possibilities, the surface area of neuroblasts fails to constrict after altering neuroblast shape or decreasing myosin activity, the neuroblasts are not as well-organized, and the overlying ventral epidermal cells fail to migrate properly. Even though different cell types are involved, we can make some analogies with dorsal closure in *Drosophila*, where the extraembryonic amnioserosa tissue is required for closure of the epidermis on the back of the embryo (Franke et al., 2005). During this process, extensive myosin contractility constricts the amnioserosal cells to decrease their surface area and influences contractility of the actin-myosin ring in the overlying dorsal epidermal cells (Franke et al., 2005).

We also saw that some of the neuroblasts that lie in the open pocket assemble into a rosette-like pattern. This pattern is highly transient, and occurs after cells first align in columns. In other organisms, rosettes are formed when five or more cells share a common vertex, and they act as intermediates in rearranging cells to elongate tissue during epithelial morphogenesis (Harding et al., 2014). The embryo elongates after ventral enclosure, and it is possible that the neuroblast tissue is re-organized prior to this event. However, it is interesting that the networks of

96

myosin appear to correlate with the rosette patterns, and one idea is that the rosettes help to organize myosin within the intercellular network.

Our data suggests that the neuroblasts can influence myosin localization in the overlying epidermal cells. We previously found that ANI-1 (anillin) is expressed predominantly in the neuroblasts, and is required for their division (Fotopoulos et al., 2013). In *ani-1*-depleted embryos, we observed the formation of large, multinucleate neuroblasts, and epidermal cells failed to migrate properly often resulting in their misalignment (Fotopoulos et al., 2013). We proposed that the abnormal neuroblasts may not present cues properly to the overlying epidermal cells, or the neuroblast tissue lacks sufficient tension for their migration. Here, we observed the asymmetric, uneven distribution of myosin in both the neuroblasts and epidermal cells in *ani-1*-depleted embryos. In the neuroblasts, myosin was not distributed evenly, and some of the cells failed to decrease in surface area, which may have caused some of the overlying epidermal cells to lag behind. Previous studies revealed that myosin accumulates in response to mechanical stress (Neujahr et al., 1997; Fernandez-Gonzalez et al., 2009). For example, during *Drosophila* germband extension, introducing ectopic forces using microaspiration induced the recruitment of myosin to the apical surface of cells (Fernandez-Gonzalez et al., 2009). One model is that since the epidermal cells are not uniformly pulled together, this could create uneven tension between epidermal cells. This uneven tension is sensed through adhesion junctions, and subsequently causes myosin to accumulate in cells with high mechanical tension, but not in cells with low tension (Neujahr et al., 1997; Kee and Robinson, 2008). Other studies have shown that actin-myosin activity in cells can change in response to changes in the rigidity of their environment, possibly via stretch-sensitive adhesion proteins (Fouchard et al., 2011). Thus, an alternative model is that tension differences in the underlying neuroblasts could lead to changes in myosin in the overlying epidermal cells, although it is not clear how the epidermal cells would sense this

change. Our studies show how changes in the mechanical properties of neuroblasts can influence the integrity of epidermal tissue during development, and should enhance our understanding of how multiple cell types are coordinated for epidermal morphogenesis in metazoans.

Chapter 4. Conclusion and Model

Tissue morphogenesis is crucial for the development of multicellular organisms and depends on the tight regulation of the actomyosin cytoskeleton, which mediates cell shape change, migration and adhesion – events that also drive the formation and metastasis of cancers (Schäfer and Werner, 2008; Friedl and Wolf, 2009). We study ventral enclosure, which is part of *C. elegans* epidermal morphogenesis, where epidermal cells change shape, migrate to and adhere at the ventral midline to encase the embryo in an epithelium (Chisholm and Hardin, 2005). The process begins with the migration of two pairs of anterior leading cells, followed by the closure of a ventral pocket formed from posterior pairs of ventral epidermal cells. It has been proposed that the neuroblasts, neuronal precursors positioned underneath the ventral epidermal cells, mediate pocket closure (Chin-Sang and Chisholm, 2000). Neuroblasts provide chemical guidance cues (*e.g.* ephrin, netrin) that influence F-actin organization and migration of the overlying ventral epidermal cells (Patel et al., 2008; Bernadskaya et al., 2013). However, it is not known whether neuroblasts, which are non-epithelial, also provide mechanical cues for ventral enclosure. Events that involve force generation (*e.g.* muscle contraction and mechanotransduction) occur in epithelial cells and cells with highly organized myosin, and few studies have explored this type of signaling in other tissues (Martin et al., 2009; Hobert, 2010; Zhang et al., 2011). This thesis elucidates a role for myosin-based contractility in neuroblasts during ventral enclosure. Based on our findings, we propose a model where mechanical forces are orchestrated between two tissues (epidermis vs. neuroblasts) to drive epidermal morphogenesis.

In Chapter 2, we describe a role for the RhoA effector and actin-myosin binding protein anillin (ANI-1) in ventral enclosure. We found that ANI-1 strongly accumulates in a subset of neuroblasts that line the ventral pocket during its closure (**Figure 12**). Loss of ANI-1 causes ventral enclosure phenotypes where the ventral epidermal cells migrate only partially, or migrate to the midline, but are misaligned, causing embryos to rupture (**Figure 11 and 15**). These phenotypes likely are due to a requirement for *ani-1* in the neuroblasts, because in *ani-1* RNAi embryos, neuroblasts, but not the epidermal cells, fail cytokinesis, and often exhibit abnormal shapes (**Figure 14**; Fotopoulos et al., 2013). Hence, we propose that *ani-1* functions in the neuroblasts to non-autonomously regulate the migration of the overlying ventral epidermal cells.

In Chapter 3, we showed for the first time that active non-muscle myosin (*nmy-2*) is required for ventral enclosure. A decrease in NMY-2 function using either a loss-of-function allele, or a chemical inhibitor caused a delay or partial failure in ventral epidermal cell migration (**Figure 23**). We found that myosin localizes as foci to the junction-free edges of ventral epidermal cells in a pattern that is reminiscent of the previously described supra-cellular F-actin ring, suggesting that the pocket closes via a contractile, purse string-like mechanism (**Figures 20 and 21**; Williams-Mason et al., 1997). In addition, we found that myosin localizes into highly dynamic star-like patterns in the neuroblasts during pocket closure (**Figure 22**). We propose that myosin activity is regulated via the RhoA pathway during ventral enclosure, since loss-of-function mutations in RhoA pathway components phenocopy loss of myosin, and myosin intensity is reduced in Rho pathway mutant embryos (**Figures 24 and 25**). In addition, our genetic data is consistent with myosin functioning in the RhoA pathway for ventral enclosure (**Tables 1 and 2**).

Showing a requirement for myosin in the neuroblasts raises an interesting question about whether these cells provide mechanical forces for successful ventral enclosure. Since ANI-1 is

expressed in neuroblasts, it would be interesting to know if ANI-1 can also function outside of cytokinesis to help organize actomyosin in these cells. Although anillin is best known most for its role in stabilizing the contractile ring during cytokinesis, recent studies showed that anillin is required for maintenance of the actomyosin belt in *Xenopus* epithelial cells to ensure tissue integrity (Piekny and Glotzer, 2008; Reyes et al., 2014). In support of this idea, we found that depleting ANI-1 causes myosin foci to be distributed more asymmetrically around the ventral pocket in both the epidermal cells and the neuroblasts (**Figure 26**). Also, while myosin foci associated with the neuroblasts often pulsed and moved toward the ventral midline in control embryos, they were static with fewer pulses and flows in *ani-1* RNAi embryos (**Figure 22**). Thus, we hypothesize that *ani-1* is required for myosin organization and dynamics during ventral enclosure. Since myosin foci in the ventral epidermal cells change in response to loss of *ani-1* in the neuroblasts, this suggests that the ventral epidermal cells may mechanosense forces in the underlying neuroblasts during ventral enclosure, which may reflect a common theme on how adjacent tissues interact on a mechanical level to drive tissue and organ development in higher metazoans.

The forces generated by myosin in the neuroblasts may be required to reorganize these cells during ventral enclosure. During pocket closure, we found that a dynamic star-like pattern of myosin in the neuroblasts coincides with their re-organization into a rosette where at least 5 cells share a common vertex (**Figure 28**). The apical surface of these neuroblasts decreases as the ventral pocket closes, which fails in *ani-1* RNAi or *ect-2* (RhoA GEF) mutant embryos. In addition, while rosettes fail to form in *ani-1* RNAi embryos or severe *ect-2* mutant embryos, they form, but fail to re-organize in mild *ect-2* mutant embryos (**Figure 29**). These results suggest that myosin activity is required for changing neuroblast shape and their organization. However, it is not clear if these events are required for pocket closure. During *Drosophila* dorsal closure, when

the epidermal cells migrate over the dorsal surface of the embryo, the underlying amnioserosal cells are contractile and pulsate to help draw the overlying epidermal cells together (Jacinto et al., 2002A; 2002B). However, the amnioserosal cells are non-embryonic epithelial cells, which raises questions about how contractility is generated and transmitted in non-epithelial cell types, such as the neuroblasts, when they lack force-transmitting junctions commonly found in epidermal cells. For example, neuroblast contractility could be associated with their apical constriction and ingression, similar to mesoderm ingression during *Drosophila* and *C. elegans* gastrulation (Nance et al., 2005). During gastrulation, pulsatile centripetal flows of changing myosin amplitude are translated into apical constriction. This occurs via the coupling of the supracellular myosin network to junctions, which serves as a clutch to transmit forces and can stabilize periodic changes in cell shape though a ratchet-like mechanism (Solon et al., 2009: Martin et al., 2010; Pohl et al., 2012; Roh-Johnson et al., 2012). For this mechanism to apply to neuroblasts, they require junctions to transmit forces into changes in cell shape. Recent studies in human glial cells and astrocytes determined that low levels of N-cadherin correlate with an increased migration capacity of these cells, which could indicate that N-cadherin is involved in mediating cell shape changes required for adhesion and/or migration (Camand et al., 2012). Also, previous studies showed that there is an isoform of cadherin analogous to N-cadherin, which is expressed in the neuroblasts (Broadband and Pettitt, 2002). We also found that α-catenin/HMP-1 is expressed in the neuroblasts during ventral enclosure and localizes in a star-like pattern reminiscent of myosin (data not shown). Therefore, this data suggests that junctions could form between non-epidermal cells, where they could function to organize and transmit actomyosin contractility for cell shape changes.

We propose a model where the neuroblasts influence ventral enclosure by promoting myosin localization to the junction free edges of the overlying epidermal cells (**Figure 30**).

Wild-type

ect-2 (ax751)

ani-1 RNAi

	Epidermal cell		F-actin
	Neuroblast	←	Direction of movement
	Myosin		Reduction in cell surface/shrinkage
	α-catenin		Mechanosensing ?
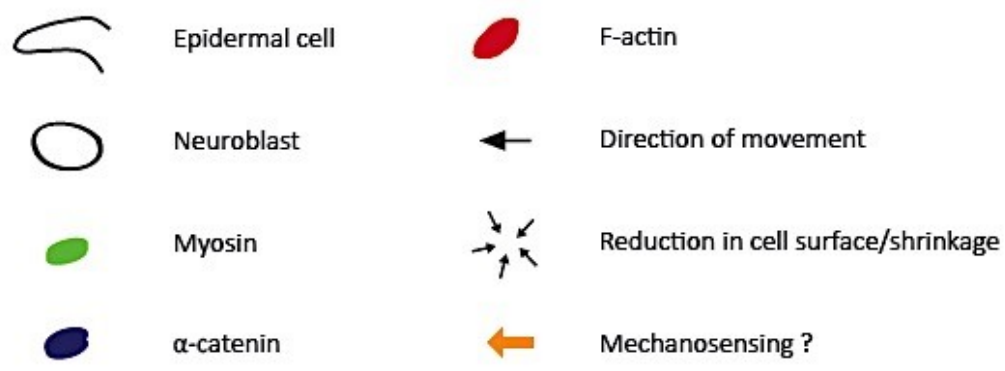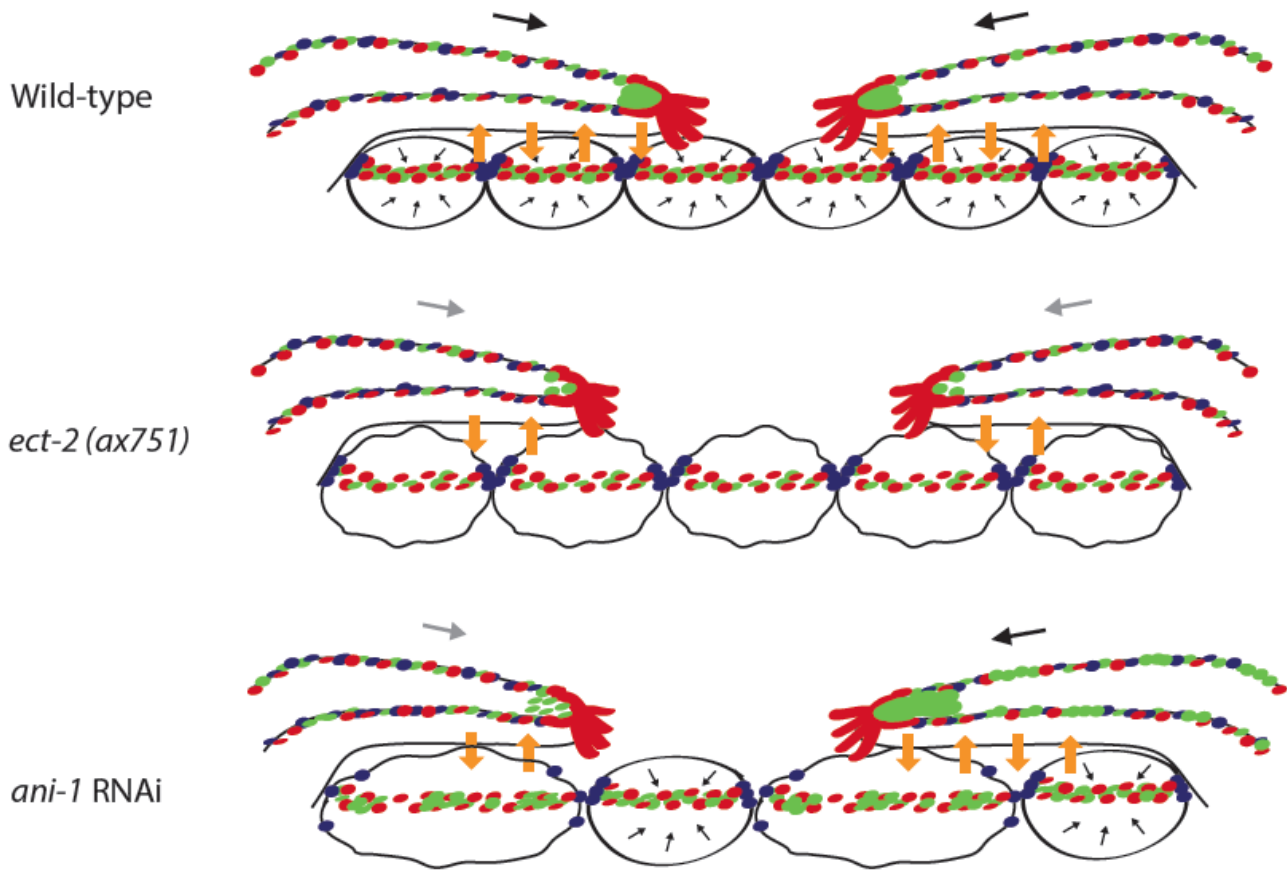
Figure 30. Model for myosin-based mechanosensing during *C. elegans* ventral enclosure. Schematic overview of the interplay between epidermal cells and neuroblasts during *C. elegans* ventral enclosure in wild-type, *ect-2 (ax751)* and *ani-1* RNAi mutant embryos. In the wild-type, neuroblasts are of spherical shape and accumulate proper amounts of myosin. We propose that this creates tension and/or contractility in the neuroblasts, which helps them reduce their surface area (small black arrows). Further, this tension/contractility can be sensed by the overlying epidermal cells, resulting in myosin accumulation there, and their forward movement. In turn, stronger myosin accumulation in the epidermal cells could help signal back to the neuroblasts, thereby promoting myosin to accumulate more strongly in both tissues (feedback loop) as ventral enclosure progresses. In *ect-2* mutants, myosin foci are reduced in both tissues. This may cause less tension/contractility in the neuroblasts, which would interfere with their ability to signal to the epidermal cells, hence leading to an even dampened myosin accumulation in epidermal cells and slower migration rates. In *ani-1* RNAi embryos, neuroblasts are multinucleate due to failed division, and exhibit abnormal shapes, causing myosin to accumulate unevenly in the neuroblasts. This, in turn, causes an improper distribution of myosin in the epidermal cells, and is associated with lower migration rates of epidermal cells in regions with less myosin levels in the neuroblasts versus faster rates in regions with higher myosin levels.

Although we did not investigate whether there are rosettes forming during leading edge cell migration or whether there are several distinct rosettes versus one rosette that transitions as ventral enclosure progresses, we propose that the supracellular distribution of myosin is coordinated between a subset of neuroblasts in the ventral pocket for their re-organization to mediate changes in their shape during ventral enclosure. These events create changes in tension in the ventral pocket that is sensed by the overlying epidermal cells and causes myosin to accumulate along their junction-free edges (Neujahr et al., 1997; Fernandez-Gonzalez et al., 2009). It would be interesting to know if there is feedback between the two tissues, where accumulated myosin in the epidermal cells could, in turn, enhance myosin accumulation in the neuroblasts. For example, this theory could be tested by disrupting ventral epidermal cell migration in 'gex' mutants and observing whether rosettes still form with their typical star-like myosin patterns. Further, it would be intriguing to elucidate if myosin activity along with neuroblast re-organization is calcium-dependent. Since both myosin phosphorylation (via increased MLCK activity) and adhesion (via increased E-cadherin activity) were shown to require calcium (Mizuno et al., 2008; Tu et al., 2008), it would be interesting to investigate whether reduced levels of calcium could phenocopy ventral enclosure defects as observed in myosin mutant embryos.

Taken together, our studies demonstrate how changes in the mechanical properties of neuroblasts can influence the integrity of epidermal tissue during development, which can help shed light on how multiple cell types are coordinated for epidermal morphogenesis in metazoans.

Chapter 5. References

Akhshi, T.K., Wernike, D. and Piekny, A.J., 2013. **Microtubules and actin crosstalk in cell migration and division**. Cytoskeleton (Hoboken) 71: 1-23.

Amann, K.J. and Pollard, T.D., 2001. **Direct real-time observation of actin filament branching mediated by Arp2/3 complex using total internal reflection microscopy**. PNAS USA 98: 15009–15013.

Arber, S., Barbayannis, F.A., Hanser, H., Schneider, C., Stanyon, C.A., Bernard, O., et al., 1998. **Regulation of actin dynamics through phosphorylation of cofilin by LIM-kinase**. Nature 393: 805-809.

Armenti, S.T. and Nance, J., 2012. **Adherens junctions in *C. elegans* morphogenesis**. Subcell Biochem 60: 279-299.

Azevedo, D., Antunes, M., Prag, S., Ma, X., Hacker, U., Brodland, G.W., et al., 2011. **DRhoGEF2 regulates cellular tension and cell pulsations in the Amnioserosa during *Drosophila* dorsal closure**. PLoS One 6: e23964.

Bastos, R.N., Penate, X., Bates, M., Hammond, D. and Barr, F., 2012. **CYK4 inhibits Rac1-dependent PAK1 and ARHGEF7 effector pathways during cytokinesis**. J Cell Biol 198: 865-880.

Benink, H.A. and Bement, W.M., 2005. **Concentric zones of active RhoA and Cdc42 around single cell wounds**. J Cell Biol 168: 429-439.

Bernadskaya, Y.Y., Wallace, A., Nguyen, J., Mohler, W.A. and Soto, M.C., 2012. **UNC-40/DCC, SAX-3/Robo, and VAB-1/Eph polarize F-actin during embryonic morphogenesis by regulating the WAVE/SCAR actin nucleation complex**. PLoS Genet 8: e1002863.

Bloor, J.W. and Kiehart, D.P., 2002. ***Drosophila* RhoA regulates the cytoskeleton and cell-cell adhesion in the developing epidermis**. Development 129: 3173-3183.

Bos, J.L., Rehmann, H. and Wittinghofer, A., 2007. **GEFs and GAPs: Critical elements in the control of small G proteins**. Cell 129: 865-877.

Brenner. S., 1974. **The genetics of *Caenorhabditis elegans***. Genetics 77, 71-94.

Broadband, I.D. and Pettitt, J., 2002. **The *C. elegans hmr-1* gene can encode a neuronal classic cadherin involved in the regulation of axon fasciculation**. Curr Biol 12: 69-63.

Bülow, H.E., Berry, K.L., Topper, L.H., Peles, E. and Hobert, O., 2002. **Heparan sulfate proteoglycan-dependent induction of axon branching and misrouting by the Kallmann syndrome gene *kal-1***. PNAS 99: 6346-6351.

Calixto, A., Chelur, D., Topalidou, I., Chen. X. and Martin, C., 2010. **Enhanced neuronal RNAi in *C. elegans* using SID-1**. Nat Methods 7: 554-559.

Camand, E., Peglion, F., Osmani, N., Sanson, M. and Etienne-Manneville, S., 2012. **N-cadherin expression level modulates integrin-mediated polarity and strongly impacts on the speed and directionality of glial cell migration.** J Cell Sci 125: 844-857.

Canevascini, S., Marti, M., Frohli, E. and Hajnal, A., 2005. **The *Caenorhabditis elegans* homologue of the proto-oncogene *ect-2* positively regulates RAS signalling during vulval development**. EMBO Rep 6: 1169-1175.

Champellone, K.G. and Welch, M.D., 2010. **A nucleator arms race: cellular control of actin assembly**. Nat Rev Mol Cell Biol 11: 237-251.

Chan, B., Rocheleau, S.K., Smit, R.B. and Mains, P.E., 2015. **The Rho guanine exchange factor RHGF-2 acts through the Rho-binding kinase LET-502 to mediate embryonic elongation in *C. elegans*.** Dev Biol 405: 250-259.

Chan, E. and Nance, J., 2013. **Mechanisms of CDC-42 activation during contact-induced cell polarization**. J Cell Sci 126: 1692-1702.

Chesarone, M.A., and Goode, B.L., 2009. **Actin nucleation and elongation factors: mechanisms and interplay**. Curr Opin Cell Biol 21: 28-37.

Chin-Sang, I.D., George, S.E., Ding, M., Moseley, S.L., Lynch, A.S. and Chisholm, A.D., 1999. **The ephrin VAB-2/EFN-1 functions in neuronal signaling to regulate epidermal morphogenesis in *C. elegans***. Cell 99: 781-790.

Chin-Sang, I.D. and Chisholm, A.D., 2000. **Form of the worm: genetics of epidermal morphogenesis in *C. elegans*.** Trends Genetics 16: 544-551.

Chin-Sang, I.D., Moseley, S.L., Ding, M., Harrington, R.J., George, S.E. and Chisholm, A.D., 2002. **The divergent *C. elegans* ephrin EFN-4 functions in embryonic morphogenesis in a pathway independent of the VAB-1 Eph receptor**. Development 129: 5499-5510.

Chisholm, A.D. and Hardin, J., 2005. **Epidermal morphogenesis**. WormBook: the online review of *C. elegans* biology: 1-22.

Clark, A.G., Miller, A.L., Vaughan, E., Yu, H.Y., Penkert, R. and Bement. W.M., 2009. **Integration of single and multicellular wound responses**. Curr Biol 19: 1389-1395.

Costa, M., Raich, W., Agbunag, C., Leung, B., Hardin, J. and Priess, J.R., 1998. **A putative catenin-cadherin system mediates morphogenesis of the *Caenorhabditis elegans* embryo**. J Cell Biol 141: 297-308.

Davies, T., Jordan, S.N., Chand, V., Sees, J.A., Laband, K., Carvalho, A.X., et al., 2014. **High-resolution temporal analysis reveals a functional timeline for the molecular regulation of cytokinesis**. Dev Cell 30: 209-223.

Davies, T. and Canman, J.C., 2012. **Stuck in the middle: Rac, adhesion and cytokinesis**. J Cell Biol 198: 769-771.

Dickinson, D.J., Ward, J.D., Reiner, D.J. and Goldstein, B., 2013. **Engineering the *Caenorhabditis elegans* genome using Cas9-triggered homologous recombination**. Nat Methods 10: 1028-1034.

Diogon, M., Wissler, F., Quintin, S., Nagamatsu, Y., Sookhareea, S., Landmann, F., et al., 2007. **The RhoGAP RGA-2 and LET-502/ROCK achieve a balance of actomyosin-dependent forces in *C. elegans* epidermis to control morphogenesis**. Development 134: 2469-2479.

Dorn, J.F., Zhang, L., Paradis, V., Edoh-Bedi, D., Jusu, S., Maddox, P.S., et al., 2010. **Actomyosin tube formation in polar body cytokinesis requires Anillin in *C. elegans***. Curr Biol 20: 2046-2051.

Dvorsky, R. and Ahmadian, M.R., 2004. **Always look on the bright site of Rho: structural implications for a conserved intermolecular interface**. EMBO Rep 12: 1130-1136.

Edwards, D.C., Sanders, L.C., Bockoch, G.M. and Gill, G.N., 1999. **Activation of LIM-kinase by Pak1 couples Rac/Cdc42 GTPase signalling to actin cytoskeletal dynamics**. Nat Cell Biol 1: 253-259.

Fernandez-Gonzalez, R., Simoes Sde, M., Röper, J.C., Eaton, S. and Zallen, J.A., 2009. **Myosin II dynamics are regulated by tension in intercalating cells**. Dev Cell 17: 736-743.

Field, C.M., Coughlin, M., Doberstein, S., Marty, T. and Sullivan, W., 2005. **Characterization of anillin mutants reveals essential roles in septin localization and plasma membrane integrity**. Development 132: 2849-2860.

Fields, A.P. and Justilien, V., 2010. **The guanine nucleotide exchange factor (GEF) Ect2 is an oncogene in human cancer**. Adv Enzyme Reg 50: 190-200.

Fire, A., Xu, S., Montgomery., M.K., Kostas, S.A., Driver, S.E. and Mello, C.C., 1998. **Potent and specific genetic interference by double-stranded RNA in *Caenorhabditis elegans***. Nature 391: 806-811.

Firestein, B.L. and Rongo, C., 2001. **DLG-1 is a MAGUK similar to SAP97 and is required for adhesion junction formation**. Mol Biol Cell 12: 3465-3475.

Fotopoulos, N., Wernike, D., Chen, Y., Makil, N., Marte, A. and Piekny, A., 2013. ***Caenorhabditis elegans* anillin (*ani-1*) regulates neuroblast cytokinesis and epidermal morphogenesis during embryonic development**. Dev Biol 383: 61-74.

Fouchard, J., Mitrossilis, D. and Asnacios, A., 2011. **Actomyosin based response to stiffness and rigidity sensing**. Cell Adh Migr 5: 16-19.

Franke, J.D., Montague, R.A. and Kiehart, D.P., 2005. **Nonmuscle myosin II generates forces that transmit tension and drive contraction in multiple tissues during dorsal closure**. Curr Biol 15: 2208-2221.

Fraser, A.G., Kamath, R.S., Zipperlen, P., Martinez-Campos, M., Sohrmann, M. and Ahringer, J., 2000. **Functional genomic analysis of *C. elegans* chromosome I by systematic RNA interference**. Nature 408: 325-330.

Friedl, P. and Wolf, K., 2009. **Proteolytic interstitial cell migration: a five-step process**. Cancer Metastasis Rev 28: 129-135.

Gally, C., Wissler, F., Zahreddine, H., Quintin, S., Landmann, F. and Labouesse, M., 2009. **Myosin II regulation during *C. elegans* embryonic elongation: LET-502/ROCK, MRCK-1 and PAK-1, three kinases with different roles**. Development 136: 3109-3119.

George, S.E., Simokat, K., Hardin, J. and Chisholm, A.D., 1998. **The VAB-1 Eph receptor tyrosine kinase functions in neural and epithelial morphogenesis in *C. elegans***. Cell 92: 633-643.

Ghenea, S., Boudreau, J.R., Lague, N.P. and Chin-Sang, I.D., 2005. **The VAB-1 Eph receptor tyrosine kinase and SAX-3/Robo neuronal receptors function together during *C. elegans* embryonic morphogenesis**. Development 132: 3679-3690.

Gitai, Z., Yu, T.W., Lundquist, E.A., Tessier-Lavigne, M. and Bargmann, C.I., 2003. **The netrin

receptor UNC-40/DCC stimulates axon attraction and outgrowth through enabled and, in parallel, Rac and UNC-115/AbLIM**. Neuron 37: 53-65.

Giurumescu, C.A., Kang, S., Planchon, T.A., Betzig, E., Bloomekatz, J., Yelon, D., et al., 2012. **Quantitative semi-automated analysis of morphogenesis with single-cell resolution in complex embryos**. Development 139: 4271-4279.

Glotzer, M. 2001. **Animal cytokinesis**. Annu Rev Cell Dev Biol 17: 351-386.

Goldbach, P., Wong, R., Beise, N., Sarpal, R., Trimble, W.S. and Brill, J.A., 2010. **Stabilization of the actomyosin ring enables spermatocyte cytokinesis in *Drosophila***. Mol Biol Cell 21: 1482-1493.

Goley, E.D. and Welch, M.D., 2006. **The ARP2/3 complex: an actin nucleator comes of age**. Nat Rev Mol Cell Biol 7: 713-726.

Goode, B.L. and Eck, M.J., 2007. **Mechanism and function of formins in the control of actin assembly**. Annu Rev Biochem 76: 593-627.

Grose, R. and Martin, P., 1999. **Parallels between wound repair and morphogenesis in the embryo**. Semin Cell Dev Biol 10: 395-404.

Guenther, C. and Garriga, G., 1996. **Asymmetric distribution of the *C. elegans* HAM-1 protein in neuroblasts enables daughter cells to adopt distinct fates**. Development 122: 3509-3518.

Guo, S. and Kemphues, K.J., 1996. **A non-muscle myosin required for embryonic polarity in *Caenorhabditis elegans***. Nature 382: 455-458.

Halbleib, J.M. and Nelson, W.J., 2006. **Cadherins in development: cell adhesion, sorting, and tissue morphogenesis**. Genes Dev 20: 3199-3214.

Hall, D.H. and Altun, Z., 2008. *C. elegans* **Atlas**. Cold Spring Harbor Laboratory Press, New York: pp348.

Hardin, J., King, R., Thomas-Virnig, C. and Raich, W.B., 2008. **Zygotic loss of ZEN-4/MKLP1 results in disruption of epidermal morphogenesis in the *C. elegans* embryo**. Dev Dyn 237: 830-836.

Harding, M.J., McGraw, H.F. and Nechiporuk, A., 2014. **The roles and regulation of multicellular rosette structures during morphogenesis**. Development 141: 2549-2558.

Harrington, R.J., Gutch, M.J., Hengartner, M.O., Tonks, N.K. and Chisholm, A.D., 2002. **The *C. elegans* LAR-like receptor tyrosine phosphatase PTP-3 and the VAB-1 Eph receptor tyrosine kinase have partly redundant functions in morphogenesis**. Development 129: 2141-2153.

Harris, T.J. and Tepass, U., 2010. **Adherens junctions: from molecules to morphogenesis**. Nature Rev Mol Cell Biol 11: 502-514.

Heisenberg, C.P. and Bellaïche, Y., 2013. **Forces in tissue morphogenesis and patterning**. Cell 153: 948-962.

Hickson, G.R. and O'Farrell, P.H., 2008. **Rho-dependent control of anillin behavior during cytokinesis**. J Cell Biol 180: 285-294.

Higashida, C., Miyoshi, T., Fujita, A., Oceguera-Yanez, F., Monypenny, J., Andou, Y., et al. 2004. **Actin polymerization-driven molecular movement of mDia1 in living cells**. Science 303: 2007-2010.

Hresko, M.C., Williams, B.D. and Waterston, R.H., 1994. **Assembly of body wall muscle and muscle cell attachment structures in _Caenorhabditis elegans_**. J Cell Biol 124: 491–506.

Hudson, M.L., Kinnunen, T., Cinar, H.N. and Chisholm, A.D., 2006. **_C. elegans_ Kallmann syndrome protein KAL-1 interacts with syndecan and glypican to regulate neuronal cell migrations**. Dev Biol 294: 352-365.

Ikegami, R., Simokat, K., Zheng, H., Brown, L., Garriga, G., Hardin, J., et al., 2012. **Smaphorin and Eph receptor signaling guide a series of cell movements for ventral enclosure in _C. elegans_**. Curr Biol 22: 1-11.

Jacinto, A., Wood, W., Woolner, S., Hiley, C., Turner, L., Wilson, C., et al., 2002B. **Dynamic analysis of actin cable function during *Drosophila* dorsal closure**. Curr Biol 12: 1245-1250.

Jacinto, A., Woolner, S. and Martin, P., 2002A. **Dynamic analysis of dorsal closure in *Drosophila*: from genetics to cell biology**. Dev Cell 3: 9-19.

Jankovics, F., Henn, L., Bujna, A., Vilmos, P., Kiss, N. and Erdélyi, M., 2011. **A functional genomic screen combined with time-lapse microscopy uncovers a novel set of genes involved in dorsal closure of Drosophila embryos**. PLoS One 6: e22229.

Justilien, V. and Fields, A.P., 2009. **Ect2 links the PKCiota-Par6alpha complex to Rac1 activation and cellular transformation**. Oncogene 28: 3597-3607.

Kamath, R.S., Fraser, A.G., Dong, Y., Poulin, G., Durbin, R., Gotta, M., et al., 2003. **Systematic functional analysis of the *Caenorhabditis elegans* genome using RNAi**. Nature 421: 231-237.

Kee, Y.S. and Robinson, D.N., 2008. **Motor proteins: myosin mechanosensors**. Curr Biol 18: R860-862.

Kiehart, D.P., Galbraith, C.G., Edwards, K.A., Rickoll, W.L. and Montague, R.A., 2000. **Multiple forces contribute to cell sheet morphogenesis for dorsal closure in *Drosophila***. J Cell Biol. 149: 471-490.

Kimura, K., Tsuji, T., Takada, Y., Miki, T. and Narumiya, S., 2000. **Accumulation of GTP-bound RhoA during cytokinesis and a critical role of ECT2 in this accumulation**. J Biol Chem 275: 17233-17236.

Kobielak, A. and Fuchs, E., 2004. **Alpha-catenin: at the junction of intracellular adhesion and actin dynamics**. Rev Mol Cell Biol 5: 614-625.

Köppen, M., Simske, J.S., Sims, P.A., Firestein, B.L., Hall, D.H., Radice, A.D., et al., 2001. **Cooperative regulation of AJM-1 controls junctional integrity in *Caenorhabditis elegans* epithelia**. Nat Cell Biol 3: 983-991.

Labouesse, M., 2006. **Epithelial junctions and attachments**. WormBook: the online review of *C. elegans* biology: 1-21.

Lee, J.Y., Marston, D.J., Walston, T., Hardin, J., Halberstadt, A. and Goldstein, B., 2009. **Wnt/Frizzled signaling controls C. elegans gastrulation by activating actomyosin contractility**. Curr Biol 16: 1986-1997.

Lee, J.Y. and Goldstein, B., 2003. **Mechanisms of cell positioning during *C. elegans* gastrulation**. Development 130: 307-320.

Lepage, S.E. and Bruce, A.E., 2010. **Zebrafish epiboly: mechanics and mechanisms**. Int J Dev Biol 54: 1213-1228.

Lin, L., Tran, T., Hu, S., Cramer, T., Komuniecki, R. and Steven, R.M., 2012. **RHGF-2 is an essential Rho-1 specific RhoGEF that binds to the multi-PDZ domain scaffold protein MPZ-1 in *Caenorhabditis elegans***. PLoS One 7: e31499.

Liu, J., Fairn, G.D., Ceccarelli, D.F., Sicheri, F. and Wilde, A., 2012. **Cleavage furrow organization requires PIP(2)-mediated recruitment of anillin**. Curr Biol 22: 64-69.

Loria, A., Longhini, K.M. and Glotzer, M., 2012. **The RhoGAP domain of CYK-4 has an essential role in RhoA activation**. Curr Biol 22: 213-219.

Lu, Y. and Settleman, J., 1999. **The *Drosophila* Pkn protein kinase is a Rho/Rac effector target required for dorsal closure during embryogenesis**. Genes Dev 13: 1168-1180.

Lundquist, E.A., Reddien, P.W., Hartwieg, E., Horvitz, H.R., and Bargmann, C.I., 2001. **Three *C. elegans* Rac proteins and several Rac regulators control axon guidance, cell migration and apoptotic phagocytosis**. Development 128: 4475-4488.

Maddox, A.S., Habermann, B., Desai, A. and Oegema, K., 2005. **Distinct roles for two *C. elegans* anillins in the gonad and early embryo**. Development 132: 2837-2848.

Maddox, A.S., Lewellyn, L., Desai, A. and Oegema, K., 2007. **Anillin and the septins promote asymmetric ingression of the cytokinetic furrow**. Dev Cell 12: 827-835.

Magie, C.R., Meyer, M.R., Gorusch, M.S., and Parkhurst, S.M., 1999. **Mutations in the Rho1 small GTPase disrupt morphogenesis and segmentation during early *Drosophila* development**. Development 126: 5353-5364.

Maiden, S.L., Harrison, N., Keegan, J., Cain, B., Lynch, A.M., Pettitt, J., et al., 2013. **Specific conserved C-terminal amino acids of *Caenorhabditis elegans* HMP-1/□-catenin modulate F-actin binding independently of vinculin**. J Biol Chem 288: 5694-5706.

Mains, P.E., Kemphues, K.J., Sprunger, S.A., Sulston, I.A. and Wood, W.B., 1990. **Mutations affecting the meiotic and mitotic divisions of the early *Caenorhabditis elegans* embryo**. Genetics 126: 593-605.

Martin, A.C., Gelbart, M., Fernandez-Gonzalez, R., Kaschube, M. and Wieschaus, E.F., 2010. **Integration of contractile forces during tissue invagination**. J Cell Biol 188: 735-749.

Martin, P. and Lewis, J., 1992. **Actin cables and epidermal movement in embryonic wound healing**. Nature 360: 179-183.

Martin, E., Harel, S., Nkengfac, B., Hamiche, K., Neault, M, and Jenna, S., 2014. ***pix-1* controls early elongation in parallel with *mel-11* and *let-502* in *Caenorhabditis elegans***. PLoS One 9: e94684.

Martin, P. and Parkhust, S.M., 2004. **Parallels between tissue repair and embryo morphogenesis**. Development 131: 3021-3034.

Mason, F.M., Tworoger, M. and Martin, A.C., 2013. **Apical domain polarization localizes actin-myosin activity to drive ratchet-like apical constriction**. Nat Cell Biol 15: 926-936.

Matsumura, F., 2005. **Regulation of myosin II during cytokinesis in higher eukaryotes**. Trends Cell Biol 15: 371-377.

Matsumura, F. and Hartshorne, D.J., 2008. **Myosin phosphatase target subunit: Many roles in cell function**. Biochem Biophysic Res Comm 369: 149-156.

McMahon, L., Legouis, R., Vonesch, J.L. and Labouesse, M., 2001. **Assembly of *C. elegans* apical junctions involves positioning and compaction by LET-413 and protein aggregation by the MAGUK protein DLG-1**. J Cell Sci 114: 2265-2277.

Miki, T., Smith, C.L., Long, J.E., Eva, A. and Fleming, T.P., 1993. **Oncogene *ect2* is related to regulators of small GTP-binding proteins**. Nature 362: 462-465.

Mizuno, Y., Isotani, E., Huang, J., Ding, H., Stull, J.T. and Kamm, K.E., 2008. **Myosin light chain kinase activation and calcium sensitization in smooth muscle in vivo.** Am J Physiol Cell Physiol 295: C358-364.

Morel, V. and Arias, A.M., 2004. **Armadillo/beta-catenin-dependent Wnt signalling is required for the polarisation of epidermal cells during dorsal closure in *Drosophila*.** Development 131: 3273-3283.

Morita, K., Hirono, K. and Han, M., 2005. **The *Caenorhabditis elegans* ect-2 RhoGEF gene regulates cytokinesis and migration of epidermal P cells**. EMBO Rep 6: 1163-1168.

Nalbant, P., Chang, Y.C., Birkenfeld, J., Chang, Z.F. and Bokoch, G.M., 2009. **Guanine nucleotide exchange factor-H1 regulates cell migration via localized activation of RhoA at the leading edge**. Mol Biol Cell 20: 4070-82.

Nance, J., Munro, E.M., and Priess, J.R., 2003. ***C. elegans* PAR-3 and PAR-6 are required for apicobasal asymmetries associated with cell adhesion and gastrulation**. Development 130: 5339-5350.

Nance, J. and Priess, J.R., 2002. **Cell polarity and gastrulation in *C. elegans***. Development 129: 387-397.

Neujahr, R., Heizer, C., Albrecht, R., Ecke, M., Schwartz, J.M., Weber, I., et al., 1997. **Three-dimensional patterns and redistribution of myosin II and actin in mitotic Dictyostelium cells**. J Cell Biol 139: 1793-1804.

Nichimura, T. and Takeichi, M., 2009. **Remodeling of the adherens junctions during morphogenesis**. Curr Top Cell Biol 89: 33-54.

Niessen, C.M. and Gumbiner, B.M., 2002. **Cadherin-mediated cell sorting not determined by binding or adhesion specificity**. J Cell Biol 156: 389-399.

Niu, W., Lu, Z.J., Zhong, M., Sarov, M., Murray, J.I., Brdlik, C.M., et al., 2011. **Diverse transcription factor binding features revealed by genome-wide ChIP-seq in *C. elegans***. Genome Res 21: 245-254.

Patel, F.B., Bernadskaya, Y.Y., Chen, E., Jobanputra, A., Pooladi, Z., Freeman, K.L., et al., 2008. **The WAVE/SCAR complex promotes polarized cell movements and actin enrichment in epithelia during *C. elegans* embryogenesis**. Dev Biol 324: 297-309.

Pettitt, J., Cox, E.A., Broadbent, I.D., Flett, A. and Hardin, J., 2003. **The *Caenorhabditis elegans* p120 catenin homologue, JAC-1, modulates cadherin-catenin function during epidermal morphogenesis**. J Cell Biol 162: 15-22.

Piekny, A.J., Wissmann, A. and Mains, P.E., 2000. **Embryonic morphogenesis in *Caenorhabditis elegans* integrates the activity of LET-502 Rho-binding kinase, MEL-11 myosin phosphatase, DAF-2 insulin receptor and FEM-2 PP2c phosphatase**. Genetics 156: 1671-1689.

Piekny, A.J. and Mains, P.E., 2002. **Rho-binding kinase (LET-502) and myosin phosphatase (MEL-11) regulate cytokinesis in the early *Caenorhabditis elegans* embryo**. J Cell Sci 115: 2271-2282.

Piekny, A.J., Johnson, J.L., Cham, G.D. and Mains, P.E., 2003. **The *Caenorhabditis elegans* nonmuscle myosin genes *nmy-1* and *nmy-2* function as redundant components of the *let-***

502/Rho-binding kinase and *mel-11*/myosin phosphatase pathway during embryonic morphogenesis. Development 130: 5695-5704.

Piekny, A., Werner, M. and Glotzer, M., 2005. **Cytokinesis: welcome to the Rho zone**. Trends Cell Biol 15: 651-658.

Piekny, A.J. and Glotzer, M., 2008. **Anillin is a scaffold protein that links RhoA, actin, and myosin during cytokinesis**. Curr Biol 18: 30-36.

Piekny, A.J. and Maddox, A.S., 2010. **The myriad roles of Anillin during cytokinesis**. Sem Cell Dev Biol 21: 881-891.

Pohl, C., Tiongson, M., Moore, J.L., Santella, A. and Bao, Z., 2012. **Actomyosin-based self-organization of cell internalization during *C. elegans* gastrulation**. BMC Biol 10: 94.

Pollard, T.D., 2007. **Regulation of actin filaments assembly by Arp2/3 complex and formins**. Annu Rev Biophys Biomol Struct 36: 451-457.

Priess, J.R. and Hirsh, D.I., 1986. *Caenorhabditis elegans* **morphogenesis: the role of the cytoskeleton in elongation of the embryo**. Dev Biol 117: 156-173.

Quinn, C.C., Pfeil, D.S. and Wadsworth, W.G., 2008. **CED-10/Rac1 mediates axon guidance by regulating the asymmetric distribution of MIG-10/lamellipodin**. Curr Biol 18: 808-813.

Raich, W.B., Agbunag, C. and Hardin, J., 1999. **Rapid epithelial-sheet sealing in the** *Caenorhabditis elegans* **embryo requires cadherin-dependent filopodial priming**. Curr Biol 9: 1139-1146.

Reyes, C.C., Jin, M., Breznau, E.B., Espino, R., Delgado-Gonzalo, R., Goryachev, A.B., et al., 2014. **Anillin regulates cell-cell junction integrity by organizing junctional accumulation of Rho-GTP and actomyosin**. Curr Biol 24: 1263-1270.

Ridley, A.J., 2011. **Life at the leading edge**. Cell 145: 1012-22.

Roh-Johnson, M., Shemer, G., Higgins, C.D., McClellan, J.H., Werts, A.D., Tulu, U.S., et al., 2012. **Triggering a cell shape change by exploiting preexisting actomyosin contractions**. Science 335: 1232-1235.

Sarov, M., Schneider, S., Pozniakovski, A., Roguev, A., Ernst, S., Zhang, Y., et al., 2006. **A recombineering pipeline for functional genomics applied to** *Caenorhabditis elegans*. Nat Methods 3: 839-844.

Sawa, M., Suetsugu, S., Sugimoto, A., Miki, H., Yamamoto, M. and Takenawa, T., 2003. **Essential role of the** *C. elegans* **Arp 2/3 complex in cell migration during ventral enclosure**. J Cell Sci 116: 1505-1518.

Schäfer, M. and Werner, S., 2008. **Cancer as an overhealing wound: an old hypothesis revisited**. Nat Rev Mol Cell Biol 9: 628-638.

Schlessinger, K., Hall, A. and Tolwinski, N., 2009. **Wnt signaling pathways meet Rho GTPases**. Genes Dev 23: 265-277.

Schmidt-Rhaesa, A., 2007. **The Evolution of Organ Systems**. New York: Oxford University Press: pp. 368.

Schumacher, S., Gryzik, T., Tannebaum, S. and Muller, H.A., 2004. **The RhoGEF Pebble is required for cell shape changes during cell migration triggered by the *Drosophila* FGF receptor Heartless**. Development 131: 2631-2640.

Segbert, C., Johnson, K., Theres, C., van Fürden, D. and Bossinger, O., 2004. **Molecular and functional analysis of apical junction formation in the gut epithelium of *Caenorhabditis elegans***. Dev Biol 266: 17-26.

Severson, A.F., Baillie, D.L. and Bowerman, B., 2002. **A Formin Homology protein and a profilin are required for cytokinesis and Arp2/3-independent assembly of cortical microfilaments in *C. elegans***. Curr Biol 12: 2066-2075.

Sheffield, M., Loveless, T., Hardin, J. and Pettitt, J., 2007. ***C. elegans* Enabled exhibits novel interactions with N-WASP, Abl, and cell-cell junctions**. Curr Biol 17: 1791-1796.

Sheikh, F., Ross, R.S. and Chen, J., 2009. **Cell-cell connection to cardiac disease**. Trends Cardiovasc Med 19: 182-190.

Shekarabi, M. and Kennedy, T.E., 2002. **The netrin-1 receptor DCC promotes filopodia formation and cell spreading by activating Cdc42 and Rac1**. Mol Cell Neurosci 19: 1-17.

Shekarabi, M., Moore, S.W., Tritsch, N.X., Morris, S.J., Bouchard, J.F., Kennedy, T.E., 2005. **Deleted in colorectal cancer binding netrin-1 mediates cell substrate adhesion and recruits Cdc42, Rac1, Pak1, and N-WASP into an intracellular signaling complex that promotes growth cone expansion**. J Neurosci 25: 3132-3141.

Shelton, C.A., Carter, J.C., Ellis, G.C. and Bowerman, B., 1999. **The nonmuscle myosin regulatory light chain gene mlc-4 is required for cytokinesis, anterior-posterior polarity, and body morphology during *Caenorhabditis elegans* embryogenesis**. J Cell Biol 146: 439-451.

Simske, J.S. and Hardin, J., 2001. **Getting into shape: epidermal morphogenesis in *Caenorhabditis elegans* embryos**. BioEssays 22: 12-23.

Smallhorn, M., Murray, M.J. and Saint, R., 2004. **The epithelial-mesenchymal transition of the *Drosophila* mesoderm requires the Rho GTP exchange factor Pebble**. Development 131: 2641-2651.

Solon, J., Kaya-Copur, A., Colombelli, J. and Brunner, D, 2009. **Pulsed forces timed by a ratchet-like mechanism drive directed tissue movement during dorsal closure**. Cell 137: 1331-1342.

Somers, W.G. and Saint, R., 2003. **A RhoGEF and Rho family GTPase-activating protein complex links the contractile ring to cortical microtubules at the onset of cytokinesis**. Dev Cell 4: 29-39.

Soto, M.C., Qadota, H., Kasuya, K., Inoue, M., Tsuboi, D., Mello, C.C., et al., 2002. **The GEX-2 and GEX-3 proteins are required for tissue morphogenesis and cell migrations in *C. elegans***. Genes Dev 16: 620-632.

Straight, A.F., Cheung, A., Limouze, J., Chen, I., Westwood, N.J., Sellers, J.R., et al., 2003. **Dissecting temporal and spatial control of cytokinesis with a myosin II inhibitor**. Science 299: 1743-1747.

Straight, A.F., Field, C.M. and Mitchison, T.J., 2005. **Anillin binds nonmuscle myosin II and regulates the contractile ring**. Mol Biol Cell 16: 193-201.

Sulston, J.E., Schierenberg, E., White, J.G. and Thomson, J.N., 1983. **The embryonic cell lineage of the nematode *Caenorhabditis elegans***. Dev Biol 100: 64-119.

Sweeney, H.L. and Houdusse, A., 2010. **Structural and functional insights into the myosin motor mechanism**. Annu Rev Biophys 39: 539-557.

Tabara, H., Sarkissian, M., Kelly W.G., Fleenor, J., Grishok, A., Timmons, L, et al., 1999. **The *rde-1* gene, RNA interference, and transposon silencing in *C. elegans***. Cell 99: 123-132.

Tatsumoto, T., Xie, X., Blumenthal, R., Okamoto, I. and Miki, T., 1999. **Human ECT2 is an exchange factor for Rho GTPases, phosphorylated in G2/M phases, and involved in cytokinesis**. J Cell Biol 147: 921-928.

Tepass, U., Truong, K., Godt, D., Ikura, M. and Peifer, M., 2000. **Cadherins in embryonic and neural morphogenesis**. Nat Rev Mol Cell Biol 1: 91-100.

Terry, S.J., Zihni, C., Elbediwy, A., Vitello, E., Leefa Chong San, I.V., Balda, M.S., et al., 2011. **Spatially restricted activation of RhoA signalling at epithelial junctions by p114RhoGEF drives junction formation and morphogenesis**. Nat Cell Biol 13: 159-166.

Tian, D., Diao, M., Jiang, Y., Sun, L., Zhang, Y., Chen, Z., et al., 2015. **Anillin Regulates Neuronal Migration and Neurite Growth by Linking RhoG to the Actin Cytoskeleton**. Curr Biol 25: 1135-1145.

Tojkander, S., Gateva, G. and Lappalainen, P., 2012. **Actin stress fibers--assembly, dynamics and biological roles**. J Cell Sci 125: 1855-1864.

Tse, Y.C., Piekny, A. and Glotzer, M., 2011. **Anillin promotes astral microtubule-directed cortical myosin polarization**. Mol Biol Cell 22: 3165-3175.

Tu, C.L., Chang, W., Xie, Z. and Bikle, D.D., 2008. **Inactivation of the calcium sensing receptor inhibits E-cadherin-mediated cell-cell adhesion and calcium-induced differentiation in human epidermal keratinocytes.** J Biol Chem 283: 3519-3528.

van Impel, A., Schumacher, S., Draga, M., Herz, H.M., Grosshans, J. and Muller, H.A., 2009. **Regulation of the Rac GTPase pathway by the multifunctional Rho GEF Pebble is essential for mesoderm migration in the *Drosophila* gastrula**. Development 136: 813-822.

van Oostende Triplet, C., Jaramillo Garcia, M., Haji Bik, H., Beaudet, D. and Piekny, A., 2014. **Anillin interacts with microtubules and is part of the astral pathway that defines cortical domains**. J Cell Sci 127: 3699-3710.

Vicente-Manzanares, M., Ma, X., Adelstein, R.S. and Horwitz A.R., 2009. **Non-muscle myosin II takes centre stage in cell adhesion and migration**. Nat Rev Mol Cell Biol 10: 778-790.

Wang, X., Roy, P.J., Holland, S.J., Zhang, L.W., Culotti, J.G. and Pawson, T., 1999. **Multiple ephrins control cell organization in *C. elegans* using kinase-dependent and -independent functions of the VAB-1 Eph receptor**. Mol Cell 4: 903-913.

Welch, M.D. and Mullins, R.D., 2002. **Cellular control of actin nucleation**. Annu Rev Cell Dev Biol 18: 247-288.

Wernike, D., van Oostende, C. and Piekny, A., 2014. **Visualizing neuroblast cytokinesis during *C. elegans* embryogenesis**. J Vis Exp 85: e51188.

White, J.G., Southgate, E., Thomson, J.N. and Brenner, S., 1986. **The structure of the nervous system of the nematode *Caenorhabditis elegans***. Phil Trans R Soc Lond B 314: 1-340.

Williams-Masson, E.M., Malik, A.N. and Hardin, J., 1997. **An actin-mediated two-step mechanism is required for ventral enclosure of the *C. elegans* hypodermis**. Development 124: 2889-2901.

Williams, B.D. and Waterston, R.H., 1994. **Genes critical for muscle development and function in *Caenorhabditis elegans* identified through lethal mutations**. J Cell Biol 124: 475–490.

Wissmann, A., Ingles, J., McGhee, J.D. and Mains, P.E., 1997. ***Caenorhabditis elegans* LET-502 is related to Rho-binding kinases and human myotonic dystrophy kinase and interacts genetically with a homolog of the regulatory subunit of smooth muscle myosin phosphatase to affect cell shape**. Genes Dev 11: 409-422.

Wissmann, A., Ingles, J. and Mains, P.E., 1999. **The *Caenorhabditis elegans mel-11* myosin phosphatase regulatory subunit affects tissue contraction in the somatic gonad and the embryonic epidermis and genetically interacts with the Rac signaling pathway**. Dev Biol 209: 111-127.

Withee, J., Galligan, B., Hawkins, N. and Garriga, G., 2004. *Caenorhabditis elegans* **WASP and Ena/VASP proteins play compensatory roles in morphogenesis and neuronal cell migration**. Genetics 167: 1165-1176.

Wong, M.C. and Schwarzbauer, J.E., 2012. **Gonad morphogenesis and distal tip cell migration in the *Caenorhabditis elegans* hermaphrodite**. Wiley Interdiscip Rev Dev Biol 1: 519-531.

Yamashiro, S., Totsukawa, G., Yamakita, Y., Sasaki, Y., Madaule, P., Ishizaki, T., et al., 2003. **Citron kinase, a Rho-dependent kinase, induces di-phosphorylation of regulatory light chain of myosin II.** Mol Biol Cell 14: 1745-1756.

Young, P.E., Richman, A.M., Ketchum, A.S. and Kiehart, D.P., 1993. **Morphogenesis in *Drosophila* requires nonmuscle myosin heavy chain function**. Gene Dev 7: 29-41.

Yüce, O., Piekny, A. and Glotzer, M., 2005. **An ECT2-centralspindlin complex regulates the localization and function of RhoA**. J Cell Biol 170: 571-582.

Zhang, H., Landmann, F., Zahreddine, H., Rodriguez, D., Koch, M. and Labouesse, M., 2011. **A tension-induced mechanotransduction pathway promotes epithelial morphogenesis**. Nature 471: 99-103.

Zhang, H., Gally, C. and Labouesse, M., 2010. **Tissue morphogenesis: how multiple cells cooperate to generate a tissue**. Curr Opin Cell Biol 22: 575-582.

Zhang, H., Landmann F., Zahreddine H., Rodriguez, D., Koch M. and Labouesse M., 2011. **A tension-induced mechanotransduction pathway promotes epithelial morphogenesis**. Nature 471: 99-103.

Zhang, H. and Labouesse, M., 2012. **Signalling through mechanical inputs: a coordinated process**. J Cell Sci 125: 3039-3049.

Zonies, S,. Motegi, F., Hao, Y. and Seydoux, G., 2010. **Symmetry breaking and polarization of the *C. elegans* zygote by the polarity protein PAR-2**. Development 137: 1669-1677.